Propagation-invariant Vector Beams

A thesis submitted during 2014 to the University of Hyderabad in the partial fulfilment of the award of a **Ph.D. degree** in School of Physics by

Geo Philip M

School of Physics
University of Hyderabad
(P.O) Central University, Gachibowli
Hyderabad – 500 046
India

DECLARATION

I **Geo Philip M** hereby declare that this thesis entitled **"Propagation-invariant Vector Beams"** submitted by me under the guidance and supervision of Professor. **Nirmal K. Viswanathan** is a bonafide research work which is also free from plagiarism. I also declare that it has not been submitted previously in part or in fill to this University or any other University or Institution for the award of any degree or diploma. I hereby agree that my thesis can be deposited in Shodganga/INFLIBNET.

Date: June 2014 Name: Geo Philip M

Signature of the Student
Regd. No. 09PHPH02

CERTIFICATE

This is to certify that the thesis entitled **"Propagation-invariant Vector Beams"** submitted by **Geo Philip M** bearing Regd. No. 09PHPH02 in partial fulfilment of the requirements for the award of **Doctor of Philosophy** in **Physics** is a bonafide work carried out by him under my supervision and guidance which is a plagiarism free thesis.

The thesis has not been submitted previously in part or in full to this or any other University or Institution for the award of any degree or diploma.

Signature of the Supervisor

//Countersigned//

Dean of the School

To Kavya and Boo Boo

Acknowledgement

First and foremost, I would like to express my gratitude to my supervisor, Prof.Nirmal K Viswanathan, for suggesting this Ph.D. topic, and for his patience helping me along the way, for his constant guidance in both the good days and bad ones. It is difficult to imagine how our student-supervisor relationship could have been better. Needless to say, I have learned a lot from him.

I would like to thank my Ph.D Doctoral Committee members Prof. Narayana Rao and Dr. Ashoka V. S for their teaching, encouragement and insightful comments.

I express my sincere thanks to University of Hyderabad and CSIR for financial support and Dean School of Physics for making available all the necessary facilities for the research work.

This work is also a testament to the breadth and friendliness of beam optics and application group. I thankfully remember Dr.V.V.G Krishna, Dr.Shankar Pidishetty, Vijay Kumar, Dr.Chandra Prajapathi and Samlan C. T for useful discussions, creating a warm and friendly research lab environment and timely help. I also acknowledge Y.V Jayasura, P. Vijay for their help with Matlab and Amala, Jabir, Midhun, Rakesh, Sandeep for their friendship and help. I also thank Giovanni Milione my co-author. Also my Msc classmate Reddy Prathap for his timely help in getting research articles.

I would like to thank Abraham, Pentiah and Laxminarayana (SEM operator) for getting my work done quckly.

Most of all, I thank my wife, my love Kavya and our little Boo Boo for their love, support, sacrifices, for putting up with my moods and grumpiness at times, for allowing me time away from family stuff to get my work completed, and to you this thesis is dedicated. I can't forget my little one, when she was 10 months old peacefully sleeping in the lab, while my wife was helping me with the final experiments. I also thank her for reducing pressure on me by talking care of the job search, at times applying on my behalf and finally finding my next job. I also thank the child care center UOH for taking care of my baby when I was at work. I am also forever indebted to my parents and in laws for their support and care.

Special thanks to my father for encouraging me to study physics and giving me the freedom to choose my way.

None of these would have been possible without the abundant blessings showered by the almighty throughout my life.

The five years I have spent working in a dark laboratory (if not all some of the times) has been very fruitful, and I owe much gratitude to a lot of people. This was my small attempt at expressing my gratitude, I hope those I forget will not take offence!

Abstract

Diffraction is an unavoidable inherent property of a wave field resulting in changes in both the transverse and longitudinal amplitude, phase and polarization distribution of the beam field, leading to the divergence of a light beam propagating in the free-space in the simplest case. In optical sciences the diffraction is a classical problem which occurs in imaging and observational devices imposing critical resolution limits which cannot be corrected for by any known techniques . The concept of non-divergence of beams during propagation started with Bessel beams which is obtained as a solution to the wave equation in free-space. The properties such as propagation-invariance, self-reconstruction and self-imaging of Bessel beams are made use of in a variety of applications including optical trapping, tweezing, microscopy, drilling of high-precision holes and controlling the propagation of ultra-short pulses in dispersive media. Higher-order Bessel beam also carry a helical wave-front and thus possess orbital angular momentum a new attribute which can also be used as information carriers. Superposing vector nature on these beam fields, the propagation-invariant vector beams are all the more attractive and finds its uses in both fundamental studies and in different applications such as microscopy, micro manipulation of particles, accelereting particles etc. This thesis is focused on studies to highlight some of the salient experimental and theoretical aspects of the propagation-invariant vector optical beams ranging from its generation methods (using bulk axicon and fiber micro-axicon) to studies on different manifestations of the fundamental aspects of the propagation-invariant beams such as its self-reconstruction beyond obstruction, and the phase and polarization evolution in the vector regime and their characterization, all geared towards making use of these beams in emerging and future applications.

Contents

CHAPTER

1

Introduction to Propagation-invariant Optical Beams

Contents

1.1 Introduction

Historically, diffraction was considered a violation from the rectilinear propagation of light. The effect of diffraction of light was first observed and characterized by Grimaldi in 1665, who also coined the term *diffraction*, from the Latin word *diffringere*, meaning 'to break into pieces', referring to light breaking up into different directions. Around the same time James Gregory observed diffraction patterns from bird feather which can hence be called the first diffraction grating. Subsequently, according to Somerfield, any deviation from the rectilinear propagation of light not caused by refraction or reflection can be called diffraction and is responsible for the divergence in free-space propagation and bending of light into the shadow region. But in modern optics diffraction is treated as a natural property of the wave field with nonhomogeneous transverse intensity distribution that leads to changes in both transverse and longitudinal amplitude, phase and polarization distribution of the wave field.

In optical science diffraction by a circular or an annular aperture is a classical problem which occurs in microscope to astronomical telescope imposing critical resolution limits which cannot be corrected for by any aberration or apodization techniques. It is however possible to have a *non-diffracting* propagation of light field within waveguides or in non-linear media as guided modes or as spatial solitons. All other cases of optical beam which is a solution of paraxial wave equation diffracts and hence diverge through its propagation. The term *diffraction-free beams* or *non-diffracting beams* in vacuum emerged first in 1987 when Durnin *et.al.,* showed that the intensity distribution in the focal region of an annular aperture placed before an aberration-free lens takes the form $J_0^2(\alpha\rho)$ where J_0 is the zeroth-order Bessel function of first kind, ρ is the radial distance and the parameter 'α' is invariant over a certain range[DuME87]. For an ideal aberration–free lens with unlimited open aperture this range can extend up to infinity leading to the formation of an ideal *non-diffracting beam*. As in the case of a plane wave, a trivial example of propagation invariant field the ideal *non-diffracting beam* also possess infinite energy since the transverse intensity falls off as $1/\rho$ [TuFr10]. The far-field diffraction pattern of the field introduced by Durnin is delta-function rings rather than concentric intensity pattern around the optic axis. Hence the term *'propagation-invariant'* is more realistic and appropriate here than '*diffraction-free'* beams.[TuFr10].

Though the term *diffraction-free* was coined in 1987 by Durnin, the *propagation-invariant field*s is historically known, going back to Stratton in 1941[Adam41]and van Nie (1964) who had considered elementary non-diffracting solutions, the Bessel beams. The Bessel beams were first generated experimentally by McLeod[Mcle54] sixty years ago by using an axicon, a conical lens. Later on different types of diffractive optical elements were used to generate Bessel beams of any order [VaTF89]. Further, rapid developments in propagation-invariant beams lead to newer ways other than using an axicon, for its generation[Inde89];[ScMc92] including laser resonator [UeKi89]; [KhKR01], dual element optical system [DaFH92];[IfAK93], spherically aberrated lens [HeWi91], holograms [TuVF88] and more recently spatial light modulators [DaCC96]. The propagation-invariance is not limited only to Bessel beams as other propagation-invariant beam solutions to wave equation and their generation were also identified which include Mathieu beams in elliptic co-o*rdinat*es [GuIC00], Weber beams in parabolic co-ordinates [BaGC04] and other self-similar Hermite-Gaussian, Laguerre-Gaussian and Ince-Gaussian beams[ABRW12]. Since the propagation-invariant vortex beams such as higher-order Bessel beams can exert radiation pressure and carry optical angular momentum they can be efficiently used in particle trapping, optical tweezers [HeHR95] and as optical wrenches[CPAN02].

As in the case of continuous propagation-invariant beam fields pulsed light fields can also maintain their intensity and shape in space and time and are called localized waves which under certain conditions can propagate at superluminal or subluminal speeds. These kind of focused wave modes were first demonstrated by Reivelt and Saari [ReSa02]. The first ultrasonic Bessel beam transducer[HsMT89] was based on the application of localized fields in acoustics. The localized pulsed fields which propagate at superluminal speed were extensively studied by Lu and Greenleaf [LuGr92a]; [LuGr92b] who generalized the Bessel beams to include broadband non-diffracting and non-dispersive pulses known as *X*-waves. The spatio-temporally localized optical waves have found applications in non-linear optics for second-harmonic generation and spontaneous generation of X-shaped light pulses. More recently, electron Bessel beams were also generated using diffraction from a nano-scale phase hologram[GKGF14] which is expected to dramatically improve the performance of electron microscope.

1.2 Propagation-invariant scalar beams

An ideal monochromatic spatially coherent propagation-invariant beam propagating along the z-axis can be comprehended as a mode-like field whose complex amplitude can be written in the form [Bouc03]:

$$U(x, y, z, t) = u(x, y)\, exp[i(\omega t - \beta z)] \tag{1.1}$$

where 'u' describes the transverse amplitude profile, 'ω' and 'β' are the angular frequency and the angular wave-number respectively[Bouc03]. The amplitude 'u' is independent of z and so the intensity $I = UU^*$ is also independent of z and thus the beam is propagation-invariant. Conventionally Equation (1.1) represents a waveguide mode or a spatial soliton which propagate in optically linear or non-linear material. But Durnin showed that there can be physically possible solutions to homogeneous wave equation having the form of Equation (1.1) thus enabling propagation-invariance in vacuum. The time-independent part of U given by Equation (1.2) should satisfy the Helmholtz equation (Equation (1.3):

$$a(x, y, z) = u(x, y)\, exp(-i\beta z) \tag{1.2}$$

$$(\nabla^2 + k^2)a(x, y, z) = 0 \tag{1.3}$$

where $k = \omega/c$ with c the velocity of light in vacuum. In cylindrical co-ordinates the solution of Equation (1.3) can be written as

$$a(\rho, \varphi, z) = P(\rho)\Phi(\varphi)\, exp(-i\beta z) \tag{1.4}$$

Assuming

$$\Phi(\varphi) = exp(im\varphi); \quad m = 0,1,2,3 \ldots \ldots \tag{1.5}$$

and substituting Equation (1.5) and (1.4) in (1.3) we get

$$\frac{\partial^2 P(\rho)}{\partial \rho^2} + \frac{1}{\rho}\frac{\partial P(\rho)}{\partial \rho} + \alpha^2 P(\rho)\left(1 - \frac{m^2}{\alpha^2 \rho^2}\right) = 0 \tag{1.6}$$

with $\alpha = k^2 - \beta^2$. The general solution to Equation (1.6) can be written as a linear combination of m^{th}-order Bessel function of the first kind and m^{th}-order Neumann function as [Bouc03]:

$$P_m(\rho) = \mu J_m(\alpha\rho) + \upsilon N_m(\alpha\rho) \tag{1.7}$$

where μ and υ are constants. Generally only the Bessel function of the first kind is considerd as physically possible solution since the Neumann function has singularities at ρ=0 when they are considered separetly. The radial solution of the Bessel equation is given by $R^j \equiv H_m^j, j = 1,2$ with the Hankel functions H_m^j given by

$$H_m^1 = J_m(\alpha\rho) + iN_m(\alpha\rho) \tag{1.8}$$

$$H_m^2 = J_m(\alpha\rho) - iN_m(\alpha\rho) \tag{1.9}$$

Now calculating the real amplitude of a rotationaly symmetric beam considering 0^{th} Hankel functions one gets

$$\overline{U}(\rho, z) = \frac{1}{2}\left[\overline{U}_0^1(\rho, z) + \overline{U}_0^2(\rho, z)\right] \tag{1.10}$$

with

$$\overline{U}_0^1(\rho, z) = J_0(\alpha\rho)\, cos(\omega t - \beta z) + N_0(\alpha\rho)\, sin(\omega t - \beta z) \tag{1.11}$$

$$\overline{U}_0^2(\rho, z) = J_0(\alpha\rho)\, cos(\omega t - \beta z) - N_0(\alpha\rho)\, sin(\omega t - \beta z) \tag{1.12}$$

Thus the real amplitude can be represented as a superposition of an out going $\overline{U}_0^1(\rho, z)$and an incoming $\overline{U}_0^2(\rho, z)$ travelling waves. To satisfy the boundary conditions at ρ = 0, each cylindrical wave must be the complex conjugate of the other. In which case the imaginary parts of the Hankel functions composing the Neumann functions cancels out so that the total field is a standing wave represented by the Bessel function only.

In the integral form, the time independent amplitude of the general propagation-invariant beam can be conveniently expressed using cylindrical coordinates as

$$a(\rho) = \frac{ik}{2\pi} \int_{-\pi}^{\pi} A(\psi) f(\rho, \psi) d\psi \tag{1.13}$$

where,

$$f(\rho,\psi) = exp(-i\beta z)\, exp[i\alpha\rho cos(\psi-\varphi)] \tag{1.14}$$

and 'A' denotes an arbitrary periodical function. The parameter 'α' can be interpreted by means of the angular spectrum, which is a function of the angular frequencies v_x and v_y and can be obtained as the two-dimensional Fourier transformation of the amplitude 'a':

$$F(v,\psi) = A(\psi)\delta(v-v_0)\,;\; v_0 = \frac{\alpha}{2\pi} \tag{1.15}$$

The special properties of the propagation-invariant beams depend on the composition of the angular spectrum, representing a coherent superposition of an infinite number of plane waves whose wave vector lies on a conical surface[Bouc03].

1.2.1 Types of propagation-invariant beams

Since a propagation-invariant beam can be considered as the interference field of an infinite number of plane waves whose propagation vectors lie on a conical surface, different types of intensity distributions are possible for the Propagation-invariant beams depending on the amplitude and phase of the constituent plane wave components of the angular spectrum. The following are some of the best known examples of propagation-invariant beams:

Bessel beams:

Bessel beams are obtained as a special case when the amplitude of the plane wave components are equal with an azimuthal phase variation of $A(\psi) = A_0 exp(im\psi)$. The complex amplitude of the Bessel beam can be then written as

$$U(\rho,\varphi,z,t) = A_0 J_m(\alpha\rho)\, exp[i(\omega t + m\varphi - \beta z)] \tag{1.16}$$

where J_m is Bessel function of the first kind. If the plane waves are coherently superposed with m=0 the resultant beam will have a bright center srrounded by cylindrically symmetric rings. Fig. 1.1 shows the intensity and phase distributions of J_0, J_1 and J_2 Bessel beams.

Mathieu beams:

These type of beam fields are obtained when the real amplitude of the superposing plane wave components are kept constant while the phase varies as:

$$A(\psi) = exp\left[-\left(\frac{\upsilon_0\, cos\psi}{\omega_0}\right)\right] \tag{1.17}$$

Where υ_0 is given by Equation (1.15) and ω_0 is the band-width of the Gaussian profile at these spatial frequencies. The transverse intensity profile of the Mathieu beam depends strongly on the parameter ω_0. Fig. 1.2 shows the intensity profile of Mathieu beams for different ω_0 [Bouc03].

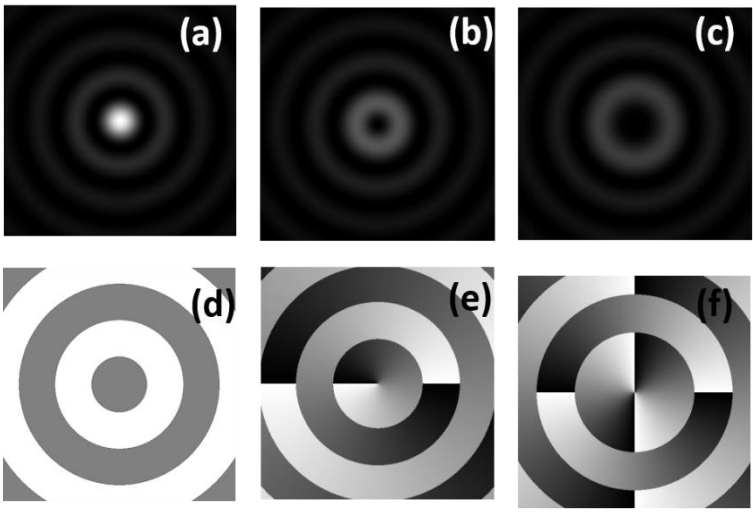

Fig. 1.1 Intensity and phase distributions of Bessel beams (a), (b) and (c) are respectively the zero, first and second order Bessel beams; (d), (e) and (f) are the corresponding phase distribution in the cross-section

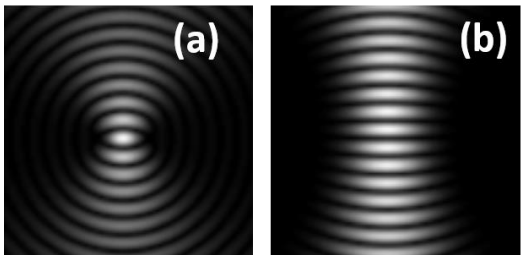

Fig. 1.2 Intensity profile of Mathieu beams with (a) $\omega_0 = 4\upsilon_0$ and (b) $\omega_0 = 2\upsilon_0$[Bouc03]

Caleidoscopic propagation-invariant beams:

In both of the above mentioned examples of propagation-invariant beam fields the phase of the superposing plane waves varies in a continous manner in the beam cross section. The Caleidoscopic beam patterns are formed when the phase variation is in discrete steps across the beam. If the phase variation is given by Dirac delta function Equation (1.18), the integration in Equation (1.13) becomes a summation and the complex amplitude of the propagation-invariant field can be written as Equation (1.19):

$$A(\psi) = \sum_{j=1}^{N} A_0(\psi)\delta(\psi - \psi_j) \tag{1.18}$$

$$a(\rho, \varphi, z) = \frac{ik}{2\pi} exp(-i\beta z) \sum_{j=1}^{N} A_0(\psi_j)\, exp[i\alpha\rho\, cos(\psi_j - \psi)] \tag{1.19}$$

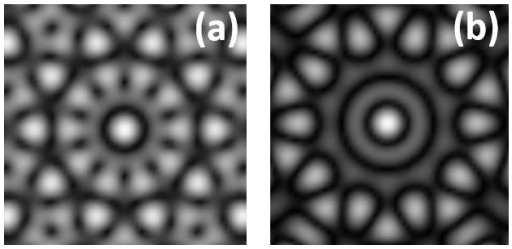

Fig. 1.3 Caleidoscopic propagation-invariant beam patterns corresponding to (a) N=5 and (b) N=10[Bouc03]

Fig. 1.3 shows the simulated intensity patterns[Bouc03] for different N values and the azimuthal angle is chosen as follows

$$\psi_j = (j - i)\Delta\psi; \quad \Delta\psi = \frac{2\pi}{N} \tag{1.20}$$

Bessel-Gauss beams:

Ideal propagation-invaraiant beams possess infinite energy and propagate from -∞ to +∞ without any change in its transverse intensity distribution. But a beam with infinite energy cannot be realized in any experiment. So, experimentally only approximate propagation-invariant beams are realizable which possess finite

energy and whose propagation characteristics can be approximated to that of an ideal propagation-invariant beam transmitted through a finite Gaussian aperture. Bessel-Gauss beams are an example for realistic propagation-invariant beams. The complex amplitude of a J_0 Bessel-Gauss beam is given by the following equation[Bouc03]:

$$\boldsymbol{a(\rho,z) = J_0\left(\frac{k\rho}{1-\frac{iz}{q}}\right) exp\left[\frac{ik^2q^2}{4k}\left(\frac{2}{k\omega^2}+\frac{i}{R_g}\right)(z - iq)\right] a_g(\rho,z)} \quad (1.21)$$

where $\boldsymbol{a_g}$ is the complex amplitude of the Gaussian beam and $\boldsymbol{q}$ is the Rayleigh range of the Gaussian beam.

1.3 Propagation-invariant vector beams

The scalar teatment for the propagation-invariant beams presented above is applicabe only in the paraxial limit and one needs to consider the longitudinal component of the electric field once the cone angle is in the non-paraxial regime. Applying representative theorem the vector complex amplitude can be deduced from the scalar amplitude a_m which satisfy the Helmholtz equation[BoOl95] and the vector complex amplitudes can be written as:

$$E = -\sum (p_m P_m + q_m Q_m)\, exp(i\omega t) \quad (1.22)$$

$$H = i\xi \sum (p_m Q_m + q_m P_m)\, exp(i\omega t) \quad (1.23)$$

where

$$P_m = -(s \times \nabla a_m), \qquad Q_m = \frac{1}{k}(\nabla \times P_m) \;\; and \;\; \frac{1}{\xi} = \sqrt{\mu_0 \epsilon_0}$$

p_m and q_m are constants and 's' is an arbitrary vector. This formalism explains the existence of azimuthally and radially polarized propagation-invariant beams by substituting suitable values for the weighing constants. Thus the propagation-invariant beams with spatially varying polarization structure are possible and can

be predicted by extending the scalar treatment into vector theory. The concepts of vector beam and propagation invariance were connected to realize vector Bessel beams, first introduced by Jordan and Hall [JoHa94] and Bouchal [BoOl95]. Recently, Dudley *et al* experimentally generated vector Bessel beam using a spatial light modulator and birefringent crystal[DLME13]. Another method based on *c*-cut Nd:YVO4 laser with a hemispherical cavity [VyKS14] is also reported for the generation of radially-polarized Bessel beams. Other methods reported for the generation of propagation-invariant vector beams include concentric-grating surface–emitting semiconductor diode laser[EKWH92] and sub-wavelength grating systems [NBKH04].

1.4 Properties of propagation-invariant beam fields

The propagation invariant beams differ from the conventional Gaussian or flat top beams in many aspects. Some of these properties which make the propagation-invariant beams more suitable for several practical applications such as trapping of particles, atom guiding and efficient imaging are discussed below:

1.4.1 Beam stability

Beam stability is a remarkable property of the propagation-invariant beams; that these beams are highly resistant towards any type of amplitude and phase disturbances while propagation. It can regain its original transverse intensity profile even after being partially obstructed by an opaque obstacle.

1.4.2 Self imaging

If two or more PI beams with suitably chosen wave numbers superimpose the transverse intensity profile of the beam repeats itself periodically along its propagation due to constructive and destructive interference between the constitutive modes. The complex amplitude of such system a beam combination can be written as:

$$a(x, y, z) = a(x, y, z + L) \tag{1.24}$$

where L is the longitudinal period. The self-imaging property of the Bessel beam is made use of in experimentally realizing optical Bottle beams[PhVi10].

1.4.3 Self-reconstruction

The propagation-invariant beam fields are also known to exhibit self-reconstruction property in both linear[BoBB98] and non-linear[BGJP02] regimes. An optical beam whose amplitude reconstructs itself after a partial obstruction, reported first in Bessel beams[BoWC98] has revolutionized micromanipulation[GMMS02] and microscopy[FaSR10] applications realizing enhanced image contrast even while imaging in optically thick inhomogeneous media such as cell clusters, embryos, skin etc.

1.4.4 Optical angular momentum

The higher-order propagation-invariant Bessel beams possess phase vortex at its center (Fig. 1.1) and thus carry orbital angular momentum. The orbital angular momentum is proportional to the topological charge of the vortex beam and is inversely proportional to its angular frequency. Propagation-invariant vortex beams can exert radiation pressure and they can be efficiently used in particle trapping, optical tweezers [HeHR95] and as optical wrenches[CPAN02].

1.5 Generation Methods

Ideal propagation-invariant beam fields possess infinite energy and so cannot be realized experimentally. The closest approximations of Propagation-invariant fields with finite energy and finite propagation-invariant range are generated in a number of ways for a variety of practical applications and fundamental studies.

1.5.1 Spatial frequency selection and modulation

This is the most trivial method for the generation of Bessel field, proposed and demonstrated by Durnin [DuME87]. J0 Bessel beam was generated by keeping an annular aperture at the focal plane of a positive lens. Fig. 1.4 shows the

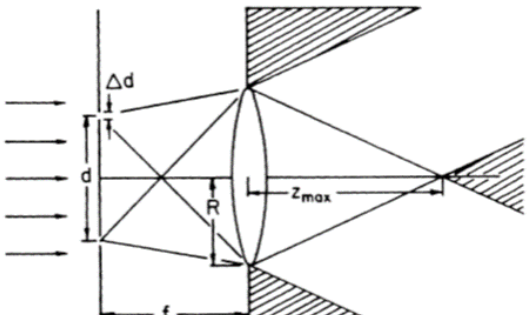

Fig. 1.4 Experimental setup used by Durnin for the generation of J0 Bessel beam via focusing of annular beam by a positive lens[DuME87].

experimental setup used for the generation of Bessel beams though low throughput efficiency is the problem with this method. The fourier lens converts the annular beam to J_0 Bessel beam in the focal plane.

1.5.2 Diffractive optics

Axicon or conical lens introduced by McLeod [Mcle54] in 1954 is a cylindrically symmetric optical device for the generation of propagation-invariant Bessel beams. Higher-order Bessel beams where also generated using the axicon by focusing of the corresponding Laguerre-Gauss modes[Jarl00]. The axicon can directly convert a Gaussian plane wave or a higher-order helical wave Lagurre-Gussian beam to a Bessel-Gauss beam by imparting a conical wave-front. The

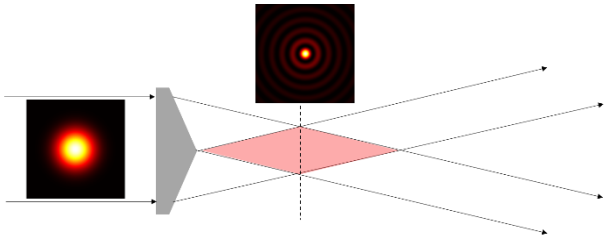

Fig. 1.5 Axicon focusing for the generation of Bessel beam

propagation-invariant range of the produced beam depends both on the small angle of the axicon and the incident beam waist[Jarl00] given by Equation (1.25):

$$Z_{max} = \frac{k}{k_r}\omega_0; \quad k_r = k\,sin\theta; \quad \theta = (n-1)\,tan\alpha \tag{1.25}$$

where ω_0 is the beam waist, n-refractive index of axicon and α- small angle of the axicon. The charecteristic property of the propagation-invariant beams formed by the axicon is the linear increase in intensity in the propagation-invariant region. Fig. 1.5 shows a the schematic of the axicon focusing to generate propagation-invariant beams.

1.5.3 Optical resonators

Optical resonator is an active source for the generation of PI beam fields. Since the propagation-invariant modes are eigen modes of an infinite aperture Fabry-Perot, the finite aperture approximation of the Bessel modes can be generated using the resonators by choosing a particular frequency[UeKi89]; [KhKR01].

Efforts to structure the active medium to an annular structure was also reported to increase the quality of the propagation-invariant beam fileds. Special optical resonator cavities are designed to produce vector Bessel-Gauss beam, for example a vertical cavity laser with circular grating mirrors[EKWH92]

1.5.4 Configurable devices

Davis *et al* in 1996 demonstrated writing axicon holograms in spatial light modulator(SLM) which can produce structured light beams and can also be electronically controlled [DaCC96]. This also allows realtime pointing and scanning of propagation-invariant fields. Because of the available pixel size of the SLM, cone angle produced by SLMs are limited. The propagation-invariant range of the beam produced by the SLM depends on the number of pixels, which puts limitation on the generated beam quality also.

1.6 Applications

Since its discovery the Bessel-Gauss beams have efficiently replaced the conventional Gaussian and flat top beams in various applications including in micro-manipulation of atoms and particles, fundamental studies in statistical physics, non-linear optics and inter-board optical data distribution, just to name a few. The first optical manipulation of particles using Bessel beams was demonstrated by Arlt *et al.* in 2001[AGSD01]. The ring structure in the Bessel-Gauss beams has made possible the simultaneous trapping of low and high refractive index beads[GMMS02]. The higher-order Bessel-Gauss beams in addition, also carry orbital angular momentum and have been used for the observation of simultaneous transfer of spin and orbital angular momentum from the laser beam to the trapped particles[GMPD03]. The self- reconstruction property of the Bessel-Gauss beams is also made use of in constructing a one-dimensional array of trapped particles[GMMS02]. Significant advances in microscopic techniques are developed in the recent times based on the self-reconstruction characteristics of the Bessel-Gauss beams[FaSR10].

Bessel-Gauss beams are also enabling applications in the area of statistical physics which examines how particles with inherent Brownian motion act in the presence of an external potential. Optical trap is an ideal tool to study the dynamics of such particles. The trapped particles undergoing Brownian motion can also be thermally agitated. In atom optics, either optical or strong magnetic forces are used to channel atoms and optical method are preferred because it is independent of the electrical charge of the particle. If the light is detuned above

the resonance, the atoms are repelled from the light intensity and thus the hollow regions fully enclosed by light in two or three dimensions can be used for atom confinement. Another area where Bessel beams have created significant interest in atom optics is a non-diffracting atom guide. The propagation-invariant hollow core higher order Bessel-Gauss beam allows the atoms to be transported over an extended distance without transverse spreading as would be the case for a normal hollow light beam. Higher-order Bessel-Gauss beams are also used to focus cold atoms[OkIK01].

The Bessel-Gauss beams were also found wanting when used in pumping of optical parametric oscillator (OPO), a device which converts the high-energy pump field into lower energy signal and idler fields. The non-diverging Bessel-Gauss beams are an ideal source in non-linear optical process such as second-harmonic generation. Wave-mixing effects have also been investigated using Bessel-Gauss beams, for instance the enhancement of photorefractive two-wave mixing[BiPD03], reation of Bessel-Gauss beams within the coherent anti-Stokes Raman scattering process[MuVa02], stimulated Raman scattering[NiMa97] etc.

In the recent times, optical beams with spatially varying state of polarization in its transverse cross-section, known as vector beams is getting more attention due the immense potential in various practical applications. The concepts of vector beam and propagation-invariance were connected to realize vector Bessel beams, first introduced by Jordan and Hall [JoHa94] and Bouchal [BoOl95b]. The Propagation-invariant vector beams finds applications in microscopy [AbTo06]; [WRWJ06], laser focusing, acceleration of electrons [RoKi90], optical tweezers, plasmonic lens formation [CANZ09] etc.

Summary

The introduction chapter gives a brief background for understanding propagation-invariant optical beam fields and some of the important contributions in the evolution of this research area which are relevant to the thesis. Also some of the important types of propagation-invariant beams are discussed. We subsequently proceed to highlight the characteristics and properties of the PI beams which makes this class of beams different from the conventional optical beams. Properties such as beam stability, optical angular momentum, self-imaging and self-reconstruction are also explained for a general propagatio-invariant beam. Some of these special properties of the PI beams are

made use of in a large variety of applications ranging from microscopy to micro-manipulation of particles, atoms and molecules. This chapter also tries to highlight some of the main applications realized using propagation-invariant beams.

References

[ABRW12] ALPMANN, C. ; BOGUSLAWSKI, M. ; ROSE, P. ; WÖRDEMANN, M. ; DENZ, C.: Tailored light fields: nondiffracting and self-similar beams for optical structuring and organization. In: . Bd. 8274, 2012, S. 82740R–82740R–12

[AbTo06] ABOURADDY, AYMAN F. ; TOUSSAINT, KIMANI C.: Three-Dimensional Polarization Control in Microscopy. In: *Physical Review Letters* Bd. 96 (2006), Nr. 15, S. 153901

[Adam41] ADAMS STRATTON JULIUS: *Electromagnetic Theory* : Mcgraw Hill Book Company, 1941. — 00015

[AGSD01] ARLT, J ; GARCES-CHAVEZ, V ; SIBBETT, W ; DHOLAKIA, K: Optical micromanipulation using a Bessel light beam. In: *Optics Communications* Bd. 197 (2001), Nr. 4–6, S. 239–245

[BaGC04] BANDRES, MIGUEL A. ; GUTIÉRREZ-VEGA, JULIO C. ; CHÁVEZ-CERDA, SABINO: Parabolic nondiffracting optical wave fields. In: *Optics Letters* Bd. 29 (2004), Nr. 1, S. 44–46. — 00136

[BGJP02] BUTKUS, R. ; GADONAS, R. ; JANUŠONIS, J. ; PISKARSKAS, A. ; REGELSKIS, K. ; SMILGEVIČIUS, V. ; STABINIS, A.: Nonlinear self-reconstruction of truncated Bessel beam. In: *Optics Communications* Bd. 206 (2002), Nr. 1–3, S. 201–209

[BiPD03] BISWAS, DHRUBA J. ; PADMA NILAYA, J. ; DANAILOV, MILTCHO B.: Enhancement of photo-refractive two-wave mixing gain with a Bessel pump beam. In: *Optics Communications* Bd. 226 (2003), Nr. 1–6, S. 387–391. — 00004

[BoBB98] BOUCHAL, Z. ; BAJER, J. ; BERTOLOTTI, M.: Vectorial spectral analysis of the nonstationary electromagnetic field. In: *Journal of the Optical Society of America A* Bd. 15 (1998), Nr. 8, S. 2172–2181

[BoOl95b] BOUCHAL, ZDENĚK ; OLIVÍK, MAREK: Non-diffractive Vector Bessel Beams. In: *Journal of Modern Optics* Bd. 42 (1995), Nr. 8, S. 1555–1566

[Bouc03] BOUCHAL, ZDENĚK: Nondiffracting Optical Beams: Physical Properties, Experiments, and Applications. In: *Czechoslovak Journal of Physics* Bd. 53 (2003), Nr. 7, S. 537–578. — 00099

[BoWC98] BOUCHAL, Z ; WAGNER, J ; CHLUP, M: Self-reconstruction of a distorted nondiffracting beam. In: *Optics Communications* Bd. 151 (1998), Nr. 4–6, S. 207–211

[CANZ09] CHEN, WEIBIN ; ABEYSINGHE, DON C. ; NELSON, ROBERT L. ; ZHAN, QIWEN: Plasmonic Lens Made of Multiple Concentric Metallic Rings under Radially Polarized Illumination. In: *Nano Letters* Bd. 9 (2009), Nr. 12, S. 4320–4325

[CPAN02] CHÁVEZ-CERDA, S. ; PADGETT, M. J. ; ALLISON, I. ; NEW, G. H. C. ; GUTIÉRREZ-VEGA, J. C. ; O'NEIL, A. T. ; MACVICAR, I. ; COURTIAL, J.: Holographic generation and orbital angular momentum of high-order Mathieu beams. In: *Journal of Optics B: Quantum and Semiclassical Optics* Bd. 4 (2002), Nr. 2, S. S52. — 00073

[DaCC96] DAVIS, JEFFREY A. ; CARCOLE, E. ; COTTRELL, DON M.: Nondiffracting interference patterns generated with programmable spatial light modulators. In: *Applied Optics* Bd. 35 (1996), Nr. 4, S. 599–602. — 00050

[DaFH92] DAVIDSON, N. ; FRIESEM, A. A. ; HASMAN, E.: Efficient formation of nondiffracting beams with uniform intensity along the propagation direction. In: *Optics Communications* Bd. 88 (1992), Nr. 4–6, S. 326–330. — 00048

[DLME13] DUDLEY, ANGELA ; LI, YANMING ; MHLANGA, THANDEKA ; ESCUTI, MICHAEL ; FORBES, ANDREW: Generating and measuring nondiffracting vector Bessel beams. In: *Optics Letters* Bd. 38 (2013), Nr. 17, S. 3429–3432

[DuME87] DURNIN, J. ; MICELI, J. J. ; EBERLY, J. H.: Diffraction-free beams. In: *Physical Review Letters* Bd. 58 (1987), Nr. 15, S. 1499–1501. — 02042

[EKWH92] ERDOGAN, T. ; KING, O. ; WICKS, G. W. ; HALL, D. G. ; ANDERSON, ERIK H. ; ROOKS, M. J.: Circularly symmetric operation of a concentric-circle-grating, surface- emitting, AlGaAs/GaAs

quantum-well semiconductor laser. In: *Applied Physics Letters* Bd. 60 (1992), Nr. 16, S. 1921–1923

[FaSR10] FAHRBACH, FLORIAN O. ; SIMON, PHILIPP ; ROHRBACH, ALEXANDER: Microscopy with self-reconstructing beams. In: *Nature Photonics* Bd. 4 (2010), Nr. 11, S. 780–785

[GKGF14] GRILLO, VINCENZO ; KARIMI, EBRAHIM ; GAZZADI, GIAN CARLO ; FRABBONI, STEFANO ; DENNIS, MARK R. ; BOYD, ROBERT W.: Generation of Nondiffracting Electron Bessel Beams. In: *Physical Review X* Bd. 4 (2014), Nr. 1, S. 011013

[GMMS02] GARCÉS-CHÁVEZ, V. ; MCGLOIN, D. ; MELVILLE, H. ; SIBBETT, W. ; DHOLAKIA, K.: Simultaneous micromanipulation in multiple planes using a self-reconstructing light beam. In: *Nature* Bd. 419 (2002), Nr. 6903, S. 145–147

[GMPD03] GARCÉS-CHÁVEZ, V. ; MCGLOIN, D. ; PADGETT, M. J. ; DULTZ, W. ; SCHMITZER, H. ; DHOLAKIA, K.: Observation of the Transfer of the Local Angular Momentum Density of a Multiringed Light Beam to an Optically Trapped Particle. In: *Physical Review Letters* Bd. 91 (2003), Nr. 9, S. 093602

[GuIC00] GUTIÉRREZ-VEGA, J. C. ; ITURBE-CASTILLO, M. D. ; CHÁVEZ-CERDA, S.: Alternative formulation for invariant optical fields: Mathieu beams. In: *Optics Letters* Bd. 25 (2000), Nr. 20, S. 1493–1495. — 00248

[HeHR95] HE, H. ; HECKENBERG, N.R. ; RUBINSZTEIN-DUNLOP, H.: Optical Particle Trapping with Higher-order Doughnut Beams Produced Using High Efficiency Computer Generated Holograms. In: *Journal of Modern Optics* Bd. 42 (1995), Nr. 1, S. 217–223. — 00294

[HeWi91] HERMAN, R. M. ; WIGGINS, T. A.: Production and uses of diffractionless beams. In: *Journal of the Optical Society of America A* Bd. 8 (1991), Nr. 6, S. 932–942. — 00448

[HsMT89] HSU, D. K. ; MARGETAN, F. J. ; THOMPSON, D. O.: Bessel beam ultrasonic transducer: Fabrication method and experimental results. In: *Applied Physics Letters* Bd. 55 (1989), Nr. 20, S. 2066–2068. — 00110

[IfAK93] IFTEKHARUDDIN, KHAN M. ; AWWAL, ABDUL A. S. ; KARIM, MOHAMMAD A.: Gaussian-to-Bessel beam transformation using a

split refracting system. In: *Applied Optics* Bd. 32 (1993), Nr. 13, S. 2252–2256. — 00000

[Inde89] INDEBETOUW, G.: Nondiffracting optical fields: some remarks on their analysis and synthesis. In: *Journal of the Optical Society of America A* Bd. 6 (1989), Nr. 1, S. 150–152. — 00269

[Jarl00] J. ARLT, K. DHOLAKIA: Generation of high-order Bessel beams by use of an axicon. In: *Optics Communications* (2000), S. 297–301. — 00377

[JoHa94] JORDAN, REBECCA H. ; HALL, DENNIS G.: Free-space azimuthal paraxial wave equation: the azimuthal Bessel?Gauss beam solution. In: *Optics Letters* Bd. 19 (1994), Nr. 7, S. 427–429

[KhKR01] KHILO, ANATOL N. ; KATRANJI, EUGENY G. ; RYZHEVICH, ANATOL A.: Axicon-based Bessel resonator: analytical description and experiment. In: *Journal of the Optical Society of America A* Bd. 18 (2001), Nr. 8, S. 1986–1992. — 00066

[LuGr92a] LU, J.-Y. ; GREENLEAF, J.F.: Nondiffracting X waves-exact solutions to free-space scalar wave equation and their finite aperture realizations. In: *IEEE Transactions on Ultrasonics, Ferroelectrics and Frequency Control* Bd. 39 (1992), Nr. 1, S. 19–31

[LuGr92b] LU, J.-Y. ; GREENLEAF, J.F.: Experimental verification of nondiffracting X waves. In: *IEEE Transactions on Ultrasonics, Ferroelectrics and Frequency Control* Bd. 39 (1992), Nr. 3, S. 441–446

[Mcle54] MCLEOD, JOHN H.: The Axicon: A New Type of Optical Element. In: *Journal of the Optical Society of America* Bd. 44 (1954), Nr. 8, S. 592–592. — 00703

[MuVa02] MUYS, PETER ; VANDAMME, EEFJE: Direct Generation of Bessel Beams. In: *Applied Optics* Bd. 41 (2002), Nr. 30, S. 6375–6379. — 00032

[NBKH04] NIV, AVI ; BIENER, GABRIEL ; KLEINER, VLADIMIR ; HASMAN, EREZ: Propagation-invariant vectorial Bessel beams obtained by use of quantized Pancharatnam-Berry phase optical elements. In: *Optics Letters* Bd. 29 (2004), Nr. 3, S. 238–240

[NiMa97] NIGGL, L. ; MAIER, MAX: Efficient conical emission of stimulated Raman Stokes light generated by a Bessel pump beam. In: *Optics Letters* Bd. 22 (1997), Nr. 12, S. 910–912. — 00044

[OkIK01] OKAMOTO, KENJI ; INOUYE, YASUSHI ; KAWATA, SATOSHI: Use of Bessel J1 Laser Beam to Focus an Atomic Beam into a Nano-scale Dot. In: *Japanese Journal of Applied Physics* Bd. 40 (2001), Nr. 7R, S. 4544

[PhVi10] PHILIP, GEO M. ; VISWANATHAN, NIRMAL K.: Generation of tunable chain of three-dimensional optical bottle beams via focused multi-ring hollow Gaussian beam. In: *Journal of the Optical Society of America A* Bd. 27 (2010), Nr. 11, S. 2394–2401. — 00009

[ReSa02] REIVELT, KAIDO ; SAARI, PEETER: Experimental demonstration of realizability of optical focus wave modes. In: *Physical Review E* Bd. 66 (2002), Nr. 5, S. 056611. — 00049

[RoKi90] ROMEA, RICHARD D. ; KIMURA, WAYNE D.: Modeling of inverse Čerenkov laser acceleration with axicon laser-beam focusing. In: *Physical Review D* Bd. 42 (1990), Nr. 5, S. 1807–1818

[ScMc92] SCOTT, GRAEME ; MCARDLE, NEIL: Efficient generation of nearly diffraction-free beams using an axicon. In: *Optical Engineering* Bd. 31 (1992), Nr. 12, S. 2640–2643. — 00148

[TuFr10] TURUNEN, JARI ; FRIBERG, ARI T.: Chapter 1 - Propagation-Invariant Optical Fields. In: EMIL WOLF (Hrsg.): *Progress in Optics*. Bd. Volume 54 : Elsevier, 2010. — 00000 — ISBN 0079-6638, S. 1–88

[TuVF88] TURUNEN, JARI ; VASARA, ANTTI ; FRIBERG, ARI T.: Holographic generation of diffraction-free beams. In: *Applied Optics* Bd. 27 (1988), Nr. 19, S. 3959–3962. — 00284

[UeKi89] UEHARA, K. ; KIKUCHI, H.: Generation of nearly diffraction-free laser beams. In: *Applied Physics B* Bd. 48 (1989), Nr. 2, S. 125–129. — 00084

[VaTF89] VASARA, ANTTI ; TURUNEN, JARI ; FRIBERG, ARI T.: Realization of general nondiffracting beams with computer-generated holograms. In: *Journal of the Optical Society of America A* Bd. 6 (1989), Nr. 11, S. 1748–1754

[VyKS14] VYAS, SUNIL ; KOZAWA, YUICHI ; SATO, SHUNICHI: Generation of radially polarized Bessel–Gaussian beams from c-cut Nd:YVO4 laser. In: *Optics Letters* Bd. 39 (2014), Nr. 4, S. 1101–1104

[WRWJ06] WILLIG, KATRIN I ; RIZZOLI, SILVIO O ; WESTPHAL, VOLKER ; JAHN, REINHARD ; HELL, STEFAN W: STED microscopy reveals that synaptotagmin remains clustered after synaptic vesicle exocytosis. In: *Nature* Bd. 440 (2006), Nr. 7086, S. 935–939. — PMID: 16612384

CHAPTER

2

Diffraction Theory for Axicon Focusing

Contents

2.1 Introduction

Axicon is a cylindrically symmetrical optical element introduced and characterized by McLeod in 1954[Mcle54]. Axicon produces a line focus rather than a point focus by a conventional spherical lens. The ability of the axicon to convert a Gaussian beam to a propagation-invariant Bessel beam[HeWi91] is well appreciated and used in multitude of applications. Though there are alternate methods such as wave-front coding[DoCa95], annular illumination [BoJW06] and adaptive optics techniques [SKMY12] available to extend the non-diverging region, the axicon lens[DPKM06] based method is one of the simplest one. The optical element axicon has been used in different areas ranging from alignment in telescope, atom guiding and trapping[MaOG98], laser machining[BéRi78] and Bose-Einstein condensates[WrAD00]. Axicon is also used for the characterization of complex light beams[HaZh11]. Micro-axicons are used to design compact imaging systems[WSSZ12], in bio-photonics[CKTG08], and compact optical tweezers for micro manipulation[KCKS14, Scab06]. All the above mentioned applications make use of the propagation-invariant Bessel-Gauss beam generated by the axicon. A complete understanding of the imaging and focusing properties of the axicon is necessary to understand the beam properties and also to design newer techniques using axicon. There has been different approaches to study the focusing and Bessel-Gauss beam formation of axicon in scientific literature including scalar Fresnel diffraction integrals[ArDh00, HeWi91, VaTF89], spatial spectrum method[JaPS00] and interference based method[LeYa04].

All the above mentioned approaches to explain the formation of Bessel-Gauss beam by an axicon are restricted to scalar beams with simple plane phase structures only, and all these methods are useful only when the focusing is in the paraxial regime. Since the focusing properties, especially in the non-paraxial regime depend on the polarization and phase structure rather than amplitude alone, a vector treatment is needed for the full understanding of axicon imaging, similar to that of high numerical aperture(NA) lenses[YoBr00, ZhLe02]. The vector theory is more relevant when dealing with the focusing of beams with spatially changing polarization.

This chapter starts with the scalar diffraction formalism and then extend it to vector diffraction theory to accommodate the polarization and non-paraxial

focusing effects. The complex focal field structures are also explained using the vector theory for axicon focusing. Also, a new method of using axicon is proposed for the generation of optical needle beams.

2.2 Scalar Diffraction through Axicon

Axicon converts a Gaussian beam to a propagation invariant J0 Bessel-Gauss(BG) beam. This transformation can be mathematically understood on the basis of scalar diffraction integrals[ArDh00, HeWi91, VaTF89]. The axicon focusing system schematic is shown in Fig.2.1 where the incident beam is a plane wave Gaussian beam and which is converted to a J_0 Bessel-Gauss beam. The propagation-invariant Bessel-Gauss beams are formed only in the range known as *non-diffracting range*. The non-diffracting range depends inversely on the small angle of the focusing axicon and the directly on the waist of the input beam.

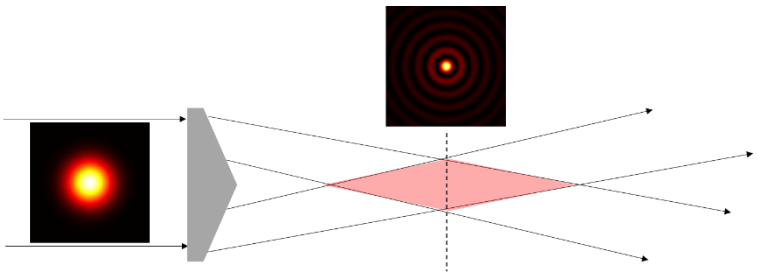

Fig. 2.1 Schematic of axicon focusing of Gaussian beam and generation of J_0 Bessel-Gauss beam

To obtain the general formalism for the formation of Bessel-Gauss beams by an axicon let us consider the input beam to be a Laguerre Gauss (LG) beam with electric field distribution given by [ArDh00]:

$$A(\rho_0, \varphi) = (\rho_0^2/\omega_0^2)^{\frac{|l|}{2}} L_p^{|l|}((2\,\rho_0^2/\omega_0^2) exp(-\rho_0^2/\omega_0^2)\, exp(il\varphi) \qquad (2.1)$$

where $L_p^{|l|}$ is the generalized Laguerre polynomial with l=0 correspond to Gaussian beam and l≥1 corresponds to higher-order LG beams. Substituting the electric field equation in the diffraction integral gives

$$E(\rho, \beta, z)$$

$$= \frac{-izexp(ikr)}{\lambda r^2} \int_0^\infty \rho_0 (\rho_0^2/\omega_0^2)^{\frac{|l|}{2}} L_p^{|l|}(2\,\rho_0^2/\omega_0^2)\, exp(-\rho_0^2/\omega_0^2)\, exp(ik\rho_0^2/2r)$$

$$exp(ik\vartheta\rho_0)\, d\rho_0 \int_0^{2\pi} exp(il\varphi)\, exp\left[\frac{-ik\rho\rho_0\, cos(\varphi-\beta)}{r}\right] d\varphi \qquad (2.2)$$

Where $exp(ik\vartheta\rho_0)$ is the axicon phase function defined as $\vartheta = (n-1)tan\alpha$ (with 'n' the refractive index of the axicon material and 'α' the axicon open angle).Simplifying Equation(2.2) using stationary phase approximation the intensity at a point (ρ, z) can be written as[ArDh00].

$$I(\rho, z) = z^{2l+1}\, exp(2z^2/z_{max}^2) J_l^2(k_\rho \rho) \qquad (2.3)$$

where $z_{max} = {\omega_0 k}/{k_\rho}$ is the range of the beam.

2.2.1 Formation characteristics of Bessel-Gauss beams

The Bessel-Gauss beam is experimentally generated by focusing a He-Ne laser beam (λ=632.8nm) by an axicon of small angle 0.5°. The characteristics of the generated J_0 Bessel-Gauss beam is studied by imaging the beam along the z direction at very close intervals using a CCD camera. Fig.2.2 shows the CCD images of the Bessel-Gauss beam with the theoretical fit to the line profile in the x direction.

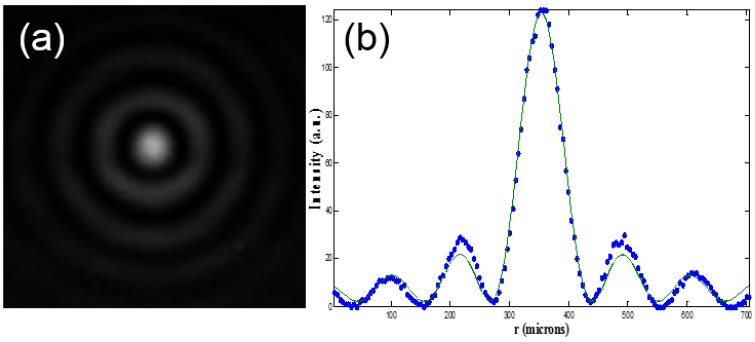

Fig. 2.2 (a) CCD image of the BG beam measured at z=70 cm from the axicon ;(b) line profile with Bessel fitting.

The propagation characteristics of the BG beam is characterized by stitching the CCD images measured at different z-positions to generate the beam propagation. The width of the centre spot is also measured at different propagation distances. Also the propagation-invariant range is experimentally measured from the

propagation characteristics of the beam. Fig.2.3 gives the beam propagation generated from the CCD images and the width of the centre maximum with propagation distance (measured from the axicon).

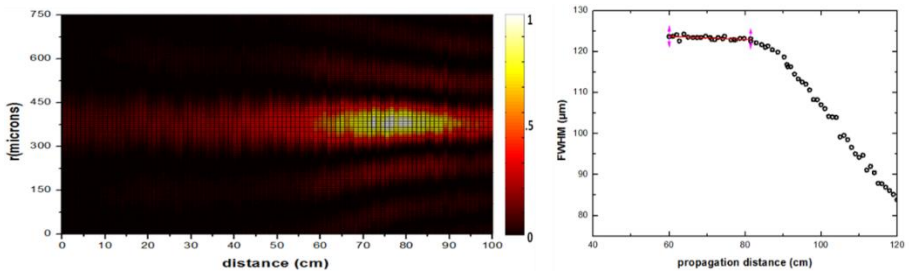

Fig. 2.3(a) Propagation of the J0 BG beam ;(b) width of the centre maximum with propagation distance

The width of the centre maximum is 123.8μm at z=60cm and remains almost the same up to z=83cm. So the non-diffracting range of the axicon system is experimentally measured to be 23cm.

According the to Equation(2.3) higher order BG beams can be generated by focusing higher order LG beams by axicon. We generated higher order LG beams using a spiral phase plate and these beams are subsequently focused by the axicon to generate corresponding higher order BG beams. Fig.2.4 shows the higher order BG beams generated using the axicon of small angle $\alpha=0.5^{o}$.

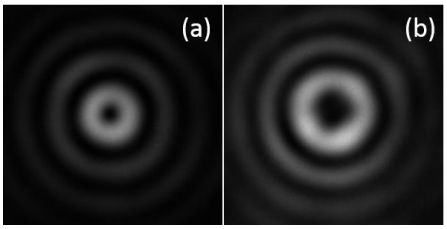

Fig. 2.4 (a) J1 and (b) J2 BG beams imaged at Z=Zmax/2

2.3 Vector Diffraction theory

Focusing properties of optical beams also depends on the polarization and phase and amplitude distribution of the input beam especially when the numerical aperture of the focusing element is high[ChHP12]. Due to this the diffraction integral given in Equation (2.2) should be modified to accommodate the

polarization also into consideration, to obtain the accurate electric filed distributions after the optical element. Tight focusing of optical beams become all the more interesting when the beams have spatially varying polarization structure coupled with non-plane phase profile. The focusing characteristics of these optical vector beams strongly depend on the state of polarization, especially in the non-paraxial regime, corresponding to high NA focusing which can result in unusual electric field distribution in the focal region[Zhan09].

Vector diffraction theory is particularly useful in the study of focusing of optical vector beams where the polarization state is spatially varying. In addition, the spatially varying polarization state vector beams can also possess helical wave-front making it a vector –vortex (VV) beam. Tight focusing of the VV beam can generate small spot sizes[YXWZ13] and transversely polarized propagation-invariant beams[YuWY11] also phase encoded vector beams can produce optical needle beams upon high NA focusing[WSLS08]. Vector beams are also known to possess V-singularity in the beam cross section where the orientation of the linear polarization is not defined[Freu02]. Superposition of orthogonal circularly polarized plane wave and helical wave-front beams can lead to the formation of C and L singularities (details see Appendix II) where the orientation of the major axis and ellipticity of the polarization ellipse respectively are not defined[Freu02, Freu02][FODP08, Freu02]. Though it is already shown that high-NA focusing of azimuthally[ZLLJ13] and radially[ScVi06] polarized beams lead to the generation of polarization singular (PS) beams, experimental realization of the PS patterns are difficult since the focal region in high NA focus is very small (few multiples of λ). Vector theory for the axicon shows that the extended line focus produced by the axicon enables one to experimentally measure the complex polarization singular patterns in the focal region[Phil14].

The mathematical formalism based on vectorial Rayleigh diffraction integrals is developed to study the focusing characteristics of VV beam by the axicon. Rayleigh diffraction integrals relate the electric field components at a point to the field distribution at the exit pupil. So the electric field components can be written using the Rayleigh diffraction integral in cylindrical coordinate system as[Lune64, ZhWZ05, ZhZZ06]

$$E_x(\rho,\beta,z) = \frac{-izexp(ikr)}{\lambda r^2}\int_0^{\infty} d\rho_0 \int_0^{2\pi} d\varphi\, E_x(r_0) ex\, p(ik\rho_0^2/2r)$$

$$exp\left[\frac{-ik\rho\rho_0\, cos(\varphi-\beta)}{r}\right]\rho_0 \qquad (2.4a)$$

$$E_y(\rho,\beta,z) = \frac{-izexp(ikr)}{\lambda r^2}\int_0^{\infty} d\rho_0 \int_0^{2\pi} d\varphi\, E_y(r_0) ex\, p(ik\rho_0^2/2r)$$

$$exp\left[\frac{-ik\rho\rho_0\, cos(\varphi-\beta)}{r}\right]\rho_0 \qquad (2.4b)$$

$$E_z(\rho,\beta,z) = \frac{-iexp(ikr)}{\lambda r^2}\int_0^{\infty} d\rho_0 \int_0^{2\pi} d\varphi\, [E_x(r_0)(\rho.cos\,\beta - \rho_0.cos\,\varphi)$$

$$+ E_y(r_0)(\rho.sin\,\beta - \rho_0.sin\,\varphi)$$

$$exp(ik\rho_0^2/2r)\, exp\left[\frac{-ik\rho\rho_0\, cos(\varphi-\beta)}{r}\right]\rho_0 \qquad (2.4c)$$

Where, (ρ,β,z) are the cylindrical coordinates at the observation point and (ρ_0,ϕ) are the polar coordinates of the plane immediately after the axicon. Taking into consideration the polarization aspects, the electric field of the input beam to the axicon can be written as

$$E(r_0) = \begin{bmatrix} E_x(r_0) \\ E_y(r_0) \\ E_z(r_0) \end{bmatrix} = P(\theta,\varphi)\, A(\rho_0,\varphi) \qquad (2.5)$$

Where $P(\theta,\varphi)$ is the polarization matrix[KhKV11] and $A(\rho_0,\varphi)$ is the amplitude and phase distribution of electric field after the axicon. In this work we consider paraxial, or purely transverse electric field distributions as input to the axicon. Then the polarization matrix can then be rewritten as[KhKV11]:

$$P(\theta,\varphi) = \begin{bmatrix} a(\theta,\varphi)(cos\theta cos^2\varphi + sin^2\varphi) + b(\theta,\varphi)(cos\theta - 1)sin\varphi cos\varphi \\ a(\theta,\varphi)(cos\theta - 1)sin\varphi cos\varphi + b(\theta,\varphi)(cos\theta sin^2\varphi + cos^2\varphi) \\ -a(\theta,\varphi)sin\theta cos\varphi - sin\theta sin\varphi \end{bmatrix}$$

$$P(\theta,\varphi)=\begin{bmatrix}P_x(\theta,\varphi)\\P_y(\theta,\varphi)\\P_z(\theta,\varphi)\end{bmatrix} \tag{2.6}$$

Where $a(\theta,\varphi)$, $b(\theta,\varphi)$ are the polarization functions for '*x*', '*y*' and '*z*' components of the incident beam. In the case of commonly used TM and TE polarized cylindrical vector beam modes these functions have a simpler form independent of θ [22].

The amplitude and phase distribution $A(\rho_0,\varphi)$ of the LG beam is[ArDh00]

$$A(\rho_0,\varphi)=(\rho_0^2/\omega_0^2)^{\frac{|l|}{2}}L_p^{|l|}((2\,\rho_0^2/\omega_0^2)exp(-\rho_0^2/\omega_0^2)\,exp(il\varphi)\,exp(ik\vartheta\rho_0) \tag{2.7}$$

Where $L_p^{|l|}$ is the generalized Laguerre polynomial and $exp(ik\vartheta\rho_0)$ is the axicon phase function defined as $\vartheta=(n-1)tan\alpha$ (with 'n' the refractive index of the axicon material and 'α' the axicon open angle). Using this the electric field distribution at any point after the axicon when a generalized vector-vortex beam is focused by the axicon is written by substituting Equs.(2.5),(2.6) and (2.7) in Equation(2.4). The electric field components any point (ρ,β,z) is written as

$$E_x(\rho,\beta,z)=\frac{-izexp(ikr)}{\lambda r^2}\int_0^{\infty}d\rho_0\int_0^{2\pi}d\varphi\,P_x(\theta,\varphi)(\rho_0^2/\omega_0^2)^{\frac{|l|}{2}}L_p^{|l|}(2\,\rho_0^2/\omega_0^2)$$
$$exp(-\rho_0^2/\omega_0^2+il\varphi-ik\vartheta\rho_0+ik\rho_0^2/2r)$$
$$exp[i\eta\,cos(\varphi-\beta)]\,\rho_0 \tag{2.8a}$$

$$E_y(\rho,\beta,z)=\frac{-izexp(ikr)}{\lambda r^2}\int_0^{\infty}d\rho_0\int_0^{2\pi}d\varphi\,P_y(\theta,\varphi)(\rho_0^2/\omega_0^2)^{\frac{|l|}{2}}L_p^{|l|}(2\,\rho_0^2/\omega_0^2)$$
$$exp(-\rho_0^2/\omega_0^2+il\varphi-ik\vartheta\rho_0+ik\rho_0^2/2r)$$
$$exp[i\eta\,cos(\varphi-\beta)]\,\rho_0 \tag{2.8b}$$

$$E_z(\rho,\beta,z) = \frac{-iexp(ikr)}{\lambda r^2}\int_0^{\infty} d\rho_0 \int_0^{2\pi} d\varphi \left[P_x(\theta,\varphi)(\rho.cos\,\beta - \rho_0.cos\,\varphi)\right.$$

$$\left. + P_y(\theta,\varphi)(\rho sin\beta - \rho_0 sin\varphi)\right](\rho_0^2/\omega_0^2)^{\frac{|l|}{2}} L_p^{|l|}(2\,\rho_0^2/\omega_0^2)$$

$$exp(-\rho_0^2/\omega_0^2 + il\varphi - ik\vartheta\rho_0 + ik\rho_0^2/2r)$$

$$exp[i\eta\, cos(\varphi-\beta)]\,\rho_0 \qquad (2.8c)$$

where $\eta = {}^{-k\rho\rho_0}/_{r}$.

2.4 Focusing of vector beams using axicon

In a vector beam the state of polarization in linear everywhere but the direction of the electric field vector varies with azimuthal angle. The polarization state of the generalized vector beam can be written as

$$\begin{bmatrix} a(\theta,\varphi) \\ b(\theta,\varphi) \\ 0 \end{bmatrix} = \begin{bmatrix} cos(m\varphi+\delta) \\ sin(m\varphi+\delta) \\ 0 \end{bmatrix} \qquad (2.9)$$

Where '*m*' denotes the order of the vector beam and 'δ' is the constant angle the polarization vector makes with radial direction. δ =0° and *m*=1, in for radial polarization and δ =90° with m=1 implies azimuthal polarization. Substituting Equation(2.9) in Equation(2.6) the polarization matrix corresponding to a generalized vector beam becomes

$$P(\theta,\varphi)$$

$$= \begin{bmatrix} cos(m\varphi+\delta)(cos\theta cos^2\varphi + sin^2\varphi) + sin(m\varphi+\delta)(cos\theta-1)sin\varphi cos\varphi \\ cos(m\varphi+\delta)(cos\theta-1)sin\varphi cos\varphi + sin(m\varphi+\delta)(cos\theta sin^2\varphi + cos^2\varphi) \\ -cos(m\varphi+\delta)sin\theta cos\varphi - sin\theta sin\varphi \end{bmatrix} (2.10)$$

Substituting this polarization matrix in Equation(2.8) one can find the electric field distribution in the focal plane when a vector-vortex beam is focused by an axicon:

$$E_x(\rho,\beta,z)=\frac{-izexp(ikr)}{\lambda r^2}\int_0^{\infty}d\rho_0\int_0^{2\pi}d\varphi\,[cos(m\varphi+\delta)(cos\theta cos^2\varphi+sin^2\varphi)$$
$$+sin(m\varphi\quad+\delta)(cos\theta-1)sin\varphi cos\varphi](\rho_0^2/\omega_0^2)^{\frac{|l|}{2}}L_p^{|l|}(2\,\rho_0^2/\omega_0^2)$$
$$exp(-\rho_0^2/\omega_0^2-ik\vartheta\rho_0$$
$$+ik\rho_0^2/2r)\,exp[i\eta\,cos(\varphi-\beta)]\,\rho_0 \qquad (2.11a)$$

$$E_y(\rho,\beta,z)=\frac{-izexp(ikr)}{\lambda r^2}\int_0^{\infty}d\rho_0\int_0^{2\pi}d\varphi\,[cos(m\varphi+\delta)\,(cos\theta$$
$$-1)sin\varphi cos\varphi$$
$$+sin(m\varphi+\delta)\,(cos\theta sin^2\varphi+cos^2\varphi)](\rho_0^2/\omega_0^2)^{\frac{|l|}{2}}L_p^{|l|}(2\,\rho_0^2/\omega_0^2)$$
$$exp(-\rho_0^2/\omega_0^2-ik\vartheta\rho_0$$
$$+ik\rho_0^2/2r)\,exp[i\eta\,cos(\varphi-\beta)]\,\rho_0 \qquad (2.11b)$$

$$E_z(\rho,\beta,z)=\frac{-iexp(ikr)}{\lambda r^2}\int_0^{\infty}d\rho_0\int_0^{2\pi}d\varphi\,\big[[cos(m\varphi+\delta)\,(cos\theta cos^2\varphi+sin^2\varphi)$$
$$+sin(m\varphi+\delta)\,(cos\theta-1)sin\varphi cos\varphi](\rho.cos\,\beta-\rho_0.cos\,\varphi)$$
$$+[cos(m\varphi+\delta)\,(cos\theta-1)sin\varphi cos\varphi$$
$$+sin(m\varphi+\delta)\,(cos\theta sin^2\varphi+cos^2\varphi)](\rho sin\beta-\rho_0 sin\varphi)\big]$$
$$(\rho_0^2/\omega_0^2)^{\frac{|l|}{2}}L_p^{|l|}(2\,\rho_0^2/\omega_0^2)\,exp(-\rho_0^2/\omega_0^2-ik\vartheta\rho_0$$
$$+ik\rho_0^2/2r)\,exp[i\eta\,cos(\varphi-\beta)]\,\rho_0 \qquad (2.11c)$$

The electric filed of a generalized vector beam can be written as Equation2.12 as a superposition of orthogonal circularly polarized beams of oppositely helical charge beams.

$$E=\left(\begin{bmatrix}1\\-i\end{bmatrix}exp(im\varphi)+exp(i\varepsilon)\begin{bmatrix}1\\i\end{bmatrix}exp(-im\varphi)\right)ex\,p(-\rho_0^2/\omega_0^2) \quad (2.12)$$

where $\varepsilon=2\delta$

For the experimental verification of the focusing of vector beams by an axicon a Sagnac interferometer setup with a spiral phase plate is used as shown in Fig.2.5. Light beam from the He-Ne laser is made linearly polarized by polarizer (P1) and then the axis of polarization is changed to 45° with respect to vertical by half wave plate(HWP1) so that the polarization beam splitter (PBS) makes counter propagating orthogonal linearly polarized beams with equal intensity in the Sagnac

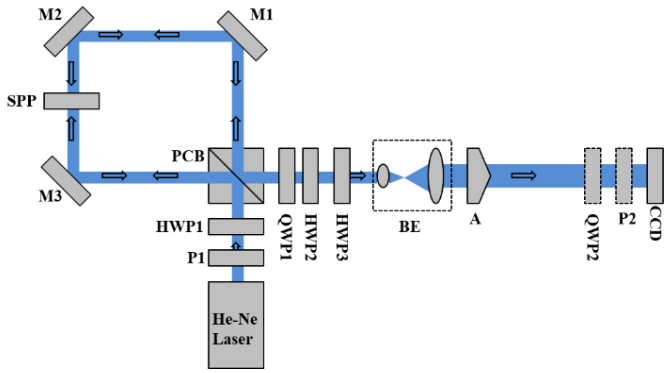

Fig. 2.5 Schematic of the experimental setup for the generation of optical vector beams.

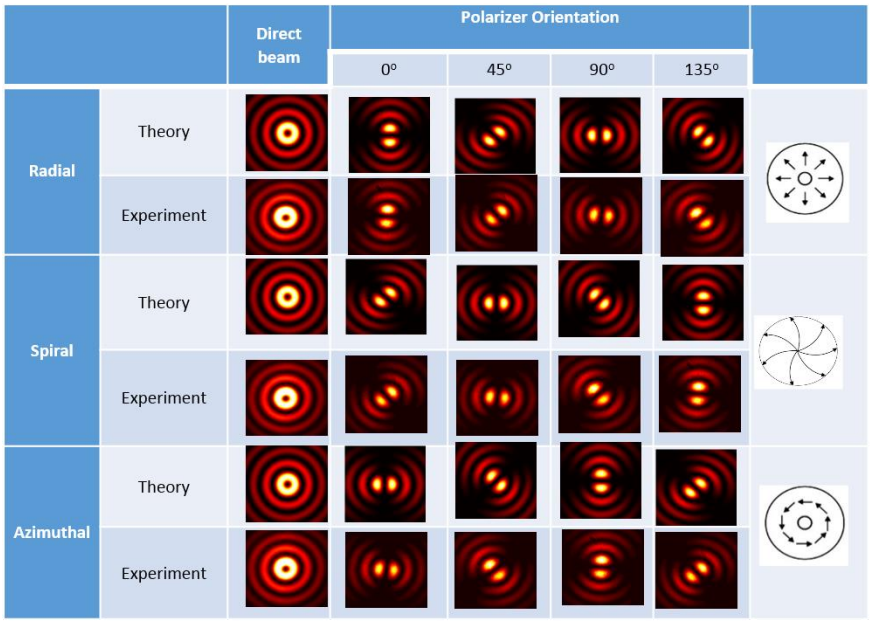

Fig. 2.6 Theoretical and experimental intensity distributions of vector BG beams generated by focusing vector beam using an axicon at z=zmax/2

interferometer. Since the beams in the interferometer are counter propagating the spiral phase plate (SPP) in the interferometer gives opposite helical charges to the beams. The quarter wave plate (QWP1) at 45° in the output of the interferometer makes the superposing beams orthogonal circular. A two HWP combination is used to rotate the polarization state to generate desired vector beam. A 3x beam expander is used to expand the beam and which is then focused by an axicon of open angle α=0.5°. The axicon focused beam is imaged using a CCD camera. Fig.2.6 shows the experimental and theoretical intensity distributions of the different vector BG beams generated by focusing of vector beams by an axicon.

2.5 Focusing of vector-vortex beams using axicon

The non-paraxial focusing of the complex vector-vortex beams are particularly interesting because of its ability to generate small spot sizes of the order of sub-wavelengths. But the reduction of the spot size happens at the cost of depth-of-focus (DOF). Some specific measurements such as polarization sensitive orientation imaging[AbTo06, NBYB01], and light-matter interaction in the nano-scale[BPQL10] need small spot size and long DOF at the same time. Though there are methods to produce optical needle beams all of them involve either

complex phase or amplitude modulation[SMRP13, WaCZ10, WSLS08, ZWWG13]. But the vector theory for axicon focusing of vector–vortex beam shows that it can directly generate different types of optical needle beams[Phil14].

The electric field components in the focal region when a vector-vortex beam is focused by an axicon can be directly calculated by using Equation(5) by substituting the corresponding polarization matrix. The schematic representation of this axicon focusing of vector-vortex beams is given in Fig.2.7

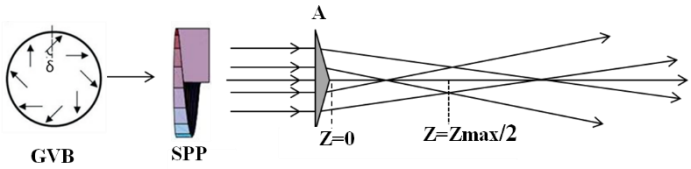

Fig. 2.7 Schematic of the axicon focusing system.

2.5.1 Focusing of azimuthally-polarized vortex beam to generate transversely polarized needle beam

The polarization matrix for azimuthally polarized beam is obtained by substituting $\delta = \pi/2$ in Equ(2.9), and the polarization matrix then becomes

$$P(\theta,\varphi) = \begin{bmatrix} sin(m\varphi) \\ -cos(m\varphi) \\ 0 \end{bmatrix} \tag{2.13}$$

Substituting the polarization matrix elements in Equation (2.8) the field components at any position after the axicon can be written as

$$E_x(\rho,\beta,z) = \frac{-izexp(ikr)}{\lambda r^2}\int_0^R d\rho_0 \left(\rho_0^{|l|+1}/\omega_0^l\right) L_p^{|l|}(2\,\rho_0^2/\omega_0^2)\, exp(-\rho_0^2/\omega_0^2 - ik\vartheta\rho_0 + ik\rho_0^2/2r)\,(\pi(-i)i^{l+m}J_{l+m}(\eta)\, exp[i(l+m)\beta] + \pi(i)i^{l-m}J_{l-m}(\eta)\, exp[i(lm)\beta]) \tag{2.14a}$$

$$E_y(\rho,\beta,z) = \frac{-izexp(ikr)}{\lambda r^2}\int_0^R d\rho_0 \left(\rho_0^{|l|+1}/\omega_0^l\right) L_p^{|l|}(2\,\rho_0^2/\omega_0^2)\, exp(-\rho_0^2/\omega_0^2 - ik\vartheta\rho_0 + ik\rho_0^2/2r)\,(\pi i^{l+m} J_{l+m}(\eta)\, exp[i(l+m)\beta] + \pi i^{l-m} J_{l-m}(\eta)\, exp[i(lm)\beta]) \quad (2.14b)$$

$$E_z(\rho,\beta,z) = \frac{-iexp(ikr)}{\lambda r^2}\int_0^R d\rho_0 \left(\rho_0^{|l|+1}/\omega_0^l\right) L_p^{|l|}(2\,\rho_0^2/\omega_0^2)\, exp(-\rho_0^2/\omega_0^2 - ik\vartheta\rho_0 + ik\rho_0^2/2r)\,(\pi i^{l+m}(-i) J_{l+m}(\eta)\, exp[i(l+m+1)\beta] + \rho\pi i^{l-m} J_{l-m}(\eta)\, exp[i(l+m-1)\beta] \quad (2.14c)$$

First the loose focusing condition is checked by focusing an azimuthally polarized beam of order m=1 and having a helical charge l=1 by an axicon of small angle α=0.5°. The vector-vortex beam generator consists of a He-Ne laser (λ = 632.8 nm) and a 27.4 cm long two-mode optical fiber. The Gaussian beam from the He-Ne laser is passed through a polarizer-half wave plate combination to enable the change of the plane of polarization of the linearly polarized input beam. This linearly polarized beam is coupled skew-off axially into the circular-core step-index two-mode optical fiber (V# = 3.805, length = 27.4 cm) using a 20x, 0.4 NA microscope objective lens mounted on a 3-axis precision fiber launch system. The linear polarization of the input beam and the coupling angle are selected such that the output beam from the two-mode optical fiber is a cylindrical vector beam[ViIn09]. The output beam from the optical fiber is then collimated using a 20x microscopic objective lens. Two cascaded half-wave plates are used after the collimated fiber output to rotate the polarization state of the vector beam[Zhan09, ZhLe02] spatially which then passes through a spiral phase plate (VPP m-633 RPC Photonics, USA) and is subsequently focused by the axicon of open angle α=0.5°. The focused beam is then imaged using a CCD camera along the direction of propagation 'z'. The polarization characteristics of the focused beam are measured via spatially-resolved Stokes polarimetry using a quarter-wave plate and polarizer combination (see Appendix I for details). The generated transverse beam field (longitudinal field E_z=0) is a superposition of orthogonal circularly polarized J_0 and J_2 Bessel functions as can be seen from Equs. (2.14). The beams described by the J_0 and J_2 Bessel functions have

respectively a central maximum intensity and a vortex of topological charge *l*=+2with intensity null at the centre. The on-axis superposition of the two beams with orthogonal circular polarization results in elliptically polarized field, leading to the formation of C-point and L-line in the beam cross-section[FODP08, Freu02] (see Appendix II for details). In the present case the C-point index defined as$I_c = 1/2\pi \oint d\psi = \pm 1$, where 'ψ' is the polarization ellipse orientation, which rotates by 2π around the *C*-point. Fig.2.8 shows the theoretical simulations and the experimentally measured intensity distribution, polarization ellipse map and the ellipse orientation at the centre of the non-diffracting range of $z = z_{max}/2$, where $z_{max} = \omega_0 k/k_\rho$ with $k_\rho = k(n-1)tan\alpha$, and $k = 2\pi/\lambda$ is the wave vector.

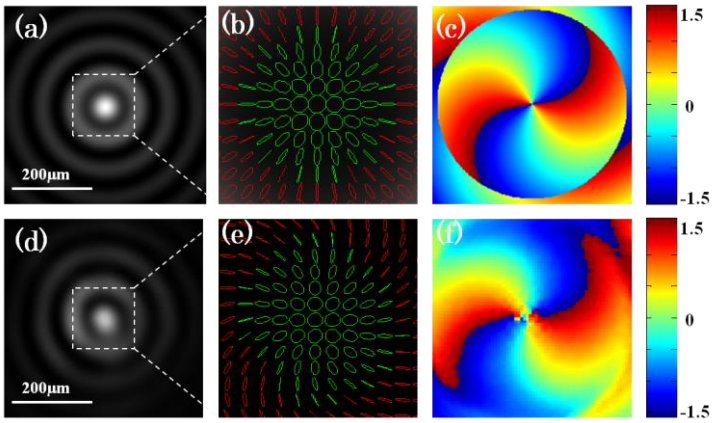

Fig. 2.8 (a)-(c) are respectively the theoretical simulations of intensity distribution, polarization ellipse map and the polarization ellipse orientation (d)- (f) are the corresponding experimental results, all are at Z = Zmax/2.

The polarization ellipse orientation around the *C*-point depends on the phase difference between the constituent superposing J_0 and J_2 beams. The radial type variation in the polarization ellipse orientation around the *C*-point in Fig. 2.8 is due to the Gouy phase difference between the constituent beams[PKMV12] (discussed in detail in Chapter 3).

After experimentally verifying the focused field structure with the one predicted by the theoretical formalism the field calculation is extended to high NA focusing of azimuthally polarized vortex beams. The high NA axicon focusing is studied theoretically by considering an azimuthally polarized vortex beam having *m*=1

and l=1 of λ=632.8nm and beam waist ω_0=5mm focused by an axicon of small angle α=70°. The electric field distribution and the propagation of the beam in the propagation-invariant region is simulated using Equation(2.11) and the results are shown in Fig.2.9. The spot size at the centre of the propagation invariant range is calculated to be 0.43λ and it propagates without divergence up to a distance of 80λ making it transversely polarized optical needle beam. Since the input beam is azimuthally polarized the focused field is free from longitudinal component of electric field. The axicon focusing of azimuthally-polarized vortex beam is an efficient way to generate transversely polarized optical needle beam. It is also important to note that the axial intensity also remains constant in the non-diverging region.

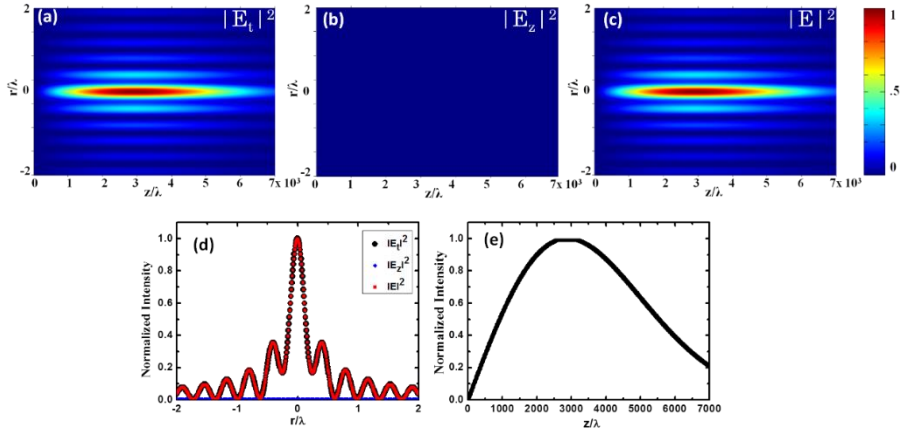

Fig. 2.9 (a),(b) and (c) are respectively the transverse, longitudinal components and the total intensity with propagation; (d) shows the line profile of the intensity distribution of (c) at Z=Zmax/2; and (e) shows the axial intensity with propagation.

2.5.2 Focusing radially-polarized vortex beam to generate longitudinally polarized needle beam

The polarization matrix for radial polarization is obtained by substituting $\delta = 0$ in Equation (2.9) for which the polarization matrix is written as

$$P(\theta, \varphi) = \begin{bmatrix} cos\theta\ cos(m\varphi) \\ cos\theta\ sin(m\varphi) \\ sin\theta \end{bmatrix} \tag{2.15}$$

The electric field components after the axicon at any position along the propagation direction 'z' is obtained by substituting the polarization elements in Equation(2.8) and we get

$$E_x(\rho,\beta,z) = \frac{-izexp(ikr)cos\theta\,\pi}{\lambda r^2}\int_0^R d\rho_0 \left(\rho_0^{|l|+1}/\omega_0^l\right) L_p^{|l|}(2\,\rho_0^2/\omega_0^2)\, exp(-\rho_0^2/\omega_0^2 - ik\vartheta\rho_0 + ik\rho_0^2/2r)\,(\pi i^{l+m} J_{l+m}(\eta)\, exp[i(l+m)\beta] + \pi i^{l-m} J_{l-m}(\eta)\, exp[i(lm)\beta]) \quad (2.16a)$$

$$E_y(\rho,\beta,z) = \frac{-izexp(ikr)cos\theta\,\pi}{\lambda r^2}\int_0^R d\rho_0 \left(\rho_0^{|l|+1}/\omega_0^l\right) L_p^{|l|}(2\,\rho_0^2/\omega_0^2)\, exp(-\rho_0^2/\omega_0^2 - ik\vartheta\rho_0 + ik\rho_0^2/2r)\,(\pi i^{l+m}(-i) J_{l+m}(\eta)\, exp[i(l+m)\beta] + \pi(i) i^{l-m} J_{l-m}(\eta)\, exp[i(lm)\beta]) \quad (2.16b)$$

$$E_z(\rho,\beta,z) = \frac{-iexp(ikr)cos\theta exp(il\beta)}{\lambda r^2}\int_0^R d\rho_0 \left(\rho_0^{|l|+1}/\omega_0^l\right) L_p^{|l|}(2\,\rho_0^2/\omega_0^2)\, exp(-\rho_0^2/\omega_0^2 - ik\vartheta\rho_0 + ik\rho_0^2/2r)\left(i^{l+m} J_{l+m}(\eta) + \pi i^{l-m} J_{l-m}(\eta) - \rho_0 2\pi i^l J_l(\eta)\right) \quad (2.16c)$$

As before the loose focusing is verified first by adjusting the output from vector beam generator to radial polarized beam and keeping spiral phase plate to give a helical charge of 1 and the focusing the beam using the axicon of small angle α=0.5°. The beam is imaged using the CCD camera and the spatially resolved stokes parameters are calculated. Fig.2.10 shows the theoretical simulation and experimentally measured intensity distribution, polarization ellipse map and its orientation in the middle of the non-diverging region ($Z=Z_{max}/2$).

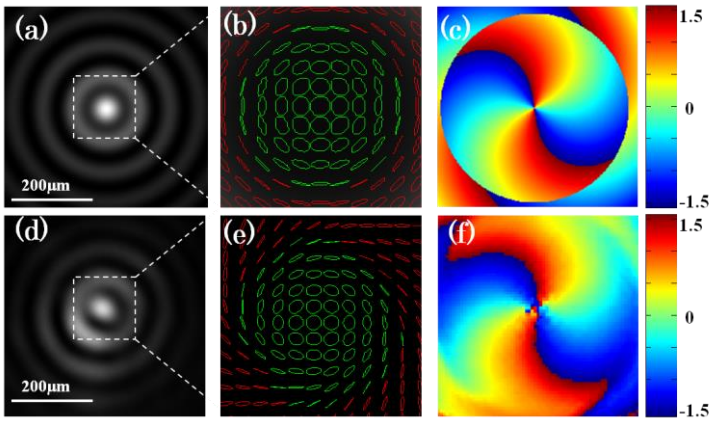

Fig. 2.10(a)-(c) are respectively the theoretical simulations of intensity distribution, polarization ellipse map and the polarization ellipse orientation. (d)-(f) are the corresponding experimental results, all are at Z = Zmax/2

The formalism is then extended to high NA focusing after verifying the paraxial case results. To generate longitudinally polarized optical needle beam a radially polarized vortex beam is focused using a high NA axicon. The electric field components are calculated from Equation (2.16). If we choose an axicon with an open angle of $\alpha=70^{o}$ the resulting longitudinally polarized central bright spot intensity is much more than the transverse component. For radially polarized vortex beam, with $l=0$ and beam width of 5mm input to the axicon Fig.2.11 shows the theoretically simulated results. From Fig.2.11 it is clear that radially polarized vortex beam focused by an axicon of small angle 70o can generate longitudinally polarized needle beam of spot size 0.44λ with a range of 80λ.

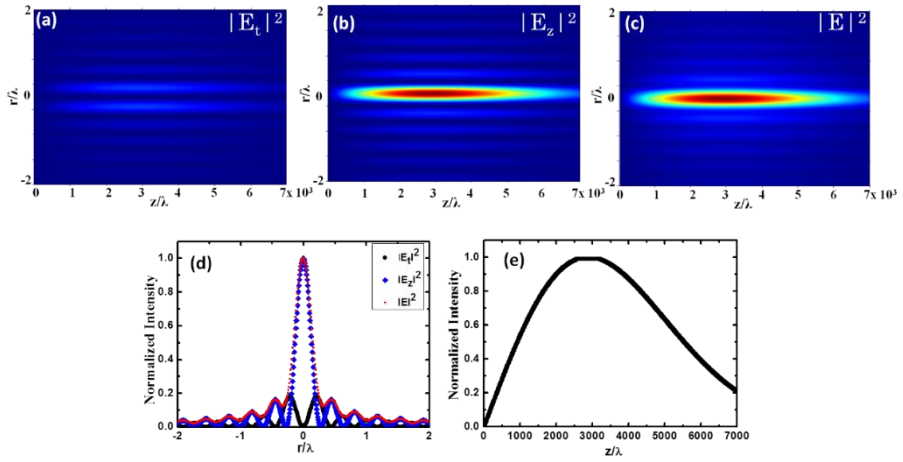

Fig. 2.11 (a), (b) and (c) respectively are the transverse and longitudinal components and total intensity distribution with propagation; (d) shows the line profiles of the intensity distribution of (a) – (c) at Z=Zmax/2; (e) shows the axial intensity with propagation

Summary

The scalar diffraction theory for axicon focusing and formation of BG beam in the paraxial regime is discussed. The vector diffraction theory to study the focusing characteristics of vector-vortex beam is developed using Rayleigh diffraction integrals. Using the vector diffraction theory the formation of vector BG beams is understood. The theoretically predicted vector BG beams are experimentally generated by focusing of vector beam using an axicon. The derived vector diffraction theory formalism is also extended to vector-vortex beam focusing and is used to explain the field structure in the focal region. The formation of higher order C-point is studied both theoretically and experimentally when a vector-vortex beam is focused by an axicon. These results lead to a novel method for generating longitudinal and transverse polarized optical needle beams based on high NA axicon focusing of vector-vortex beams.

References

[AbTo06] ABOURADDY, AYMAN F. ; TOUSSAINT, KIMANI C.: Three-Dimensional Polarization Control in Microscopy. In: *Physical Review Letters* Bd. 96 (2006), Nr. 15, S. 153901. — 00040

[ArDh00] ARLT, J. ; DHOLAKIA, K.: Generation of high-order Bessel beams by use of an axicon. In: *Optics Communications* Bd. 177 (2000), Nr. 1–6, S. 297–301. — 00378

[BéRi78] BÉLANGER, PIERRE-ANDRÉ ; RIOUX, MARC: Ring pattern of a lens?axicon doublet illuminated by a Gaussian beam. In: *Applied Optics* Bd. 17 (1978), Nr. 7, S. 1080–1088. — 00000

[BoJW06] BOTCHERBY, E. J. ; JUŠKAITIS, R. ; WILSON, T.: Scanning two photon fluorescence microscopy with extended depth of field. In: *Optics Communications* Bd. 268 (2006), Nr. 2, S. 253–260. — 00047

[BPQL10] BANZER, PETER ; PESCHEL, ULF ; QUABIS, SUSANNE ; LEUCHS, GERD: On the experimental investigation of the electric and magnetic response of a single nano-structure. In: *Optics Express* Bd. 18 (2010), Nr. 10, S. 10905–10923. — 00040

[ChHP12] CHEN, ZIYANG ; HUA, LIMIN ; PU, JIXIONG: Chapter 4 - Tight Focusing of Light Beams: Effect of Polarization, Phase, and Coherence. In: EMIL WOLF (Hrsg.): *Progress in Optics*, *Progress in Optics*. Bd. Volume 57 : Elsevier, 2012. — 00000 — ISBN 0079-6638, S. 219–260

[CKTG08] CI?MÁR, TOMAS ; KOLLÁROVÁ, V. ; TSAMPOULA, X. ; GUNN-MOORE, F. ; SIBBETT, W. ; BOUCHAL, Z. ; DHOLAKIA, K.: Generation of multiple Bessel beams for a biophotonics workstation. In: *Optics Express* Bd. 16 (2008), Nr. 18, S. 14024–14035. — 00000

[DoCa95] DOWSKI, EDWARD R. ; CATHEY, W. THOMAS: Extended depth of field through wave-front coding. In: *Applied Optics* Bd. 34 (1995), Nr. 11, S. 1859–1866. — 00887

[DPKM06] DUFOUR, PASCAL ; PICHÉ, MICHEL ; DE KONINCK, YVES ; MCCARTHY, NATHALIE: Two-photon excitation fluorescence

microscopy with a high depth of field using an axicon. In: *Applied Optics* Bd. 45 (2006), Nr. 36, S. 9246–9252. — 00055

[FODP08] FLOSSMANN, FLORIAN ; O'HOLLERAN, KEVIN ; DENNIS, MARK R ; PADGETT, MILES J: Polarization singularities in 2D and 3D speckle fields. In: *Physical review letters* Bd. 100 (2008), Nr. 20, S. 203902. — 00046 PMID: 18518537

[Freu02] FREUND, ISAAC: Polarization singularity indices in Gaussian laser beams. In: *Optics Communications* Bd. 201 (2002), Nr. 4–6, S. 251–270. — 00068

[HaZh11] HAN, YUJING ; ZHAO, GUANGHUI: Measuring the topological charge of optical vortices with an axicon. In: *Optics Letters* Bd. 36 (2011), Nr. 11, S. 2017–2019. — 00013

[HeWi91] HERMAN, R. M. ; WIGGINS, T. A.: Production and uses of diffractionless beams. In: *Journal of the Optical Society of America A* Bd. 8 (1991), Nr. 6, S. 932–942. — 00457

[JaPS00] JARUTIS, V. ; PAŠKAUSKAS, R. ; STABINIS, A.: Focusing of Laguerre–Gaussian beams by axicon. In: *Optics Communications* Bd. 184 (2000), Nr. 1–4, S. 105–112. — 00095

[KCKS14] KAMPMANN, R. ; CHALL, A. K. ; KLEINDIENST, R. ; SINZINGER, S.: Optical system for trapping particles in air. In: *Applied Optics* Bd. 53 (2014), Nr. 4, S. 777–784. — 00000

[KhKV11] KHONINA, S. N. ; KAZANSKIY, N. L. ; VOLOTOVSKY, S. G.: Influence of vortex transmission phase function on intensity distribution in the focal area of high-aperture focusing system. In: *Optical Memory and Neural Networks* Bd. 20 (2011), Nr. 1, S. 23–42. — 00009

[LeYa04] LEI, MING ; YAO, BAOLI: Characteristics of beam profile of Gaussian beam passing through an axicon. In: *Optics Communications* Bd. 239 (2004), Nr. 4–6, S. 367–372. — 00036

[Lune64] LUNEBURG, RUDOLF KARL: *Mathematical Theory of Optics* : University of California Press, 1964. — 00006

[MaOG98] MANEK, I ; OVCHINNIKOV, YU. B ; GRIMM, R: Generation of a hollow laser beam for atom trapping using an axicon. In: *Optics Communications* Bd. 147 (1998), Nr. 1–3, S. 67–70. — 00136

[Mcle54] MCLEOD, JOHN H.: The Axicon: A New Type of Optical Element. In: *Journal of the Optical Society of America* Bd. 44 (1954), Nr. 8, S. 592–592. — 00710

[NBYB01] NOVOTNY, L. ; BEVERSLUIS, M. R. ; YOUNGWORTH, K. S. ; BROWN, T. G.: Longitudinal Field Modes Probed by Single Molecules. In: *Physical Review Letters* Bd. 86 (2001), Nr. 23, S. 5251–5254. — 00421

[Phil14] PHILIP, GEO: Focusing of Optical Vector-vortex Beams. In: *Physical Science International Journal* Bd. 4 (2014), Nr. 3, S. 434–446. — 00000

[PKMV12] PHILIP, GEO M. ; KUMAR, VIJAY ; MILIONE, GIOVANNI ; VISWANATHAN, NIRMAL K.: Manifestation of the Gouy phase in vector-vortex beams. In: *Optics Letters* Bd. 37 (2012), Nr. 13, S. 2667–2669. — 00006

[Scab06] S. CABRINI, C. LIBERALE: Axicon lens on optical fiber forming optical tweezers, made by focused ion beam milling. In: *Microelectronic Engineering* Bd. 83 (2006), S. 804–807. — 00029

[ScVi06] SCHOONOVER, R. W. ; VISSER, T. D.: Polarization singularities of focused, radially polarized fields. In: *Optics Express* Bd. 14 (2006), Nr. 12, S. 5733–5745. — 00055

[SKMY12] SASAKI, KAZUHIRO ; KUROKAWA, KAZUHIRO ; MAKITA, SHUICHI ; YASUNO, YOSHIAKI: Extended depth of focus adaptive optics spectral domain optical coherence tomography. In: *Biomedical Optics Express* Bd. 3 (2012), Nr. 10, S. 2353–2370. — 00005

[SMRP13] SURESH, P. ; MARIYAL, C. ; RAJESH, K. B. ; PILLAI, T. V. S. ; JAROSZEWICZ, Z.: Generation of a strong uniform transversely polarized nondiffracting beam using a high-numerical-aperture lens axicon with a binary phase mask. In: *Applied Optics* Bd. 52 (2013), Nr. 4, S. 849–853. — 00004

[VaTF89] VASARA, ANTTI ; TURUNEN, JARI ; FRIBERG, ARI T.: Realization of general nondiffracting beams with computer-generated holograms.

In: *Journal of the Optical Society of America A* Bd. 6 (1989), Nr. 11, S. 1748–1754. — 00512

[ViIn09] VISWANATHAN, NIRMAL K. ; INAVALLI, V. V. G.: Generation of optical vector beams using a two-mode fiber. In: *Optics Letters* Bd. 34 (2009), Nr. 8, S. 1189–1191. — 00022

[WaCZ10] WANG, JIMING ; CHEN, WEIBIN ; ZHAN, QIWEN: Engineering of high purity ultra-long optical needle field through reversing the electric dipole array radiation. In: *Optics Express* Bd. 18 (2010), Nr. 21, S. 21965–21972. — 00029

[WrAD00] WRIGHT, E. M. ; ARLT, J. ; DHOLAKIA, K.: Toroidal optical dipole traps for atomic Bose-Einstein condensates using Laguerre-Gaussian beams. In: *Physical Review A* Bd. 63 (2000), Nr. 1, S. 013608. — 00117

[WSLS08] WANG, HAIFENG ; SHI, LUPING ; LUKYANCHUK, BORIS ; SHEPPARD, COLIN ; CHONG, CHONG TOW: Creation of a needle of longitudinally polarized light in vacuum using binary optics. In: *Nature Photonics* Bd. 2 (2008), Nr. 8, S. 501–505. — 00243

[WSSZ12] WEBER, NIKLAS ; SPETHER, DOMINIK ; SEIFERT, ANDREAS ; ZAPPE, HANS: Highly compact imaging using Bessel beams generated by ultraminiaturized multi-micro-axicon systems. In: *Journal of the Optical Society of America. A, Optics, image science, and vision* Bd. 29 (2012), Nr. 5, S. 808–816. — 00003 PMID: 22561940

[YoBr00] YOUNGWORTH, KATHLEEN ; BROWN, THOMAS: Focusing of high numerical aperture cylindrical-vector beams. In: *Optics Express* Bd. 7 (2000), Nr. 2, S. 77–87. — 00746

[YuWY11] YUAN, G. H. ; WEI, S. B. ; YUAN, X.-C.: Nondiffracting transversally polarized beam. In: *Optics Letters* Bd. 36 (2011), Nr. 17, S. 3479–3481. — 00031

[YXWZ13] YANG, LIANGXIN ; XIE, XIANGSHENG ; WANG, SICONG ; ZHOU, JIANYING: Minimized spot of annular radially polarized focusing beam. In: *Optics Letters* Bd. 38 (2013), Nr. 8, S. 1331–1333. — 00014

[Zhan09] ZHAN, QIWEN: Cylindrical vector beams: from mathematical concepts to applications. In: *Advances in Optics and Photonics* Bd. 1 (2009), Nr. 1, S. 1–57. — 00515

[ZhLe02] ZHAN, QIWEN ; LEGER, JAMES: Focus shaping using cylindrical vector beams. In: *Optics Express* Bd. 10 (2002), Nr. 7, S. 324–331. — 00361

[ZhWZ05] ZHANG, YAOJU ; WANG, LING ; ZHENG, CHONGWEI: Vector propagation of radially polarized Gaussian beams diffracted by an axicon. In: *Journal of the Optical Society of America A* Bd. 22 (2005), Nr. 11, S. 2542–2546. — 00028

[ZhZZ06] ZHENG, CHONGWEI ; ZHANG, YAOJU ; ZHAO, DAOMU: Calculation of the vectorial field distribution of an axicon illuminated by a linearly polarized Guassian beam. In: *Optik - International Journal for Light and Electron Optics* Bd. 117 (2006), Nr. 3, S. 118–122. — 00006

[ZLLJ13] ZHANG, WEI ; LIU, SHENG ; LI, PENG ; JIAO, XIANGYANG ; ZHAO, JIANLIN: Controlling the polarization singularities of the focused azimuthally polarized beams. In: *Optics Express* Bd. 21 (2013), Nr. 1, S. 974–983. — 00007

[ZWWG13] ZHA, YIKUN ; WEI, JINGSONG ; WANG, HAIFENG ; GAN, FUXI: Creation of an ultra-long depth of focus super-resolution longitudinally polarized beam with a ternary optical element. In: *Journal of Optics* Bd. 15 (2013), Nr. 7, S. 075703. — 00002

CHAPTER

3

Phase Evolution of Propagation-invariant Beams

Contents

3.1 Introduction

L. G. Gouy in 1890 discovered that a spherical converging wave experiences an abrupt phase change of π when it passes through the focal region[Gouy90]. This phase shift also explains the imaginary factor i in the Huygens' integral, corresponding to a phase shift of $\pi/2$ acquired by the secondary wavelets diverging from each point of the primary incident wavefront[Sieg86].The Hermite-Gaussian(HG) and Laguerre-Gaussian(LG) beams with respective indexes (m, n) and (p, l) show a Gouy phase shift equal to $(m+n+1)\,tan^{-1}\,z/z_R$ and $(p+l+1)\,tan^{-1}\,z/z_R$, respectively, where z_R is the Rayleigh range[KoLi66]. For the Gaussian beam the indices m,n,p,l all are equal to zero and the accumulated Gouy phase for z= -∞ to +∞ becomes π. Though the phase evolution upon focusing of the Hermite-Gaussian and Laguerre-Gaussian beams have been studied in some detail, very less attention was given to the Bessel-Gauss beams formed by axicon focusing which produce a line focus. Also, the astigmatic beam field with wavefront dislocation shows twirling behaviour upon propagation, resulting in rotation of the intensity contour of the beam[Denn04].

This chapter explains in detail the phase anomalies and intensity contour rotation upon axicon focusing of astigmatic anisotropic vector-vortex beams. After a brief introduction to astigmatic and anisotropic beam fields and the phase anomalies associated with them upon propagation we describe our experimental results on the rotation of the constant intensity contour with propagation for a vector vortex beam focused by a forward axicon. Moving towards the focus, the constant intensity ellipse twirls around the axis with a simultaneous decrease in the core anisotropy, becoming isotropic at the focus due to the different Gouy phase acquired by the constituent HG_{10} and HG_{01} modes. The non-canonical (elliptic) constant intensity vortex core twirls by around $\pi/2$ in the neighbourhood of the two foci of the conical waves but remain irrotational in the propagation-invariant region. Apart from this the phase and polarization characteristics of the vector-vortex beam also evolves upon propagation. The measured rotation of the polarization singular pattern, formed due to the coherent superposition of orthogonal circularly polarized J_0 and J_1 beams, around the C-point quantifies precisely the Gouy phase accumulated by the constituent modes during propagation. The results on the rotation of constant intensity contour and the polarization singular pattern are manifestations of the universal form of the Gouy phase, as reported here.

3.2 Astigmatic and anisotropic beam propagation

Consider the focusing of an aberated or astigmatic wavefront resulting in the modification of the diffraction integrals. The modified diffraction integrals can be represented by the following relation[BoWo99].

$$U(P) = --iCexp(-ikf)/(\lambda f)\iint exp(ik[\varphi + s]) \tag{3.1}$$

where φ denotes the wave-front aberration function and 's' is the distance from a point of integration Q to the observation point P (Fig.3.1)[ViWo10] and the astigmatic or aberration function in spherical polar coordinate is given by the relation[ViWo10]:

$$\varphi(\rho,\theta) = A_0\rho^2(cos\,\theta)^2\,; \qquad (0 \le \rho \le 1, 0 \le \theta \le 2\pi) \tag{3.2}$$

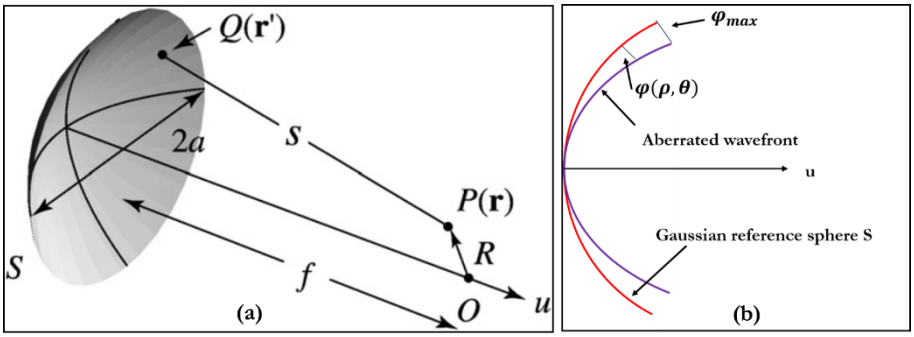

Fig. 3.1 (a) showing the of the spherical S in the co-ordinate system where the origin is the geometric focus of the converging spherical wave; (b) shows the aberrated wave-front

Now using the aberration function and the diffraction integral given in Equ.(3.1) one can calculate the amplitude and the phase distribution at any observation point P. Consider a point P on the axis 'u' (see fig.3.1(a)) and the electric filed distribution at that point is given by,

$$U(u,0) = -\frac{-i2\pi a^2 Cexp(-ifu/a^2)}{\lambda f^2}\int_0^1 exp\{(i[kA_0 - u]\,\rho^2/2)\}$$

$$\rho J_0(kA_0\,\rho^2/2)d\rho \tag{3.3}$$

The axial phase anomaly can be calculated by taking the difference in the phase of diffracted wave and that of a non-diffracted spherical wave. Thus the axial phase anomaly is given by[ViWo10]:

$$\delta(u,0) = arg\left[\int_0^1 exp\{(i[kA_0 - u]\,\rho^2/2)\}\,\rho J_0(kA_0\,\rho^2/2)d\rho\right] - \frac{\pi}{2} \quad (3.4)$$

Using this the axial phase anomalies can be calculated as shown in Fig. 3.2 upon propagation for wavefronts with different astigmaism or aberration (taken from[ViWo10]). From the plot it is clear that with increase in the astigmatism the two focal planes get separated more and more and also the phase difference of $\pi/2$ happens at each of the focal planes as in the case of an aberrated Gaussian beam field.

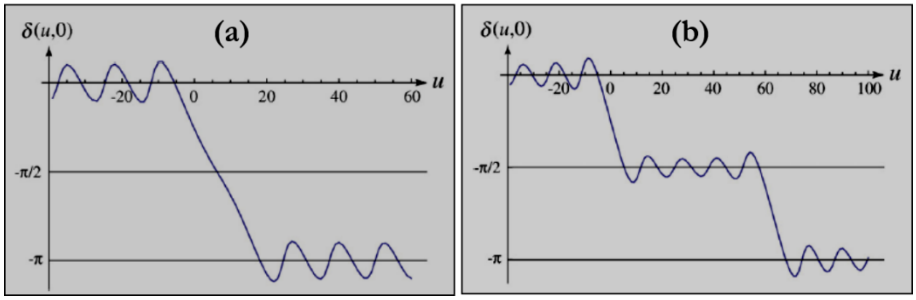

Fig. 3.2 Plot of the axial phase anomalies for astigmatic wave-front with (a) $\varphi_{max}=1\lambda$, f=2m, a=3cm and $\lambda=1\mu$m and (b) $\varphi_{max}=5\lambda$ all other conditions remains the same[ViWo10].

3.3 Rotation of intensity contour with propagation

In the case of optical vortices the beam intensity is tied to its phase structure, for example, an anisotropic vortex (vortex with an anisotropic phase profile) will have its contour around the vortex core in elliptic shape. This leads to the fact that the phase evolution and rotation of the intensity structure of an optical vortex beam are strongly correlated with each other. The intensity rotation upon focusing is a direct manifestation of Gouy phase[BKMG09]. Thus the beam rotation studies are significant in the case of vortex beams which process an anisotropic phase profiled singularity at the centre[NyBe74], mainly beacuase the vortex beams can efficiently replace conventional Gaussian beams in many applications such as optical tweezers[CuKG02], actuators for micro-electro-mechanical systems[FRGH01] and multi-dimensional quantum entanglement[MVWZ01] studies, where the phase

evolution and the beam rotation play key role. The propagation charecteristics under certain conditions are known to have knots and twists[BeDe01a; BeDe01b; LDCP05] in the case of a vortex beam. Though the dynamics of the vortex beam propagation and its focusing charecteristics are studied well, the dynamics of the general class of anisotropic and astigmatic propagation-invariant vortex beam is still being researched to enable a generalized picture. This section presents a study of the dynamics of propagation-invariant vortex beam formed by focuisng an astigmatic Laguerre-Gauss beam by an axicon.

Fig. 3.3 shows the schematic of the experimental setup used for the study of intensity contour rotation of a vector-vortex beam upon axicon focusing. The

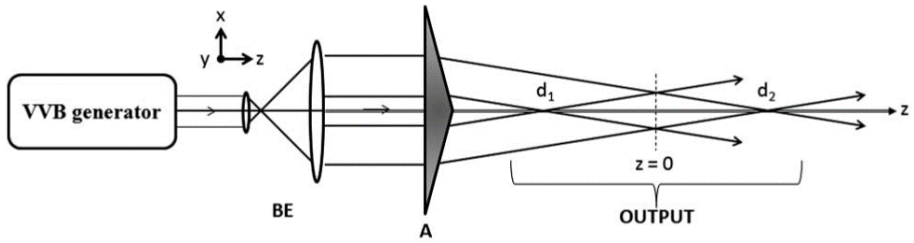

Fig. 3.3 Schematic of the experimental setup: BE-beam expander; A-axicon.

vortex beam generator consists of a two-mode optical fiber with a properly selected circularly polaried light launched into it[JaKV11]. The launching conditions are adjusted so that the output of the fiber is a vortex beam due to the combination of fiber modes excited in the fiber. The expanded and collimated fiber output is then focused by a linear axicon of small angle α=0.5°. The focused beam is imaged using a CCD camera connected to a computer and the image analysis is carried out using Matlab codes.

To devolope the theoretical formalism to understand the core intensity dynamics of the vortex beam, the vortex beam at the output of the optical fiber is treated as a linear superposition of Hermite-Gauss beams:

$$E(x,y,z) = xF + iyF = HG_{10} + iHG_{01} \tag{3.5}$$

where $F(x,y,z)$ is the host beam profile. In the most generalized form a single charged vortex beam can be written as follows:

$$E(x,y,z) = \left\{px + exp\left[i\left(\frac{\pi}{2} \pm \varphi_s\right)\right] qy\right\} F(x,y,z) \tag{3.6}$$

where *p* and *q* are constants and the additional phase φ_s makes the vortex beam a non-canoical one with φ_s=0 implies canonical (symmetric) vortex due to the $\pi/2$ phase difference between two Hermite-Gauss modes. The intensity corresponding to the field distribution given by Equ(3.6) can be expessed as:

$$I = E \times E^* = (px)^2 + (qy)^2 + 2pq\, cos(\frac{\pi}{2} \pm \varphi_s)xy \tag{3.7}$$

Now considering the intensity core of the vortex forms an elliptical shape (non-canonical vortex) with major and minor axis 'a', 'b' respectively and having an orientation of ϑ with respect to the horizondal(x) axis, the equation of the ellipse can be written as:

$$\left[\frac{(cos\vartheta)^2}{a^2} + \frac{(sin\vartheta)^2}{b^2}\right]x^2 + \left[\frac{(sin\vartheta)^2}{a^2} + \frac{(cos\vartheta)^2}{b^2}\right]y^2 + 2cos\vartheta sin\vartheta\left[\frac{1}{a^2} + \frac{1}{b^2}\right]xy \tag{3.8}$$

Comparing Equ. (3.7) and (3.8)

$$cos(\frac{\pi}{2} \pm \varphi_s) = \frac{cos\vartheta sin\vartheta\left[\frac{1}{a^2} + \frac{1}{b^2}\right]}{pq}$$

$$p^2 = \left[\frac{(cos\vartheta)^2}{a^2} + \frac{(sin\vartheta)^2}{b^2}\right] and \quad q^2 = \left[\frac{(sin\vartheta)^2}{a^2} + \frac{(cos\vartheta)^2}{b^2}\right] \tag{3.9}$$

The intensity characteristics of the vortex beam are measured, after the axicon, at different transverse planes (in 10 mm intervals) along the propagation axis from the first focus distance (d_1) to the second (d_2) through the propagationinvariant region, covering the Rayleigh ranges of both the converging and diverging regions of the conical waves. From the captured CCD images the anisotropy[BeVS06] of the core in first ring of the J_1- Bessel-Gauss beam is calculated using the following equation[BeVS06]:

$$cos\psi = 2\left[{}^{a}/_{b} + {}^{b}/_{a}\right]^{-1} \tag{3.10}$$

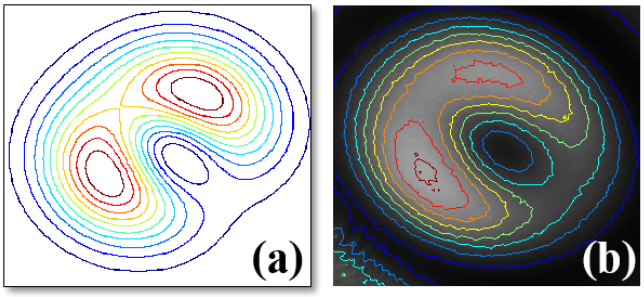

Fig. 3.4 (a) Theoretically simulated intensity contour of the vortex beam and (b) experimentally measured intensity contour at z=-25cm.

Fig. 3.4 shows the theoretically calculated and experimentally observed astigmatic vortex beam structure measured at a distance z=-25 cm. The theoretical simulation is done using Equ.(3.6). It is seen from Fig. 3.4 that the vortex core is elliptic shaped with anisotropy factor cos ψ=0.958, and is oriented at an angle ϑ =37° with respect to the horizontal (x) axis. From the images captured using the CCD as a function of z, the average intensity of the first ring of the J_1-Bessel-Gauss beam is plotted as a function of 'z' in Fig. 3.5 and is found to be similar to that of the linear axicon: linear increase in intensity within the region $d_1 < z < d_2$ [Frib96]. More importantly, this result indicates that the conical waves from within the core region of the astigmatic vortex beam crosses the z-axis at $z= d_1 (\neq 0)$ and that from the outer region at $z=d_2$. The different Gouy phase acquired by the astigmatic beam (in the "xz" and "yz" planes) due to the misaligned constituent Hermite-Gauss beams, results in two Rayleigh ranges, leading to the transformation of the noncanonical vortex to a canonical vortex. This is evidenced by the reduction in the core anisotropy as shown in Fig 3.5. The constant inetnsity contour becomes more circular, $cos\psi \approx 1$ at $z=d_1$. The canonical vortex remains so in the propagation-invariant region and becomes noncanonical beyond $z=d_2$. This behavior is clear from the plot of the anisotropy factor $cos\psi$ of the core region of the J_1 Bessel-Gauss beam as a function of z calculated from the measured intensity images (Fig. 3.5). Fig. 3.6 shows that the behaviour of the elliptic core of the first ring of the J_1 Bessel-Gauss beam: 'a' and 'b' and their changes upon propagation. From Equ. (3.9) it can be seen that any change in 'a', 'b' and φ_s leads to the change

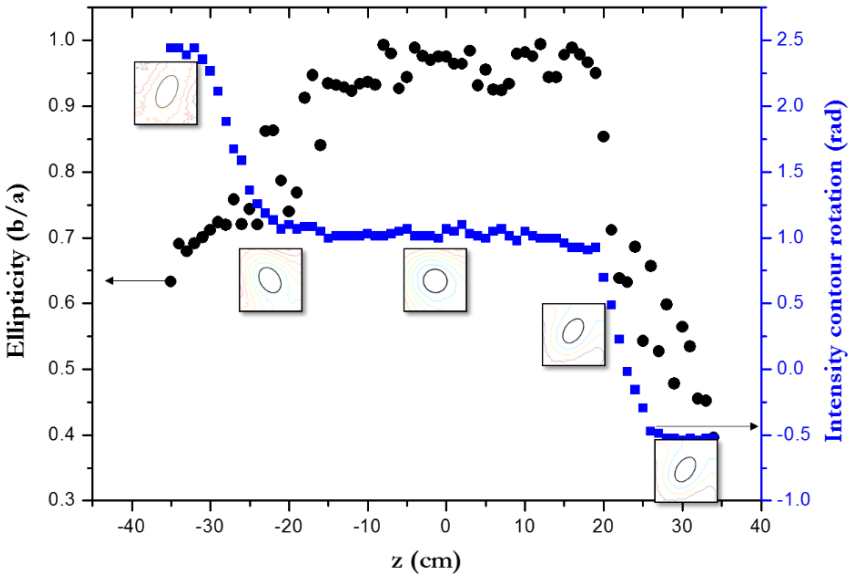

Fig. 3.6 Plot of intensity contour rotation(blue colour) and ellipticity (b/a) (black) with propagation distance 'z'. Inset intensity contour at corresponding z- positions.

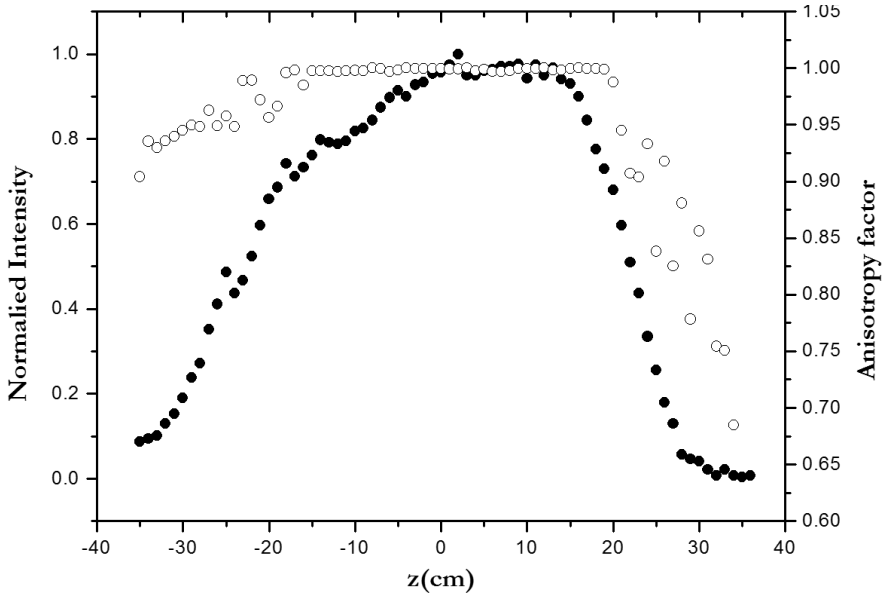

Fig. 3.5 Normalized intensity(black filled dots) and anisotropy(open circles) factor of the first ring of the J1-BG beam with propagation distance 'z'

in major axis orientation of the constant intensity ellipse and thus causes rotation

of the intensity pattern upon propagation. From the captured CCD images the constant intensity contour rotation angle is measured and Fig. 3.6 shows the plot of intensity contour rotation and ellipticity (b/a) with propagation distance 'z'. Moving towards the first focus, the constant intensity ellipse twirls around the axis with a simultaneous decrease in the core anisotropy, becoming isotropic at the focus due to the different Gouy phase acquired by the misaligned constituent HG_{10} and HG_{01} modes. The ellipticity (b/a) also remains constant in the propagation-invariant region suggesting that all the intensity related parameters of the beam are invariant in the propagation-invariant region.

3.4 Gouy phase of propagation-invariant beams

In 1890 L. G. Gouy proposed and demonstrated the anomalous behaviour of phase of an optical beam when it converges and passes through a focus. He defined the anomolous behaviour of the axial phase of a spherical beam as

"*If one considers a converging wave that has passed through a focus and has then become divergent, a simple calculation shows that the vibration of that wave has advanced half a period compared to what it should be according to the distance traveled and the speed of light*"

Over the years, researchers tried to explain this phase anomaly fom different perspectives. The main efforts towards explaining the Gouy phase include the description relating the Gouy phase to the Heisenberg uncetainity principle[HaRo96; FeWi01], geometric phase or Berry's phase[Subb95]; [SiMu93] and also to the geometrical properties of the Gaussian beam[Boyd80]. Being a general wave phenomena Gouy phase shift is also observed in a varity of different senarios including in acoustic pulses[HDMN03], electron votex beams[GSBN13], terahertz pulses[RRWF99]; [WSCY13], photonic jets[BRBW12] and in propagating optical vortex beams[HMOM06]. Gouy phase shift is also mentioned in the case of matter waves[Igda10] and surface plasmon polaritons[ZhAN07]. Different methods including the spatial mode intereference[CVGM04] and super-continum spectral interference[WZLX00] methods were devoloped for the measurment of Gouy phase.

This fundamental wave property is of significant practical importance in several applications as well. Further the Gouy effect has to be considered to achieve the phase matching in non-linear optics [Boyd68], Gouy phase of fundamental mode plays crucial role in resonant cavity alignment for gravitational

wave detection[MaSS98] and in optical trapping of atoms[ArPa00]. Almost all the measurement and studies of Gouy effect is carried out using either the fundamental mode or the first-order vortex beams and that too only for the conventional lens focusing. Very less attention is given for line focusing and propagation-invariant beams and the role of Gouy phase in their propagation. This section gives an expeimental method for the direct measurement of Gouy phase of a vector-vortex beam upon line focusing by an axicon.

3.4.1 Measurement of Gouy phase using polarization singularity

Any optical phase measurement is relative and thus needs a reference beam to extract phase. Convetionally a two-beam ineterference experiment is used to measure the phase difference, where the stability requirement of the interferometer is crucial. To overcome the difficulties due to the beam stability in the interferometer the method presented here use the superposition of orthogonal polarized light beams which makes use of polarization (field) interference effect. Orthogonal circular polarized vortex beam and fundamental Gaussian beam interfere to generate polarization singularities (see appendix A.II for details) which are very sensitive to any changes in the phase and intensity of the superposed beams. As a result polariation singularity can be effectively used as a marker pattern in the beam cross-section to track the phase evolution in constituent beams.

The experimental setup shown in Fig. 3.3 is used for the Gouy phase measurement of propagation-invariant vector-vortex beams. The two-mode optical fiber which is the heart of the vector-vortex beam generator is excited with skew rays of appropriate polarization-either left circular or right circular-to get an output beam which is a superposition of orthogonal circular polarized vortex and fundamental mode[JaKV11]. The collimated output from the fiber is subsiquently focused by a forward axicon to generate BG beams[ArDh00]. The Bessel-Gauss beam from the axicon is imaged using a CCD camera and the spatial polarization structure of the beam is measures by calculating the spatially resolved Stokes parameters of the beam using a quarter-wave plate and polarizer combination[Gold11]. This measurement set is repeated at regular intervals along the propagation to study the phase evolution of the beam. The polarization ellipse parameters are calculted from the measuremnts and the polarization ellipse is plotted in the beam cross-section. From the generated polarization ellipse map the

rotation of the polarization singularity is measured with propagation, which is directly propotional to the phase evolution relative to the fundamental mode.

The output from the two-mode optical fiber is a superposition of orthogonal circularly polarized vortex mode and fundamental mode whose electric field components can be written as[JaKV11]:

$$E_x = \left[\varepsilon\, exp(i\emptyset_F) + (x + ily)^{|l|}\, exp(i\emptyset_V)\right] \tag{3.11}$$

$$E_y = \left[i\varepsilon\sigma_F exp(i\emptyset_F) + i\sigma_V(x + ily)^{|l|}\, exp(i\emptyset_V)\right] \tag{3.12}$$

where the first and second terms in the square brackets represent the fundamental (*F*) and vortex (*V*) modes respectively, and ε is the real amplitude corresponding to the perturbed fundamental mode. If the polarization ellipse map is simulated using the above equations for a vortex of charge l=+1 with circular polarization σ_V=-1 (LCP) and σ_F=1 (RCP) for the fundamental mode, a lemon-type polarization singularity pattern surrounding the C-point is generated(Fig. 3.7). The orientation of the polarization ellipse pattern is determined by the relative phase difference between the fundamental and vortex modes, i.e.,

$$\Delta\emptyset = \emptyset_V \sim \emptyset_F \tag{3.13}$$

The resulting polarization singular lemon pattern rotates as the beam evolves around the foci due to the Gouy phase difference between the constituent modes[KMTS08]. Fig. 3.7 shows the experimentally observed and theorectically predicted polarization maps and the polarization ellipse orientations at z=-25cm. The polarization characteristics of the vector-vortex beam are measured, after the axicon, at different transverse planes (in 10 mm intervals) along the propagation axis by calculating the spatially resolved Stoke's parameters using a polarizer and quarter-wave plate arranegement (see Appendix A.I for details). From the calculated Stokes parameters the orientation of the lemon polarization singular pattern is measured with propagation distance. The rotation angle of the lemon pattern is a direct measure of the Gouy phase accumulated by the J_1- Bessel-Gauss beam with propagation, with respect to a fundamental Gaussian beam. Fig. 3.8 shows the rotation angle of the lemon polarization singular pattern with propagation for the conventional double convex lens and an axicon.

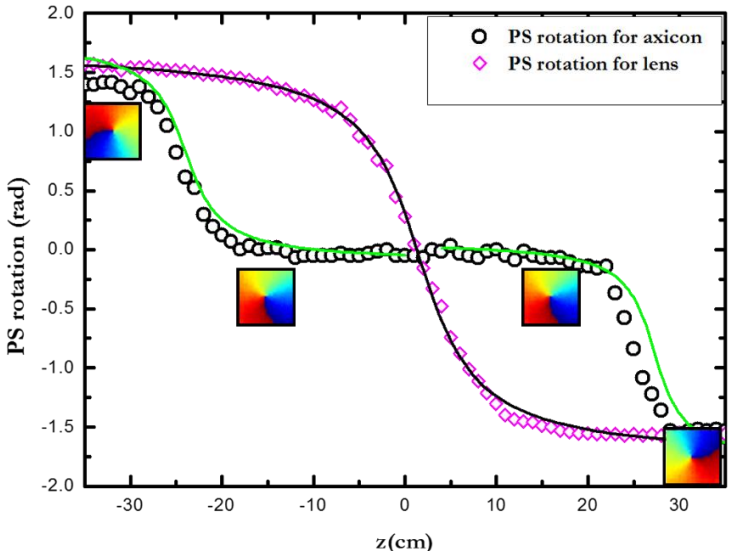

Fig. 3.8 Polarization singularity rotation angle for axicon and lens focusing of a vector-vortex beam.

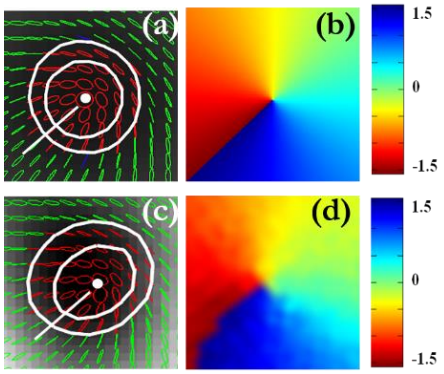

Fig. 3.7 (a) and (c) are theoretical and experimental polarization ellipse map of the core of the J1-BG beam; (b) and (d) are the corresponding ellipse orientations

The polarization singular pattern of the vector-vortex beam focused by the axicon clearly shows that the orientation of the lemon pattern rotates fast around the two foci (d1 and d2) but remains irrotational in the propagation-invariant region of the J_1-Bessel-Gauss beam, as shown in Fig. 3.8. A rotation angle of $\pi/2$, following Equ. (3.14)

$$\phi(z) = \frac{1}{2} arctan\left(\frac{z}{z_R}\right) = \phi_G(z) \tag{3.14}$$

is measured around the two foci of the conical waves, resulting in the overall Gouy phase change of π for the propagation-invariant J_1-Bessel-Gauss beam with respect to the fundamental Gaussian beam. The above measurement is compared with the double convex lens focusing of the vector-vortex beam which shows a continuous phase change of π. Our measurements thus confirms that in the propagation-invaraint region of J_1-BG beam the phase of the beam also remains invariant upon propagation.

Summary

After giving a brief introduction to the phase anomaly associated with the focusing of astigmatic beam fields our result of the constant intensity contour rotation upon axicon focusing of an astigmatic vortex beam is presented. . Moving towards the focus, the constant intensity ellipse twirls around the axis with a simultaneous decrease in the core anisotropy, becoming isotropic at the focus due to the different Gouy phase acquired by the misaligned constituent HG_{10} and HG_{01} modes. Also, a polarization interference and polarization singularity based method is used for the direct measurement of Gouy phase of vector-vortex beam upon axicon focusing. The rotation of the *lemon* type polarization singularity pattern observed with propagation is a direct manifestation of the Gouy phase.

References

[ArDh00] ARLT, J. ; DHOLAKIA, K.: Generation of high-order Bessel beams by use of an axicon. In: *Optics Communications* Bd. 177 (2000), Nr. 1–6, S. 297–301

[ArPa00] ARLT, J. ; PADGETT, M. J.: Generation of a beam with a dark focus surrounded by regions of higher intensity: the optical bottle beam. In: *Optics Letters* Bd. 25 (2000), Nr. 4, S. 191–193

[BeDe01a] BERRY, M. V. ; DENNIS, M. R.: Knotted and linked phase singularities in monochromatic waves. In: *Proceedings of the Royal Society of London. Series A: Mathematical, Physical and Engineering Sciences* Bd. 457 (2001), Nr. 2013, S. 2251–2263

[BeDe01b] BERRY, M V ; DENNIS, M R: Knotting and unknotting of phase singularities: Helmholtz waves, paraxial waves and waves in z34 (2001), Nr. 42, S. 8877–8888

[BeVS06] BEKSHAEV, A. YA ; VASNETSOV, M. V. ; SOSKIN, M. S.: Description of the morphology of optical vortices using the orbital angular momentum and its components. In: *Optics and Spectroscopy* Bd. 100 (2006), Nr. 6, S. 910–915

[BKMG09] BAUMANN, S. M. ; KALB, D. M. ; MACMILLAN, L. H. ; GALVEZ, E. J.: Propagation dynamics of optical vortices due to Gouy phase. In: *Optics Express* Bd. 17 (2009), Nr. 12, S. 9818–9827

[BoWo99] BORN, MAX ; WOLF, EMIL: *Principles of Optics: Electromagnetic Theory of Propagation, Interference and Diffraction of Light* : CUP Archive, 1999 — ISBN 9780521784498

[Boyd68] BOYD, G. D.: Parametric Interaction of Focused Gaussian Light Beams. In: *Journal of Applied Physics* Bd. 39 (1968), Nr. 8, S. 3597

[Boyd80] BOYD, ROBERT W.: Intuitive explanation of the phase anomaly of focused light beams. In: *Journal of the Optical Society of America* Bd. 70 (1980), Nr. 7, S. 877–880

[BRBW12] BON, PIERRE ; ROLLY, BRICE ; BONOD, NICOLAS ; WENGER, JÉRÔME ; STOUT, BRIAN ; MONNERET, SERGE ; RIGNEAULT, HERVÉ: Imaging the Gouy phase shift in photonic jets with a wavefront sensor. In: *Optics Letters* Bd. 37 (2012), Nr. 17, S. 3531–3533

[CuKG02] CURTIS, JENNIFER E. ; KOSS, BRIAN A. ; GRIER, DAVID G.: Dynamic holographic optical tweezers. In: *Optics Communications* Bd. 207 (2002), Nr. 1–6, S. 169–175

[CVGM04] CHOW, JONG H. ; DE VINE, GLENN ; GRAY, MALCOLM B. ; MCCLELLAND, DAVID E.: Measurement of Gouy phase evolution by use of spatialmode interference. In: *Optics Letters* Bd. 29 (2004), Nr. 20, S. 2339–2341

[Denn04] DENNIS, M. R.: Local phase structure of wave dislocation lines: twist and twirl. In: *Journal of Optics A: Pure and Applied Optics* Bd. 6 (2004), Nr. 5, S. S202

[FeWi01] FENG, SIMIN ; WINFUL, HERBERT G.: Physical origin of the Gouy phase shift. In: *Optics Letters* Bd. 26 (2001), Nr. 8, S. 485–487

[FRGH01] FRIESE, M. E. J. ; RUBINSZTEIN-DUNLOP, H. ; GOLD, J. ; HAGBERG, P. ; HANSTORP, D.: Optically driven micromachine elements. In: *Applied Physics Letters* Bd. 78 (2001), Nr. 4, S. 547–549

[Frib96] FRIBERG, ARI T.: Stationary-phase analysis of generalized axicons. In: *Journal of the Optical Society of America A* Bd. 13 (1996), Nr. 4, S. 743–750

[Gold11] GOLDSTEIN, DENNIS H.: *Polarized Light, Third Edition*. 3 edition. Aufl. Boca Raton, FL : CRC Press, 2011 — ISBN 9781439830406

[Gouy90] GOUY, LÉON GEORGES: *Sur une propriété nouvelle des ondes lumineuses* : Gauthier-Villars, 1890

[GSBN13] GUZZINATI, GIULIO ; SCHATTSCHNEIDER, PETER ; BLIOKH, KONSTANTIN Y. ; NORI, FRANCO ; VERBEECK, JO: Observation of the Larmor and Gouy Rotations with Electron Vortex Beams. In: *Physical Review Letters* Bd. 110 (2013), Nr. 9, S. 093601

[HaRo96] HARIHARAN, P. ; ROBINSON, P. A.: The gouy phase shift as a geometrical quantum effect. In: *Journal of Modern Optics* Bd. 43 (1996), Nr. 2, S. 219–221

[HDMN03] HOLME, N. C. R. ; DALY, B. C. ; MYAING, M. T. ; NORRIS, T. B.: Gouy phase shift of single-cycle picosecond acoustic pulses. In: *Applied Physics Letters* Bd. 83 (2003), Nr. 2, S. 392–394

[HMOM06] HAMAZAKI, JUNICHI ; MINETA, YURIYA ; OKA, KAZUHIRO ; MORITA, RYUJI: Direct observation of Gouy phase shift in a propagating optical vortex. In: *Optics Express* Bd. 14 (2006), Nr. 18, S. 8382–8392

[Igda10] I. G. DA PAZ, P. L. SALDANHA: Experimental proposal for measuring the Gouy phase of matter waves (2010)

[JaKV11] JAYASURYA, Y. V. ; KRISHNA INAVALLI, V. V. G. ; VISWANATHAN, NIRMAL K.: Polarization singularities in the two-mode optical fiber output. In: *Applied Optics* Bd. 50 (2011), Nr. 25, S. E131–E137

[KMTS08] KAWASE, DAISUKE ; MIYAMOTO, YOKO ; TAKEDA, MITSUO ; SASAKI, KEIJI ; TAKEUCHI, SHIGEKI: Observing Quantum Correlation of Photons in Laguerre-Gauss Modes Using the Gouy Phase. In: *Physical Review Letters* Bd. 101 (2008), Nr. 5, S. 050501

[KoLi66] KOGELNIK, H. ; LI, T.: Laser Beams and Resonators. In: *Applied Optics* Bd. 5 (1966), Nr. 10, S. 1550–1567

[LDCP05] LEACH, J. ; DENNIS, M. R. ; COURTIAL, J. ; PADGETT, M. J.: Vortex knots in light. In: *New Journal of Physics* Bd. 7 (2005), Nr. 1, S. 55

[MaSS98] MAVALVALA, NERGIS ; SIGG, DANIEL ; SHOEMAKER, DAVID: Experimental Test of an Alignment-Sensing Scheme for a Gravitational-Wave Interferometer. In: *Applied Optics* Bd. 37 (1998), Nr. 33, S. 7743–7746

[MVWZ01] MAIR, ALOIS ; VAZIRI, ALIPASHA ; WEIHS, GREGOR ; ZEILINGER, ANTON: Entanglement of the orbital angular momentum states of photons. In: *Nature* Bd. 412 (2001), Nr. 6844, S. 313–316

[NyBe74] NYE, J. F. ; BERRY, M. V.: Dislocations in Wave Trains. In: *Proceedings of the Royal Society of London. A. Mathematical and Physical Sciences* Bd. 336 (1974), Nr. 1605, S. 165–190

[RRWF99] RUFFIN, A. B. ; RUDD, J. V. ; WHITAKER, J. F. ; FENG, S. ; WINFUL, H. G.: Direct Observation of the Gouy Phase Shift with Single-Cycle Terahertz Pulses. In: *Physical Review Letters* Bd. 83 (1999), Nr. 17, S. 3410–3413

[Sieg86] SIEGMAN, A. E: *Lasers*. Mill Valley, Calif. : University Science Books, 1986 — ISBN 9780935702118 0935702113 0198557132 9780198557135 0685055957 9780685055953

[SiMu93] SIMON, R. ; MUKUNDA, N.: Bargmann invariant and the geometry of the Güoy effect. In: *Physical Review Letters* Bd. 70 (1993), Nr. 7, S. 880–883

[Subb95] SUBBARAO, D.: Topological phase in Gaussian beam optics. In: *Optics Letters* Bd. 20 (1995), Nr. 21, S. 2162–2164

[ViWo10] VISSER, T. D. ; WOLF, E.: The origin of the Gouy phase anomaly and its generalization to astigmatic wavefields. In: *Optics Communications* Bd. 283 (2010), Nr. 18, S. 3371–3375

[WSCY13] WANG, XINKE ; SUN, WENFENG ; CUI, YE ; YE, JIASHENG ; FENG, SHENGFEI ; ZHANG, YAN: Complete presentation of the Gouy phase shift with the THz digital holography. In: *Optics Express* Bd. 21 (2013), Nr. 2, S. 2337–2346

[WZLX00] WANG, ZHIGUANG ; ZENG, ZHINAN ; LI, RUXIN ; XU, ZHIZHAN: Measurement of Gouy phase shift by use of supercontinuum spectral interference. In: *Chiese Optics Letters* Bd. 05, Nr. S1, S. 183.

[ZhAN07] ZHU, WENQI ; AGRAWAL, AMIT ; NAHATA, AJAY: Direct measurement of the Gouy phase shift for surface plasmon-polaritons. In: *Optics express* Bd. 15 (2007), Nr. 16, S. 9995–10001. — PMID: 19547350

CHAPTER

4

Self-reconstruction of Propagation-invariant Beam

Contents

4.1 Introduction

An optical beam whose amplitude reconstructs after partial obstruction, reported first in Bessel beams[BoWC98], has revolutionized micromanipulation [GMMS02] and microscopy[FaSR10] realizing enhanced image contrast even in optically thick inhomogeneous media such as cell clusters, embryos, skin etc.,[FaRo12, FaSR10]. The self-reconstruction process has also been demonstrated in caustic beams[AMIC07], Airy beams[BSDC08], Parcey beams[RLMM12], non-paraxial Mathieu and Weber accelerating beams and in ring lattice beams[HeRT13]. Until now the intensity self-reconstruction process has been demonstrated behind a partial obstruction of the beam which changes locally the intensity and phase or partially absorbs the beam energy, leaving the polarization obstruction of the beam open for further investigation. Also, most of the biological samples for example neuron cells, tissues etc. which are being imaged using microscopy are naturally birefringent and significantly modify the phase and polarization characteristics of the light beam incident on them. Light beams which are immune or repair itself to local changes in phase and polarization would be immensely useful in developing novel imaging techniques for the naturally bifringent biological samples.

This chapter addresses the self-reconstruction properties of the Bessel-Gauss beams in detail, starting with the simple intensity reconstruction to self-reconstruction of complex phase and polarization structured light fields. Recently it has also been shown that the azimuthally polarized Bessel-Gauss beams do reconstruct in the focal plane after being partially obstructed[WuWC14]. To study all aspects of the self-reconstruction a Bessel–Gauss beam with embedded polarization singularity wherein the intensity, phase and polarization characteristics of the beam are tied together to form a topological pattern is generated and its evolution characteristics beyond a partial obstruction of its amplitude, phase and polarization are experimentally studied.

4.2 Self-reconstruction of caustic beams

Optical Bessel beams generated either using an axicon or a device fabricated in an optical fiber or any other method results in a line image along the propagation axis of the element for a collimated, normal incident Gaussian input beam[JaBF05, McDh05]. The quality of the generated Bessel beam however is very sensitive to aberrations, arising either due to oblique illumination, illuminating with a

cylindrical wave forms or due to the optical element itself[BiZh98, ThJF03]. The aberration and oblique illumination results in the broadening of the focal line and resulting in complex beam patterns including optical caustic patterns[BiZh98, TaYa00, ThJF03, ThJF03].

Schematic of the experimental setup used for the demonstration is shown in Fig 4.1. The He-Ne laser beam (λ = 632.8 nm) after spatial filtering and a expanding, is pass through a circular axicon (small angle $\alpha = 4^{o}$) at normal incidence and the emerging beam is imaged onto a CCD using a lens L. The biconvex lens (f = 25mm) and the CCD are mounted together at a fixed distance of d_2 = 75 mm from each other on a translation stage along the axis of the axicon to measure the spatial evolution of the transverse intensity pattern at a constant magnification of 2. First the spatial evolution of the asteroid shaped cau-

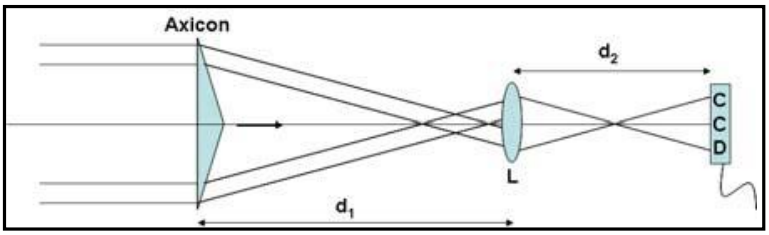

Fig. 4.1 Schematic of the experimental setup for the self-reconstruction study of the caustic beam

stic pattern emerging from the astigmatic axicon is studied by imaging the pattern along the propagation direction, and the dimensions of the pattern are recorded at different distances from the axicon along the propagation axis. For each observation the distances between the diagonally opposite corners of the pattern are recorded as a measure of the size of the pattern. These measurements are designated as 'x' and 'y' distances. To study the self-reconstruction of the generated caustic beam the patterns is obstructed using an opaque obstruction (150 μm diameter metal wire placed 40 cm away from the axicon) and the evolution dynamics beyond the obstruction is studied by measuring the CCD images at different distances from the obstruction. Fig. 4.2 (a) shows the asteroid pattern at a distance 40 com away from the axicon and 4.2(b) shows the pattern at the obstruction plane which shows that the wire which is placed vertically obstructs the pattern (dark shadow made by the wire can be seen in Fig. 4.2(b). Fig. 4.2(c) shows the reconstructed pattern.

.Beyond the obstruction the caustic pattern reconstructs itself gradually over a certain distance along with the appearance of the rings surrounding it. Depending on the position of the obstruction in the image plane of the axicon the pattern begins to reconstruct itself either completely or partially. Fig. 4.3 shows the physical dimensions of the caustic pattern with propagation with and without partial obstruction. Thus even with obstruction, the astroid shaped caustic pattern generated by the astigmatic axicon reconstructs itself almost completely after propagating some distance.

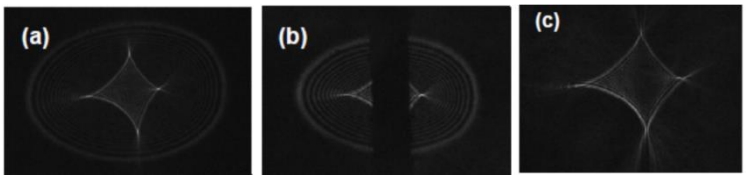

Fig. 4.2 (a) generated caustic pattern by the axicon; (b) the pattern at the obstruction plane; (c) reconstructed caustic pattern after the opaque obstruction.

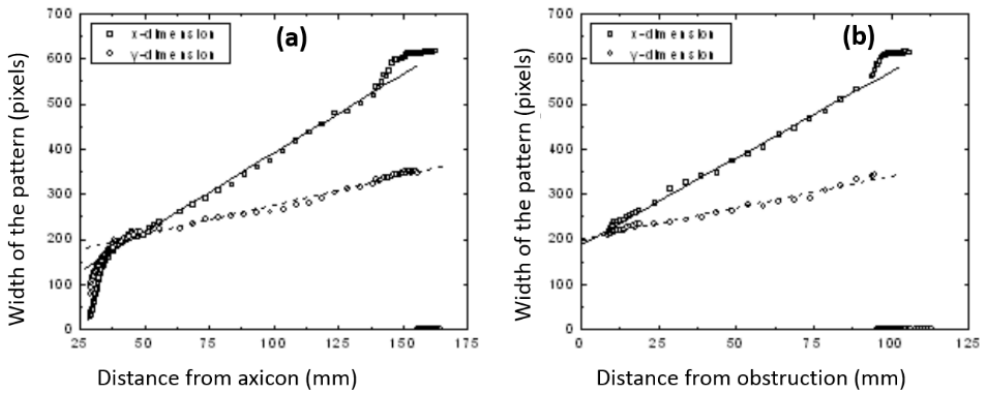

Fig. 4.3 Evolution of the physical dimensions of the caustic pattern (a) without obstruction and (b) with obstruction

The slope of x and y dimension of the astroid pattern is calculated to study the evolution of the pattern with and wihout obstruction. In the un obstructed case the slope of the linear portions of the graph are 3.5 and 1.32 for the x-dimension and the y-dimension. Similarly, a linear fit of the spatial evolution of the reconstructed pattern results in a slope of 3.85 and 1.40 for the x- and y-dimensions of the pattern. The values of the slope are almost the same as what was obtained for the un-obstructed beam. It is clear from the above-mentioned results that generation of caustic beams by illuminating an astigmatic circular axicon with plane

wavefront, when obstructed by an opaque object, reappears at a given plane with the same transverse intensity pattern of that generated by an un-obstructed caustic beam.

4.3 Self-reconstruction of vector beams

Spatially inhomogeneously polarized optical beams are known as vector beams. The inhomogeneous polarization structure in the beam cross-section can be radial, azimuthal or hybrid polarized and have received particular a lot of attention in the recent times for their applications in areas like particle acceleration[VaPi02], single molecule imaging[NBYB01], non-linear optics[BBHN03] etc. Although the self-reconstruction characteristics of scalar Bessel-Gauss beams in the intensity domain have been studied widely, the phase and polarization aspects of the beam are limited only to theoretical treatment[VyKS11], or to the high-numerical aperture focusing experiments[WuWC14]. The experiments with propagation-invariant azimuthally polarized Bessel-Gauss beams generated using a paraxial circular axicon shows that the tight focusing condition is not necessary for the reconstruction of the vector beams after being partially obstructed. Complete reconstruction of paraxial vector beams is verified here using imaging Stokes Polarimetry.

Azimuthally-polarized BG beam is generated using a Sagnac interferometer with a spiral phase plate (SPP) within the interferometer and an axicon outside it. Fig.4.4 shows a schematic of the experimental setup that was used in this study. The Gaussian beam from a He-Ne laser (632.8 nm) polarized vertical using polarizer P1 and is passed through a half-wave plate (HWP) with its fast axis oriented at an angle of 22.5^{o} with respect to the vertical to produce linear polarized light that makes 45^{o} angle with the vertical. This light is the input to the Sagnac interferometer constructed with a polarization beam splitter (PBS).

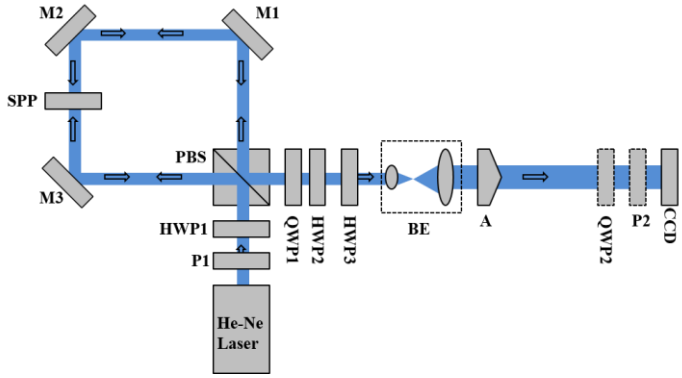

Fig. 4.4 Schematic of the experimental setup used for the study of self-reconstruction of azimuthally polarized BG beam

Orthogonal linear polarized counter propagating Gaussian beams in the interferometer are converted to Laguerre-Gauss (LG) beams with opposite helicity by the SPP kept inside the interferometer. The output beam from the interferometer is a combination of orthogonal linearly polarized LG beams with opposite helical charges (l). A quarter-wave plate (QWP) oriented at 45° at the interferometer output converts this beam combination into orthogonal circular polarized vortex beams with l=+1 and -1. Such a combination produces optical vector beams wherein the polarization state at any point is linear but its orientation is different at different points due to the phase difference between the interfering beams. In Sagnac interferometer the counter propagating beams travel through the same path and the phase difference between them is zero. But the in phase superposition of orthogonal circularly polarized LG beams with opposite helicity produces radial polarized vector beam as now the phase variation across the beam cross-section. This radial polarized vector beam is converted to azimuthal polarization using two HWP combination which rotates the state of polarization

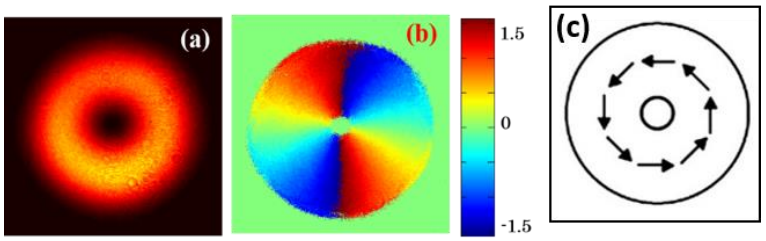

Fig. 4.5 (a) Intensity of the azimuthally-polarized LG beam generated using the Sagnac interferometer, (b) polarization orientation map and (c) polarization orientation in the beam cross-section.

at every point in the beam cross-section by 90°. An axicon of open angle α=0.5° placed at the interferometer output, focuses the expanded azimuthally polarized beam to produce azimuthal polarized Bessel-Gauss beams. The propagation-invariant range of the BG beam depends on the beam waist (ω_0) and the open angle and the refractive index of the axicon given by the relation: $Z_{max} = \omega_0(k/k_r)$ with $k_r = (n-1)\gamma k$, k being wave vector. In our experiment we make sure that all the measurements are made within the propagation-invariant range. An opaque obstruction such as a thin metallic wire (100μm diameter) is positioned in the beam using a two dimensional translation stage and 20 cm away from the axicon, partially obstructing the beam. The beam intensity and polarization characteristics are measured using a CCD camera and a QWP-polarizer combination which is used for calculating the spatially-resolved Stokes parameters of the beam[GoGo11]. Fig. 4.5 shows the CCD image of the interferometer output and corresponding polarization ellipse map. The azimuthally polarized beam is then focused by an axicon of open angle α=0.5°. the electric field components of the axicon focus field can be calculated using the diffraction integrals given in Chapter 2, Section 2.4 by substituting δ=90° for azimuthal polarization and m=1 for the order of the vector beam. The diffraction integrals are:

$$E_x(\rho,\beta,z) = \frac{-izexp(ikr)}{\lambda r^2}\int_0^R d\rho_0\,(\rho_0^1/1)(2\,\rho_0^2/\omega_0^2)\,exp(\rho_0^2/\omega_0^2 - ik\vartheta\rho_0 + ik\rho_0^2/2r)\,(\pi(-i)iJ_1(\eta)\,exp[i\beta] + \pi(i)i^{-1}J_{-1}(\eta)\,exp[-i\beta]) \quad (4.1a)$$

$$E_y(\rho,\beta,z) = \frac{-izexp(ikr)}{\lambda r^2}\int_0^R d\rho_0\,(\rho_0^1/1)(2\,\rho_0^2/\omega_0^2)\,exp(\rho_0^2/\omega_0^2 - ik\vartheta\rho_0 + ik\rho_0^2/2r)\,(\pi iJ_1(\eta)\,exp[i\beta] + \pi i^{-1}J_{-1}(\eta)\,exp[-i\beta]) \quad (4.1b)$$

$$E_z(\rho,\beta,z) = \frac{-iexp(ikr)}{\lambda r^2}\int_0^R d\rho_0\,(\rho_0^1/1)(2\,\rho_0^2/\omega_0^2)\,exp(\rho_0^2/\omega_0^2 - ik\vartheta\rho_0 + ik\rho_0^2/2r)\,(\pi i(-i)J_1(\eta)\,exp[i(2)\beta]$$

$$+\rho\pi i^{-1}J_{-1}(\eta) \qquad (4.1c)$$

The integration is performed numerically from which we find that the longitudinal electric field component is 10^7 times smaller than the transverse component and so can be neglected, leaving the beam a purely transverse azimuthally polarized Bessel-Gauss beam. The opaque obstruction is placed after the BG beam is fully formed (in the middle of the propagation-invariant region) and the Stokes parameters are measured after the obstruction at regular intervals along the propagation. Fig .4.6 shows the intensity and polarization ellipse orientation map of the direct, obstructed and then reconstructed Bessel-Gauss beam at different distances from the opaque wire obstruction. It is seen from our experimental result that the azimuthally-polarized Bessel-Gauss beam completely reconstructs both its intensity and the polarization structure after 18 cm from the partial opaque obstruction. This emphasis that the self-healing property of this class of beams is not limited only to the intensity but extends to the polarization domain as well.

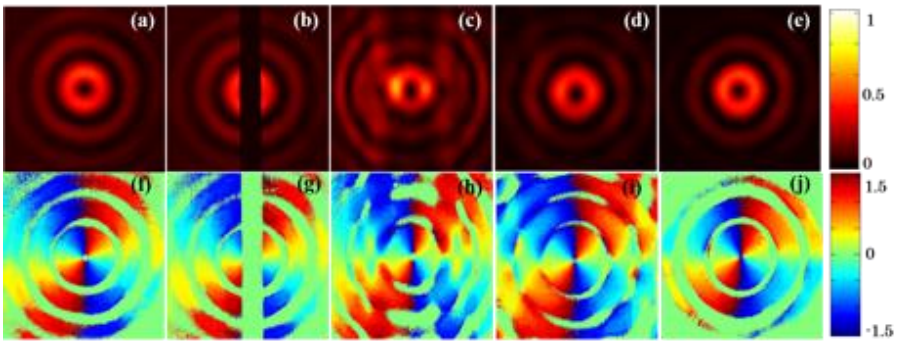

Fig. 4.6 (a)-(e) Intensity of the BG beam at different propagation distances before, at and after the opaque obstruction; (f)-(j) corresponding polarization ellipse orientations; (a) and (f) for the direct beam; (b) and (g) at obstruction plane; (c) and (h) 6cm; (d) and (i) 12 cm; (e) and (j) 18 cm away from the obstruction.

4.4 Self- reconstruction of polarization singular beams

A complete reconstruction of any optical beam means the reconstruction of all three aspects which define an optical beam: amplitude, phase and polarization. This requirement demands that the optical beam can show easily measurable and well-identifiable changes in the individual or collective changes of these three parameters upon partial obstruction. A unique combination of two orthogonal

circular polarized beams with topological charges $l = 0$ and ± 1 results in an optical beam with a polarization singular C-point surrounded by characteristically organized polarization ellipses either in a star or lemon type formation and a L-line singularity at the boundary where the intensity of the two beams are equal. The C-point is a point in the beam cross-section where the orientation of the major axis of the polarization ellipse is undefined and L-line is where its ellipticity is undefined [FODP08, Freu02]. The orientation of the polarization ellipse pattern is determined by the phase difference between the two superposing beams. This kind of complex transverse electric beam field structure can be achieved in Bessel-Gauss beams if orthogonal circularly polarized J_0 and J_1 beams are superposed. The field interference between orthogonal circularly polarized J_0 and J_1 beams has additional advantage that any small changes in the constituent beam's amplitude, phase or polarization shows well-distinguishable change in the overall polarization characteristics of the resultant beam. Thus such structured beams make it easy to experimentally measure the changes via imaging Stokes polarimetry of the resultant beam using a simple quarter-wave plate, polarizer and CCD arrangement. The L-singularity contour, the locus of all points with linear polarization state, is characterised by the amplitude ratios between the constituent orthogonal circularly polarized beam fields. Also, the L-contour can be easily calculated by taking the fourth Stokes parameter $S_3 = 0$[FODP08]. For the present case the L-contours are concentric rings in the on-axis superposition and the ring radius changes with the amplitude ratio between the constituent beams. Any change in on-axis superposition can be experimentally detected as a change in the eccentricity of the L-contours. In addition, any modification in the phase difference between the constituent beams results in rotation of the polarization singular pattern[PKMV12] and changes in wave-front of the constituent beams results in the distortion or even vanishing of the definite polarization singular pattern, which is a '*star*' type in the present case. Fig. 4.7 shows the versatility of the polarization singular patterns as a measuring tool, where the amplitude, phase and polarization is combined in a unique way. Any change in amplitude, phase and polarization state of the component beams results in changes in the polarization singular pattern. The polarization singular pattern showed n Fig. 4.7 is formed by the superposition of orthogonally circularly polarized J_1 and J_0 Bessel beams. Any changes in the amplitude of the superposing beams results in the change of L-contour which is the locus of linearly polarized states. The L-contour forms where the amplitude of the superposing beams are equal. The relative phase difference between the

component beams results in the rotation of the polarization singular pattern. The white dotted line is the L-contour and the centre pattern is the *star* type polarization singular pattern. Fig. 4.7(a) the amplitude ration of the J_0 and J_1 beams is unity ($J_1/J_0=1$) and the phase difference between the beams is set to be π. In the case of Fig 4.7(b) the amplitude ratio is changed to 0.5 and the relative phase difference to $\pi/2$. This makes noticeable change in the radius of the L contour and the orientation of the *star* pattern. The *star* pattern is rotated by an angle $\pi/2$ in Fig. 4.7(b). Similar changes can be observed in Fig. 4.7(c) where the amplitude ration is changed to 0.25 and the relative phase difference to 0.

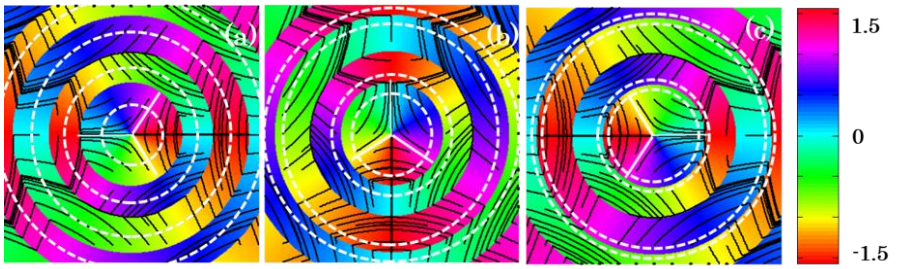

Fig. 4.7 Simulation results for the star pattern (at the centre) with the L-contours (dotted line) formed by the superposition of orthogonal circularly polarized J0 and J1 beams with different amplitude ratios and phase difference between the constituent beams: (a) amplitude ratio (J_1/J_0)=1 and phase difference between J_1 and $J_0=\pi$; (b) $J_1/J_0=0.5$ and phase difference=$\pi/2$; (c) $J_1/J_0=0.25$ and phase difference=0.

4.4.1 Opaque obstruction

Fig. 4.8 shows the schematic of the experimental setup used for the demonstration of self-reconstruction characteristics of the polarization-singular Bessel-Gauss beams beyond a partial obstruction. In the vortex beam generator linearly polarized light from the He-Ne laser after passing through a Quarter-wave plate (QWP) oriented at 45° becomes right circularly-polarized (RCP) light which is then coupled using a 20x microscope objective lens (Olympus) as skew-off-axis beam into the horizontally-held 37.4 cm long two-mode optical fiber (TMF). The launch conditions are adjusted such that the RCP input beam excites both the fundamental and first higher-order vortex modes simultaneously but with orthogonal circular polarization resulting in the star type polarization singular pattern of interest to us here.

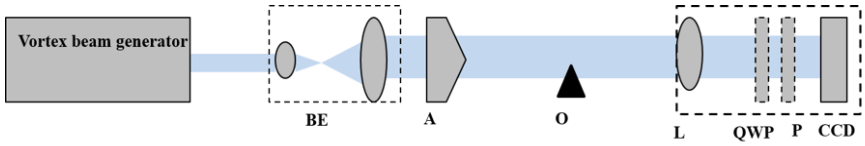

Fig. 4.8 Schematic of the experimental setup for the study of self-reconstruction of polarization singular beams

The collimated fiber output focused by the axicon is partially obstructed using an opaque object which is a 0.375 mm diameter metallic wire placed 20 cm away from the axicon. At this distance the polarization singular pattern with star-type polarization singularity structure is completely formed. The intensity and Stokes images are measured at the obstruction plane using a magnifying lens and CCD camera system with a QWP and polarizer combination in front of it. The opaque metallic wire obstruction is placed precisely using a two dimensional translation stage such that the C-point in the beam cross-section is completely blocked. First the imaging lens focuses the obstruction plane onto the CCD and the Stokes parameters of the obstructed beam is measured. Then the CCD and the imaging lens system mounted on a rail are moved along the propagation direction keeping the distance between the CCD and the imaging lens fixed same to keep the magnification a constant. Fig. 4.9 shows the direct beam, partially obstructed beam and the beam after partial obstruction at different distances from the obstruction plane with the polarization ellipse orientation and stream line plots. Fig. 4.9 clearly shows that the opaque obstruction blocks the C-point in the Bessel-Gauss beam and the C-point with the polarization singular pattern reconstructs itself completely at a plane which is 25 cm away from the obstruction. Even though the C-point reconstructs earlier, the intensity the polarization ellipse orientation and the stream lines reconstruct completely only at 25 cm as shown Fig. 4.9. For the polarization singularity to reconstruct itself after being obstructed, the two constituent beams have to reconstruct to the same amplitude, phase and polarization characteristics of the parent beam. At 25 cm away from the obstruction the Bessel-Gauss beam completely reconstructs to the characters of the parent beam.

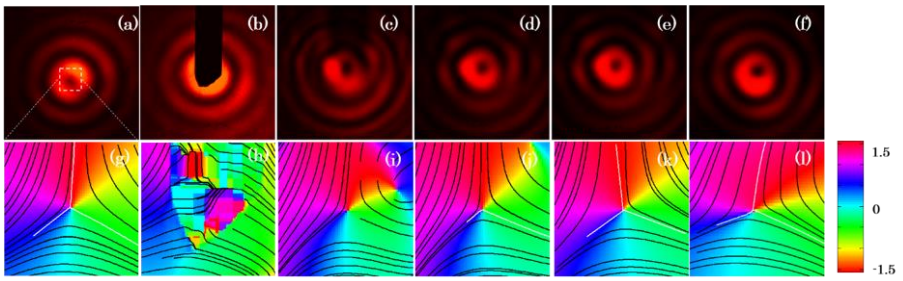

Fig.4.9 (a)-(f) Intensity distribution of BG beam at different distances from the opaque obstruction and (g)-(l) corresponding polarization ellipse orientations and stream line: (a) and (g) direct beam; (b) and (h) at obstruction plane; (c) and (i) at 6cm; (d) and (j) at 12 cm; (e) and (k) at 18 cm; (f) and (l) at 25 cm from the obstruction.

4.4.2 Phase obstruction

The phase of the beam alone can be partially disturbed by delaying a part of the beam by inserting a thin glass plate of thickness 150 μm using a two dimensional translation stage. The intensity and the polarization structure of the beam at the obstruction plane is measured using the imaging lens and CCD arrangement with QWP-polarizer combination before it. The polarization structure around the C-point is studied from the spatially-resolved Stokes polarimeter measurements. Fig. 4.10 shows the direct beam, obstructed beam and the reconstructed beam intensity along with the polarization ellipse orientation maps, which shows an almost complete self-reconstruction of the beam beyond phase only obstruction.

4.4.3 Polarization modification

Next the state of polarization of the polarization singular Bessel-Gauss beam is locally changed using a polarizer wedge placed carefully to obstruct the C-point. As this filters the polarization orientation of the C-point and the nearby areas resulting in the removal of the C-point and modification of the polarization ellipse orientations nearby. As mentioned earlier the intensity and the polarization structure at the obstruction plane is studied first, using the imaging lens and CCD system. The evolution of the polarization structure of the beam after the polarizer obstruction is studied by measuring the Stokes parameter at regular intervals from the obstruction. Fig. 4.11 shows the polarization pattern near to the C-point for the direct beam, beam obstructed by polarizer wedge and the reconstructed beam after the obstruction. From the results it is clear that though the polarizer wedge completely changes the state of polarization of the Bessel-Gauss beam, in the

obstruction plane by removing the C-point from the beam and also modifying all the polarization ellipses to orient along the polarizer axis direction. Still at 25 cm away from the obstruction the polarization singular star pattern is reconstructed as in the parent beam. This shows that the polarization singular patterns in the Bessel-Gauss beam is unaffected by local polarization disturbances.

A HWP wedge is also used to locally modify the state of polarization of the Bessel-Gauss beam combination. A HWP wedge is inserted carefully into the beam at 20 cm from the axicon using a translation stage. The HWP wedge orientation is placed such that the C-point index is inverted due to the interchanging of the polarization states between the J_0 and J_1 beams from the RCP to LCP and vice-versa. The HWP wedge locally convert the RCP J1 and LCP J_0 to LCP J_1 and RCP J_0 resulting in the change of 'star' to 'lemon' type polarization singularity pattern. For the lemon type of polarization singularity the polarization ellipses around the C-point rotate by π rad in the clock wise direction, thus the C-point index for lemon become +1/2. This even changes the direction of energy flow within the Bessel-Gauss beam locally. The intensity and the polarization of the beam at the obstruction plane is first measured via the Stokes parameters. Further, the evolution of the beam after the obstruction is also studied by measuring the polarization structure of the beam at regular intervals after the obstruction along the propagation. Fig. 4.12 shows the direct beam, beam at the obstruction plane and the reconstructed beam with the corresponding polarization ellipse orientation map and streamlines. Though the HWP changes the polarization structure of the beam locally by interchanging the state of polarization of the constituent Bessel-Gauss beams to change a star to lemon pattern as shown, locally changing the polarization ellipse orientation around the C-point. But after the obstruction by 25 cm the beam heals its local polarization disturbance, the C-point index inversion and also the diffraction caused by the edges of the HWP as shown in Fig. 4.12. Thus the Bessel beam is also immune to local polarization changes in addition to reconstructing beyond

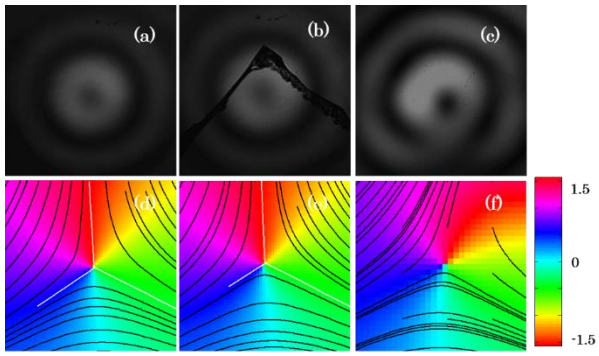

Fig. 4.10 (a)-(c) Intensity distributions and (d)-(f) polarization ellipse orientations with and without plane glass plate obstruction and its reconstruction; (a) and (d) direct beam; (b) and (e) at obstruction plane; (c) and (f) reconstructed beam at 25 cm from the obstruction.

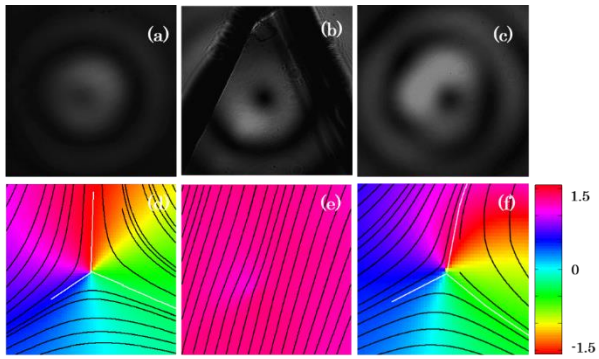

Fig. 4.11 (a)-(c) Intensity distributions and (d)-(f) polarization ellipse orientation for polarizer obstruction; (a) and (d) direct beam; (b) and (e) at obstruction plane; (c) and (f) reconstructed beam at 25 cm from the obstruction plane.

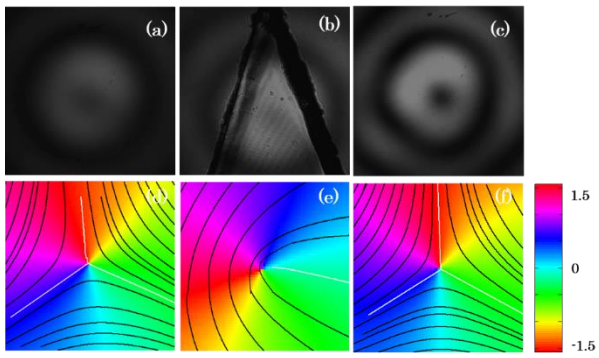

Fig. 4.12 (a)-(c) Intensity distributions and (d)-(f) polarization ellipse orientation map with streamlines for HWP wedge obstruction; (a) and (d)direct beam; (b) and (e) at obstruction plane; (c) and (f) reconstructed beam at 25 cm from the obstruction.

opaque and polarization obstructions. The polarization singular patterns embedded in Bessel-Gauss beams are relentless to the local phase and polarization disturbances.

Summary

The self-reconstruction property of Bessel-Gauss beams is experimentally studied. Beyond the well-studied intensity reconstruction after a partial obstruction the Bessel-Gauss beams can also reconstruct its polarization and phase structure after the corresponding obstructions. The reconstruction of Bessel-Gauss beam is studied using azimuthally-polarized and polarization singular beams where the amplitude, phase and polarization aspects of the beam are tied together. The polarization singular beams also have the advantage that the reconstruction aspects of the beam can be measured using imaging Stokes polarimetry. All these results indicated that a complete 3D reconstruction of the Bessel-Gauss beams beyond a partial obstruction.

References

[AMIC07] ANGUIANO-MORALES, MARCELINO ; MARTÍNEZ, AMALIA ; ITURBE-CASTILLO, M. DAVID ; CHÁVEZ-CERDA, SABINO ; ALCALÁ-OCHOA, N.: Self-healing property of a caustic optical beam. In: *Applied Optics* Bd. 46 (2007), Nr. 34, S. 8284–8290. — 00014

[BBHN03] BOUHELIER, A. ; BEVERSLUIS, M. ; HARTSCHUH, A. ; NOVOTNY, L.: Near-Field Second-Harmonic Generation Induced by Local Field Enhancement. In: *Physical Review Letters* Bd. 90 (2003), Nr. 1, S. 013903. — 00365

[BiZh98] BIN, ZHAO ; ZHU, LI: Diffraction Property of an Axicon in Oblique Illumination. In: *Applied Optics* Bd. 37 (1998), Nr. 13, S. 2563–2568. — 00044

[BoWC98] BOUCHAL, Z ; WAGNER, J ; CHLUP, M: Self-reconstruction of a distorted nondiffracting beam. In: *Optics Communications* Bd. 151 (1998), Nr. 4–6, S. 207–211. — 00252

[BSDC08] BROKY, JOHN ; SIVILOGLOU, GEORGIOS A. ; DOGARIU, ARISTIDE ; CHRISTODOULIDES, DEMETRIOS N.: Self-healing properties of optical

Airy beams. In: *Optics Express* Bd. 16 (2008), Nr. 17, S. 12880–12891. — 00197

[FaRo12] FAHRBACH, FLORIAN O. ; ROHRBACH, ALEXANDER: Propagation stability of self-reconstructing Bessel beams enables contrast-enhanced imaging in thick media. In: *Nature Communications* Bd. 3 (2012), S. 632. — 00046

[FaSR10] FAHRBACH, FLORIAN O. ; SIMON, PHILIPP ; ROHRBACH, ALEXANDER: Microscopy with self-reconstructing beams. In: *Nature Photonics* Bd. 4 (2010), Nr. 11, S. 780–785. — 00117

[FODP08] FLOSSMANN, FLORIAN ; O'HOLLERAN, KEVIN ; DENNIS, MARK R ; PADGETT, MILES J: Polarization singularities in 2D and 3D speckle fields. In: *Physical review letters* Bd. 100 (2008), Nr. 20, S. 203902. — 00046 PMID: 18518537

[Freu02] FREUND, ISAAC: Polarization singularity indices in Gaussian laser beams. In: *Optics Communications* Bd. 201 (2002), Nr. 4–6, S. 251–270. — 00068

[GMMS02] GARCÉS-CHÁVEZ, V. ; MCGLOIN, D. ; MELVILLE, H. ; SIBBETT, W. ; DHOLAKIA, K.: Simultaneous micromanipulation in multiple planes using a self-reconstructing light beam. In: *Nature* Bd. 419 (2002), Nr. 6903, S. 145–147. — 00575

[GoGo11] GOLDSTEIN, DENNIS ; GOLDSTEIN, DENNIS H.: *Polarized Light, Revised and Expanded* : CRC Press, 2011. — 00520 — ISBN 9780203911587

[HeRT13] HERMOSA, N. ; ROSALES-GUZMÁN, C. ; TORRES, J. P.: Helico-conical optical beams self-heal. In: *Optics Letters* Bd. 38 (2013), Nr. 3, S. 383–385. — 00005

[JaBF05] JAROSZEWICZ, ZBIGNIEW ; BURVALL, ANNA ; FRIBERG, ARI T.: Axicon - the Most Important Optical Element. In: *Optics and Photonics News* Bd. 16 (2005), Nr. 4, S. 34–39. — 00058

[McDh05] MCGLOIN, D ; DHOLAKIA, K: Bessel beams: Diffraction in a new light. In: *Contemporary Physics* Bd. 46 (2005), Nr. 1, S. 15–28. — 00388

[NBYB01] NOVOTNY, L. ; BEVERSLUIS, M. R. ; YOUNGWORTH, K. S. ; BROWN, T. G.: Longitudinal Field Modes Probed by Single Molecules. In: *Physical Review Letters* Bd. 86 (2001), Nr. 23, S. 5251–5254. — 00421

[PKMV12] PHILIP, GEO M. ; KUMAR, VIJAY ; MILIONE, GIOVANNI ; VISWANATHAN, NIRMAL K.: Manifestation of the Gouy phase in vector-vortex beams. In: *Optics Letters* Bd. 37 (2012), Nr. 13, S. 2667–2669. — 00006

[RLMM12] RING, JAMES D. ; LINDBERG, JARI ; MOURKA, ARETI ; MAZILU, MICHAEL ; DHOLAKIA, KISHAN ; DENNIS, MARK R.: Auto-focusing and self-healing of Pearcey beams. In: *Optics Express* Bd. 20 (2012), Nr. 17, S. 18955–18966. — 00018

[TaYa00] TANAKA, TAKUO ; YAMAMOTO, SADAHIKO: Comparison of aberration between axicon and lens. In: *Optics Communications* Bd. 184 (2000), Nr. 1–4, S. 113–118. — 00048

[ThJF03] THANING, ANNA ; JAROSZEWICZ, ZBIGNIEW ; FRIBERG, ARI T.: Diffractive Axicons in Oblique Illumination: Analysis and Experiments and Comparison with Elliptical Axicons. In: *Applied Optics* Bd. 42 (2003), Nr. 1, S. 9–17. — 00047

[VaPi02] VARIN, C. ; PICHÉ, M.: Acceleration of ultra-relativistic electrons using high-intensity TM01 laser beams. In: *Applied Physics B* Bd. 74 (2002), Nr. 1, S. s83–s88. — 00065

[VyKS11] VYAS, SUNIL ; KOZAWA, YUICHI ; SATO, SHUNICHI: Self-healing of tightly focused scalar and vector Bessel?Gauss beams at the focal plane. In: *Journal of the Optical Society of America A* Bd. 28 (2011), Nr. 5, S. 837–843. — 00020

[WuWC14] WU, GAOFENG ; WANG, FEI ; CAI, YANGJIAN: Generation and self-healing of a radially polarized Bessel-Gauss beam. In: *Physical Review A* Bd. 89 (2014), Nr. 4, S. 043807. — 00000

CHAPTER

5

Fabrication of Fiber Micro-axicon and Sculpting Propagation-invariant beam

Contents

5.1 Introduction

Bulk axicons are always in the front line of optical research from the time of its introduction more than 60 years ago[Mcle60] mainly due to its capability to generate propagation-invariant Bessel-Gauss beams with an extended depth of focus(DOF)[ShWi78,DuME87]. This optical element finds use in several applications such in high-order harmonic generation[PSSJ99], nonlinear optics[WuHe93], sub-wavelength focusing[KSOS11], material processing[MJMM01] etc., though the optical alignment with the axicon is always very tricky especially under non-paraxial conditions. The optical alignment with axicon systems has to be done very carefully because even a small misalignment can lead to astigmatism[ASTK92, BKGJ07,TaYa00] related issues especially when dealing with high-numerical aperture axicons. Micro-axicons fabricated in the extremity of an optical fiber can help in designing compact and flexible experimental systems. The extra flexible, high efficiency and miniature combination of optical fiber and micro-axicon can further extend the applications range of axicon. The use of micro-axicon has been recently demonstrated in the manipulation of microscopic objects in liquids and in tweezers[MoMB08, Vgar02], optical tomography[TMCL09], and laser breakdown spectroscopy[HYSW08]. The micro-axicons can also be used as optical probes in near field scanning microscopy for luminescence detection from semiconductor quantum dots[EaJA03,YNHN06], mapping of plasmonic fields[NoHe06] and nano-structuring of solids[KKVS13].

Recently it has been experimentally demonstrated that optical vector-vortex beams can be generated from two-mode optical fiber by adjusting the input polarization and launch conditions[ViIn09]. It is also known that Bessel-Gauss beams can be generated by focusing Laguerre-Gauss beams by an axicon[ArDh00]. So a compact source of vector Bessel beam can be achieved if one can fabricate a micro-axicon at the tip of the optical fiber. It also gives the freedom to generate different types of intensity,phase and polarization structured light beams by mode selection and by varying the physical parameters of the micro axicon such as the apex angle, tip radius and the flat top size . In an effort towards designing a compact source for the generation of structured light beams, selective chemical etching method for optical fibers with different core-cladding dopant and size ratios is calibrated to obtain the optimum micro-axicon parameters for the generation of special beams reported here. Of all the different methods available

for the fabrication of fiber micro-axicon we preferred the selective chemical etching method due to its high reproducibility and the quality of the resulting micro-axicons. This chapter discusses in detail the merits and demerits of different fiber micro-axicon fabrication methods, the experimental calibration of the selective chemical etching method for the fabrication of concave and convex micro-axicons and subsequently sculpting of propagation-invariant beams using the fabricated micro-axicons.

5.2 Methods for fabricating fiber micro-axicon

The methods for micro-axicon fabrication can be broadly classified into two: mechanical and chemical methods. Mechanical methods involve physically changing the shape of the optical fiber tip either using micro machines or by heating and pulling. Chemical methods on the other hand involve chemically etching the silica based optical fiber using a strong acid such as Hydro Fluoric (HF) acid. An appropriate method can be chosen considering the intended use and the required physical parameters of the micro-axicon.

5.2.1 Mechanical methods

Heating and pulling and mechanical polishing are the two techniques in this category. Though the reproducibility of around 80% of these methods are reasonable the flexibility (fabricating different shape and size) of micro-axicons are limited. Heating and pulling gives good surface quality but the range of apex angle one can achieve using this method is limited. On the other hand with the mechanical polishing method the surface smoothness of the fabricated micro-axicon is not good.

5.2.1.1 Heating and pulling

In the heating-and-pulling technique[Betz93, Ohts04], a silica-based optical fiber is heated using a CO_2-gas laser and pulled apart by a computer controlled micropipette puller as shown in Fig. 5.1. One can fabricate a tapered fiber with an apex diameter of 50 nm and a cone angle of 20–40° by using a commercial micropipette puller. This tapering method can be used with any type of optical fiber with a diameter of more than 125 μm by suitably adjusting the laser power, the strength of the pull, and the delay time between the end of the heating and the beginning of the pulling.

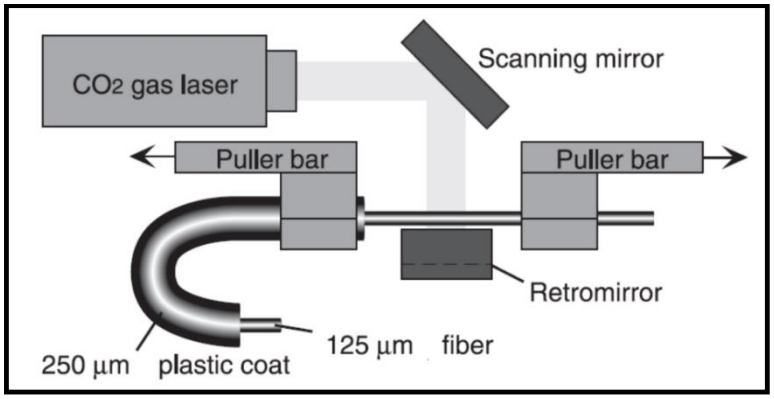

Fig. 5.1 Schematic of the heating and pulling technique for the fabrication of fiber micro-axicons[Ohts04]

It is however, difficult to control the cone angle while maintaining the apex diameter. These sharp fiber tips find their application as light collecting probe in Scanning Near-field Optical Microscopy (SNOM) [Ohts04].

5.2.1.2 Mechanical polishing method

In mechanical polishing method the optical fiber is fixed on a system which can rotate the fiber with respect to its axis. Fig. 5.2 shows the schematic of the setup used for micro axicon fabrication by mechanical polishing. The rotation control is done by an electric motor and belt arrangement[GSSI07].

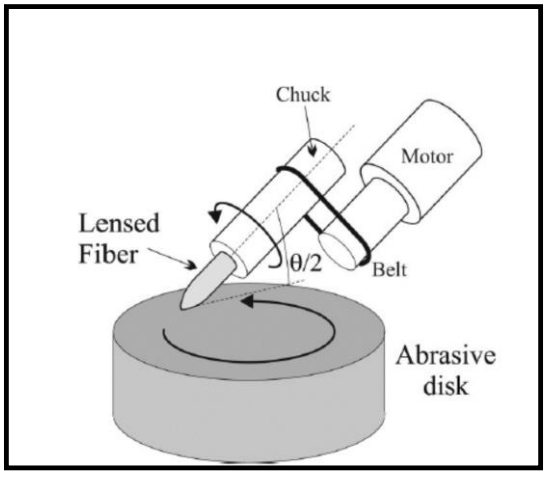

Fig. 5.2 Schematic of the setup used for micro-axicon fabrication via mechanical polishing[GSSI07].

The fiber is given a small tilt angle using a rotation stage and the apex angle of the micro-axicon is decided by the tilt angle. The fiber is in contact with a spinning disk of grinding and polishing material for the micro-axicon fabrication. Though the range of the apex angle that can be obtained by this method is large, the surface quality due to vibrations in the disc and the large size of diamond abrasive particles (around 1 μm) used are a major concern, especially when dealing with high end applications where the output beam quality cannot be compromised.

5.2.2 Chemical methods

Chemical methods involve the use of chemical for etching of the silica based optical fiber using a strong acids such as Hydro fluoric (HF) acid to fabricate micro-axicons [Ohts04]. Two different types of chemical etching methods are widely used for the generation of micro-axicon: meniscus etching and selective chemical etching. While the meniscus etching method makes use of the viscosity and capillary effects for the generation of micro-axicons the selective chemical etching method utilizes the difference in the chemical reaction etch rates of the germanium dioxide (GeO_2) doped core and the pure silica cladding of the optical fiber. Out of these two the selective chemical etching gives almost 100% reproducibility and a wide range of apex angles are also achievable. With the meniscus etching method the device surface smoothness and reproducibility are less since the viscosity and capillary forces depend strongly on the environment parameters such as temperature where the experiment is carried out.

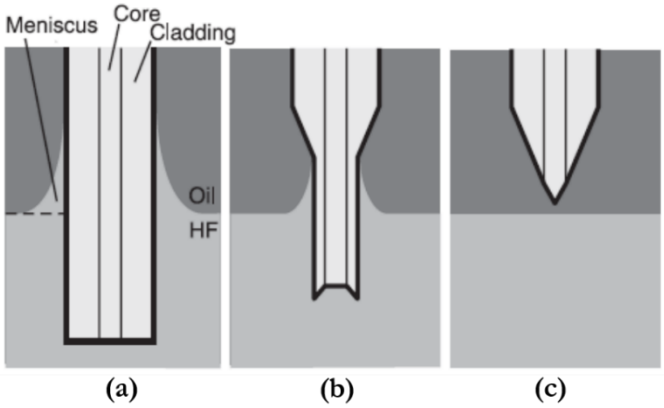

Fig. 5.3 Schematic of the meniscus etching process for the fabrication of micro axicon in an optical fiber;(a) start of the process ;(b) midway of the process and(c) etching process stops

5.2.2.1 Meniscus Etching

Fig.5.3 shows the schematic of the meniscus etching method for the fabrication of fiber micro-axicons. First, the polymer covering of the optical fiber is removed and cleaned and the bare fiber is set in the etchant solution containing HF acid with organic oil such as silicon oil layer in the top surface[Turn84, HGWK93, HoDS95, SMOS96]. The oil layer forms a meniscus and also prevent the evaporation of the highly volatile HF acid which can be hazardous and will also change the etch rate. The optical fiber gets etched into a taper because the height of the meniscus depend on the diameter of the fiber and the etching eventually stops once the taper is fully formed. Using the meniscus etching method one can fabricate micro-axicons of apex angle 30^{o}-40^{o}. After the formation of the micro-axicon the tip of the optical fiber is cleaned using H_2SO_4 to remove the oil completely.

5.2.2.2 Selective chemical etching

Selective chemical etching method is based on the difference in the reaction rated between the GeO_2 doped silica core and pure silica cladding of the optical fiber. By using the selective-etching method to a 3-5 mole percentage GeO_2-doped fiber, one can obtain micro-axicons with a small apex diameter of less than 10 nm. By varying the concentration of etching solution, a combination of hydrofluoric (HF) acid and ammonium fluoride (NH_4F), the cone angle can be controlled over a wide region from 20^{o} to 180^{o} with an apex diameter less than 20 nm [Ohts04]. Furthermore, the selective etching is the most highly reproducible technique among all the fiber tapering techniques. This method can be applied to any single, few and multi-mode fiber produced by axial deposition techniques.

The fiber is first cleaved very close to the plastic jacket and dipped perpendicular in the etchant solution which constitutes HF (50%), NH_4F (40%) and de-ionised water in specific volume ratios[JOYP92, MaMO95, Toma93, MoOh98, MSSK98]. The equations given below are the chemical reactions involved in the etching process:

$$\mathbf{SiO_2 + 4HF + 2NH_4F \longrightarrow (NH_4)_2SiF_6 + 2H_2O}$$
$$\mathbf{GeO_2 + 4HF + 2NH_4F \longrightarrow (NH_4)_2GeF_6 + 2H_2O}$$

Typically, the solubility of $(NH_4)_2SiF_6$ is less than that of $(NH_4)_2GeF_6$. So if more NH_4F is present in the etchant solution, more and $(NH_4)_2SiF_6$ precepitate in the etchant solution and leads to the decreseing of the cladding etch rate compared to

the core and this kind of a situation will lead to negative cone in the fiber tip and if NH_4F volume is less then the reaction will result in a positive cone. By changing the volume ratios of the components in the etchant solution we are able to get a variety of positive and negative cones with different cone angle and cone height in the fiber tip.

Tip formation Analysis:

An optical fiber is a cylindrically symmetric system in which the solubility or the etch rate depends only of the radial distance 'ρ' from the centre of the core. Let $S(\rho)$ be the dissolving rate at a distance ρ from the core. Then it can be represented mathematically as given in[PuDa00]:

$$\frac{\partial \rho}{\partial t} = -S(\rho) \tag{5.1}$$

$$S(\rho) = S_{co}; 0 < \rho \leq d_{co} \,\&\, S(\rho) = S_{cl};\ d_{co} < \rho \leq\ d_{cl} \tag{5.2}$$

Where '*co*' and '*cl*' denote the core and cladding respectively of the fiber. The height of the tip structure generated after time t can be expressed as [PuDa00]:

$$h(t) = (S_{cl} - S_{co})t, \quad 0 \leq t \leq t_{min} \tag{5.3}$$

where t_{min} is the minimum time required for the tip formation. Since the fiber is a cylindrical system the differential etching process will naturally result in a conical structure. The generated cone angle θ can be represented as[PuDa00]:

$$tan\left(\frac{\theta}{2}\right) = \frac{S_{co}}{(S_{cl} - S_{co})} \tag{5.4}$$

The final tip height and the etch time t_{min} can be written as[PuDa00]:

$$h_{tip} = \frac{d_{co}}{2tan(\theta/2)} = \frac{d_{co}(S_{cl} - S_{co})}{2S_{co}} \tag{5.5}$$

$$t_{min} = \frac{h_{tip}}{(S_{cl} - S_{co})} = \frac{d_{co}}{2S_{co}} \tag{5.6}$$

From the formalism it can be understood that the difference in etch rates of cladding and core can generate a conical structure symmetric with respect to the axis of the core. Also, Equ. (5.2) & (5.4) shows that the height of the cone is

positive if the cladding etch rate is more than that of the core representing a convex micro-axicon. On the other hand, if the cladding etch rate is smaller compared to that of core, the process will result in a cone with negative height, a concave micro-axicon.

5.3 Etch rate calibration for selective chemical etching

For the controllable fabrication of micro-axicons in the core of an optical fiber first the etching rates of the core and cladding should be understood thoroughly. Once the reaction rates are known, one can predict the time required and the volume ratios of the etching solution required for the fabrication of a specific micro-axicons. For studying the etching rates, the etchant solution is prepared by mixing different volume ratios of HF (50%), NH_4F (40%)-the buffer- and de-ionized water as (1: x: 1) in a Teflon vial and the cleaved end of the optical fiber is dipped in it. It was also noted that if the etching was carried out with the polymer cover, the generated micro-axicons are relatively smoother than that with bare fiber methods. The fiber is taken out of the etchant solution at fixed time intervals and cleaned in de-ionized water and again in an alkali solution to remove the acid remaining on the surface of the optical fiber. This fiber is then imaged using a Scanning electron microscope (SEM) and the etch rate of the cladding is calculated from the decrease in thickness of the cladding and the time taken to etch. Fig. 5.4 shows the SEM images of the optical fibers etched in a solution of volume ratio 1:8:1 (x=8) at different timings. The images clearly show the cladding thickness decreases with time and a micro-axicon is being formed at the tip. Fig 5.5 shows the etch rate plots for cladding for different etchant solution volume ratios, calculated from the decrease in the cladding thickness.

5.3.1 Concave and convex micro-axicons

According to the Equ. (5.2-5.4) the etching rate can be controlled such that one can produce a concave or convex micro-axicon in the core of the optical fiber. It is found from the experiments that the volume ratio of HF/NH_4F =1.7 is the critical point, below which the etching process leads to a convex micro-axicon and above which the process results in concave micro-axicon. In other words, the etching rate of the core and the cladding is equal if the etchant solution volume ratio is 1.7. By Equ.(5.3) the cone angle also depends on the reaction rates of the core and cladding. So by changing the volume ratios one can effectively change the

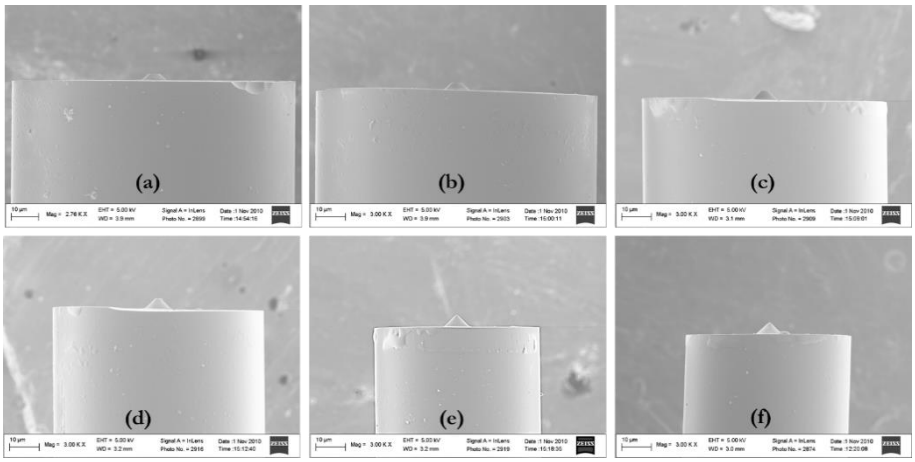

Fig. 5.4 SEM images of the optical fiber etched in an etchant solution of HF:NH4F:DW=1:8:1 and removed after;(a) 90 min;(b) 135 min; (c) 180 min; (d) 225 min; (e) 285 min and (f) 300 min.

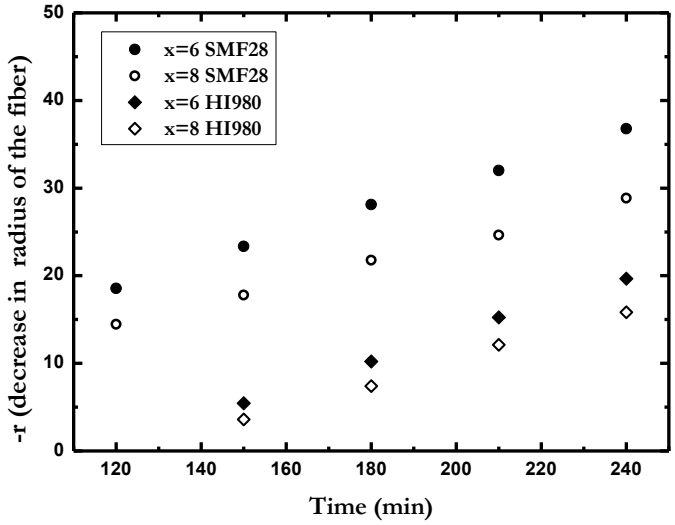

Fig. 5.5 Decrease in radius of the SMF28 and HI 980 optical fibers due chemical etching with time.

micro-axicon apex angles. Fig. 5.6 shows the microscope images of concave micro axicons fabricated in the core of SM28 fiber. Closer inspection of the concave micro-axicons etched fibers, using higher magnification, clearly shows the different angle and depth of the negative cones etched in the fiber tip. Also clear are the difference in the etch angles for the cladding and the core due to the difference in the concentration of the GeO_2 dopant material.

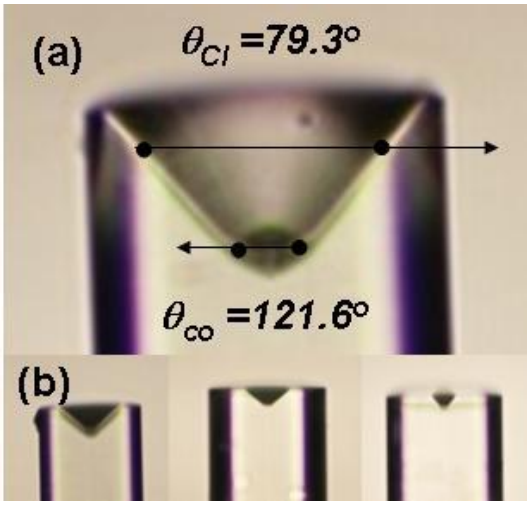

Fig. 5.6 Microscope images of concave micro-axicons etched in the core of the SM28 optical fiber. (a) Magnified image of the concave micro-axicon showing different cone angles in the core and cladding (b) concave micro-axicons with different cone angles obtained using different HF/NH_4F valued etchant solution.

Convex micro-axicons are also fabricated in the tip of optical fiber via selective chemical etching method. The cone angle of the convex axicons are changed in a wide range by changing the volume ratios of the etchant solution. Fig. 5.7 shows the SEM images of different convex micro-axicons obtained using different HF/NH4F valued etchant solution.

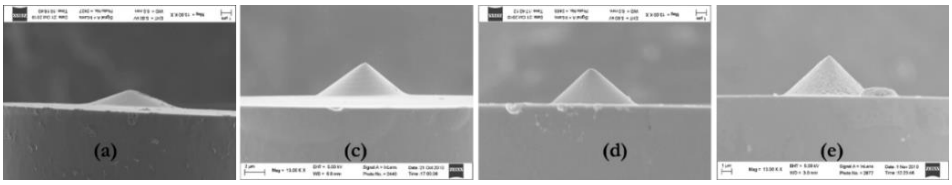

Fig. 5.7 SEM images of the convex micro-axicons fabricated in the tip of SM28 optical fiber for different etchant solution: (a) apex angle 140° with x=0.5; (b) apex angle 105° with x=0.25; (c) apex angle 86° with x=0.166; (d) apex angle 78° with x=0.125.

As mentioned earlier, the tube etching of optical fiber provides very good surface smoothness to the micro-axicons with lesser tip diameter. Using carefully prepared etchant solution and adjusting the reaction timings properly one can reduce the tip diameter to 20-30 nm. Fig. 5.8 shows the magnified SEM image of a micro-axicon fabricated on HI980 fiber whose tip diameter is measured to be 25nm. The tip diameter defines the resolution of the probe in SNOMs.

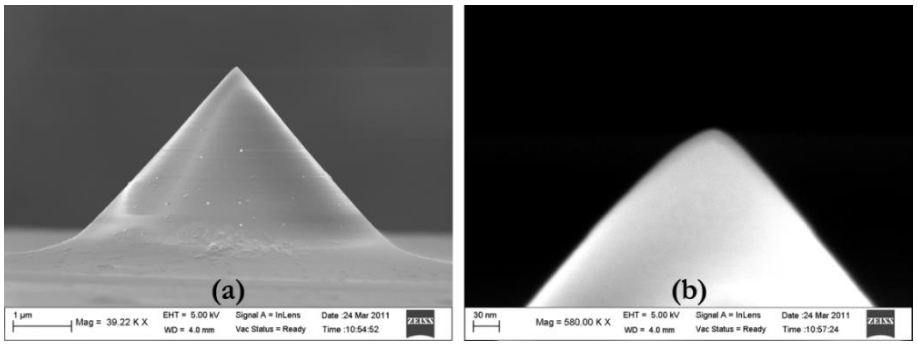

Fig. 5.8 SEM images of convex micro-axicon etched in HI980 fiber with an etchant solution of x=0.125: (a) micro-axicon with apex angle=86°; (b) magnified image of the same micro-axicon showing a tip diameter of 25nm.

5.3.2 Controlling the cladding diameter

In some experimental situations such as cellular transfection[TTCG08], where the stability of the biological system is also important, the cladding diameter also matters. In selective chemical etching method the cladding diameter can be controlled by adjusting the etching timing keeping the apex angle the same. Fig.5.9 shows the micro-axicons etched in SM28 fiber with different cladding diameters but with same apex angles, obtained by adjusting the etching time.

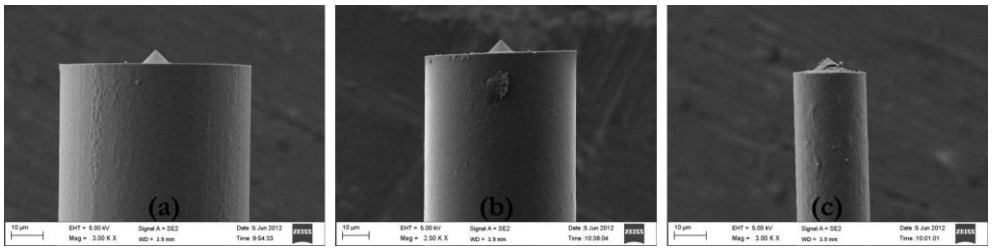

Fig. 5.9 SEM images of micro axicons fabricated in SM28 fiber using an etchant solution of x=0.0833: (a) cladding diameter 60μm and etching time 8hours; (b)cladding diameter 41μm and etching time 10 hours; (c) cladding diameter 21.8μm and etching time 12 hours.

5.4 Sculpting of propagation-invariant beams

The axicon fabricated in the fiber tip can convert the fundamental mode of the optical fiber (Gaussian beam) to a propagating-invariant Bessel-Gauss beam[ASTK92]. So a micro-axicon fabricated at the output tip of an optical fiber with the fundamental mode excited in it should become a source of propagation-

invariant Bessel-Gauss beam. The conversion of a Gaussian beam to a BG beam is studied using the setup shown in Fig.5.10 (a). A micro-axicon is fabricated in the tip of a SM 28 fiber using an enchant solution of volume ratio x=0.125 with an apex angle of 94° by etching for 225 minutes. Flat top cones of different widths can be generated in the core if we remove the fiber before this time. We removed the partially etched fibers at different times to generate different flat top cones in the fiber core. Fig. 5.10 (b) shows the SEM images of fully developed and flat top micro-axicons.

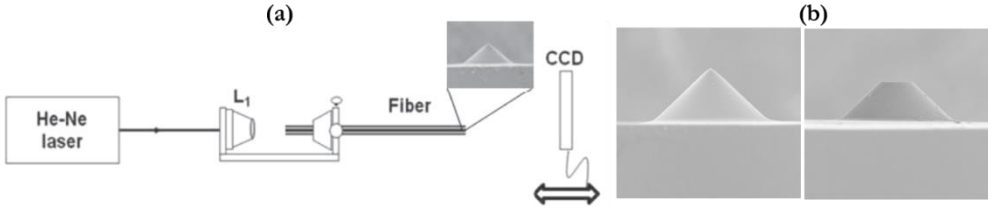

Fig. 5.10 (a) Schematic of the experimental setup used for sculpting propagation invariant beam: (b) SEM images of fully developed and flat top micro-axicons.

A SM630 fiber which is single mode at λ=633 nm is spliced into the SM28 fiber with different micro-axicons to make sure that the fundamental mode is excited in the fiber with the micro-axicon. Unpolarised laser light (λ = 628.3 nm) is launched into the SM630 fiber using a microscope objective lens (4x, NA = 0.10). The output beam from the micro-axicon is imaged using a CCD camera connected to a computer through IEEE port. The free-space propagation characteristic of the output beam is measured by imaging the output beam at different planes along 'z' by moving the CCD mounted on a translation stage. The fiber with a flat topped cone modifies the Gaussian beam intensity significantly leading to a Bessel intensity distribution modulated by Gaussian envelope (Fig. 5.11b). The propagation characteristics of the beams generated by the different cones shows propagation-invariant character up to some distance and this propagation-invariant distance increases with decrease in the flat top size, with the fully-developed cone giving maximum non-diffracting range. Fig 5.11(c) shows the plot between the Rayleigh range of the beam and the dimension of flat-top of the axicon and Fig. 5.11 (d) shows the propagation of the Bessel-Gauss beam generated using the fully developed micro-axicon. The Rayleigh range of the central spot beam extends up to 528μm with the central spot size of 44 μm. thus a Gaussian beam is converted into a propagation invariant BG beam by continuously decreasing the flat-top size of the micro-axicon chemically etched in tip of an optical fiber.

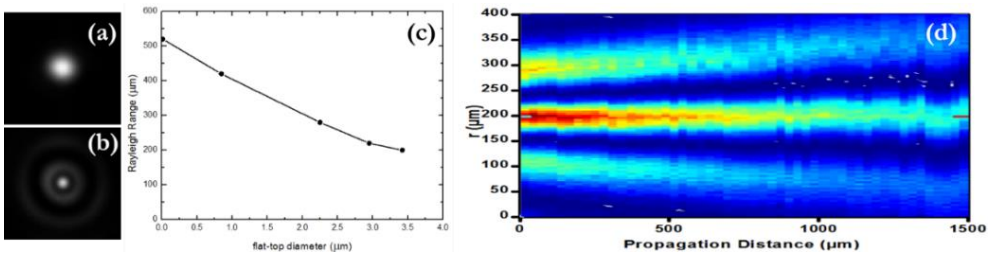

Fig. 5.11 (a) Gaussian output from a cleaved SM28 fiber; (b) BG beam from a fully developed micro-axicon; (c) the plot between Rayleigh range and flat top dimension; (d) the propagation of BG beam from the fully-developed micro-axicon.

Summary

Different methods for the fabrication of fiber micro-axicons are introduced. The taper fabrication method is analysed using the differential etch rates between the core and the cladding for selective chemical etching method. The analysis can predict the formation of concave and convex micro-axicons under different etching conditions. The etch rate for the cladding of different optical fibers are calibrated and the optimum condition for the fabrication of micro-axicons of different physical dimensions are determined experimentally for the optical fibers. Double concave micro-axicons with different cone angles are also fabricated in the optical fibers. Concave micro-axicons fabricated in optical fibers transform the fundamental Gaussian beam to a propagation-invariant Bessel-Gauss beam which is experimentally demonstrated with convex micro-axicons with different flat-top dimensions.

References

[ArDh00] ARLT, J. ; DHOLAKIA, K.: Generation of high-order Bessel beams by use of an axicon. In: *Optics Communications* Bd. 177 (2000), Nr. 1–6, S. 297–301

[ASTK92] ARIMOTO, RIEKO ; SALOMA, CAESAR ; TANAKA, TAKUO ; KAWATA, SATOSHI: Imaging properties of axicon in a scanning optical system. In: *Applied Optics* Bd. 31 (1992), Nr. 31, S. 6653–6657

[Betz93] BETZIG, E.: Principles and Applications of Near-Field Scanning Optical Microscopy (NSOM). In: POHL, D. W. ; COURJON, D. (Hrsg.): *Near Field Optics*, *NATO ASI Series* : Springer Netherlands, 1993 — ISBN 978-94-010-4873-6, 978-94-011-1978-8, S. 7–15

[BKGJ07] BURVALL, ANNA ; KOLACZ, KATARZYNA ; GONCHAROV, ALEXANDER V. ; JAROSZEWICZ, ZBIGNIEW ; DAINTY, CHRISTOPHER: Lens axicons in oblique illumination. In: *Applied Optics* Bd. 46 (2007), Nr. 3, S. 312–318

[DuME87] DURNIN, J. ; MICELI, J. J. ; EBERLY, J. H.: Diffraction-free beams. In: *Physical Review Letters* Bd. 58 (1987), Nr. 15, S. 1499–1501

[EaJA03] EAH, SANG-KEE ; JHE, WONHO ; ARAKAWA, YASUHIKO: Nearly diffraction-limited focusing of a fiber axicon microlens. In: *Review of Scientific Instruments* Bd. 74 (2003), Nr. 11, S. 4969–4971

[GSSI07] GROSJEAN, THIERRY ; SALEH, SAID SADAT ; SUAREZ, MIGUEL ANGEL ; IBRAHIM, IDRISS ABDOULKADER ; PIQUEREY, VINCENT ; CHARRAUT, DANIEL ; SANDOZ, PATRICK: Fiber microaxicons fabricated by a polishing technique for the generation of Bessel-like beams. In: *Applied Optics* Bd. 46 (2007), Nr. 33, S. 8061–8067

[HGWK93] HARTMANN, T. ; GATZ, R. ; WIEGRÄBE, W. ; KRAMER, A. ; HILLEBRAND, A. ; LIEBERMAN, K. ; BAUMEISTER, W. ; GUCKENBERGER, R.: A Scanning Near-Field Optical Microscope (SNOM) for Biological Applications. In: POHL, D. W. ; COURJON, D. (Hrsg.): *Near Field Optics*, *NATO ASI Series* : Springer Netherlands, 1993 — ISBN 978-94-010-4873-6, 978-94-011-1978-8, S. 35–44

[HoDS95] HOFFMANN, PATRIK ; DUTOIT, BERTRAND ; SALATHÉ, RENÉ-PAUL: Comparison of mechanically drawn and protection layer chemically etched optical fiber tips. In: *Ultramicroscopy*, *Selected Papers from the 3rd International Conference on Near-Field Optics and Related Techniques*. Bd. 61 (1995), Nr. 1–4, S. 165–170

[HYSW08] HEITZ, JOHANNES ; YAKUNIN, SERGEY ; STEHRER, THOMAS ; WYSOCKI, GERARD ; BÄUERLE, DIETER: <title>Laser-induced nanopatterning, ablation, and plasma spectroscopy in the near-field of an optical fiber tip</title> In: VILAR, R. ; CONDE, O. ; FAJARDO, M. ; SILVA, L. O. ; PIRES, M. ; UTKIN, A. (Hrsg.): , 2008, S. 71311W–71311W–8

[JOYP92] JIANG, SHUDONG ; OHSAWA, HISAO ; YAMADA, KAZUNOBU ; PANGARIBUAN, TOGAR ; OHTSU, MOTOICHI ; IMAI, KENSAKU ; IKAI, ATSUSHI: Nanometric Scale Biosample Observation Using a Photon

Scanning Tunneling Microscope. In: *Japanese Journal of Applied Physics* Bd. 31 (1992), Nr. Part 1, No. 7, S. 2282–2287

[KKVS13] KUCHMIZHAK, ALEKSANDR. A. ; KULCHIN, YURI N. ; VITRIK, OLEG B. ; SAVCHUK, ANDREY G. ; MAKAROV, SERGEY V. ; KUDRYASHOV, SERGEY I. ; IONIN, ANDREY A.: Optical apertureless fiber microprobe for surface laser modification of metal films with sub-100 nm resolution. In: *Optics Communications* Bd. 308 (2013), S. 125–129

[KSOS11] KOTLYAR, V. V. ; STAFEEV, S. S. ; O?FAOLAIN, L. ; SOIFER, V. A.: Tight focusing with a binary microaxicon. In: *Optics Letters* Bd. 36 (2011), Nr. 16, S. 3100–3102

[MaMO95] MAHESWARI, R.U. ; MONONOBE, S. ; OHTSU, MOTOICHI: Control of apex shape of the fiber probe employed in photon scanning tunneling microscope by a multistep etching method. In: *Journal of Lightwave Technology* Bd. 13 (1995), Nr. 12, S. 2308–2313

[Mcle60] MCLEOD, JOHN H.: Axicons and Their Uses. In: *Journal of the Optical Society of America* Bd. 50 (1960), Nr. 2, S. 166–166

[MJMM01] MARCINKEVIČIUS, ANDRIUS ; JUODKAZIS, SAULIUS ; MATSUO, SHIGEKI ; MIZEIKIS, VYGANTAS ; MISAWA, HIROAKI: Application of Bessel Beams for Microfabrication of Dielectrics by Femtosecond Laser. In: *Japanese Journal of Applied Physics* Bd. 40 (2001), Nr. Part 2, No. 11A, S. L1197–L1199

[MoMB08] MOHANTY, S. K. ; MOHANTY, K. S. ; BERNS, M. W.: Organization of microscale objects using a microfabricated optical fiber. In: *Optics Letters* Bd. 33 (2008), Nr. 18, S. 2155–2157

[MoOh98] MONONOBE, S. ; OHTSU, MOTOICHI: Development of a fiber used for fabricating application oriented near-field optical probes. In: *IEEE Photonics Technology Letters* Bd. 10 (1998), Nr. 1, S. 99–101

[MSSK98] MONONOBE, SHUJI ; SAIKI, TOSHIHARU ; SUZUKI, T ; KOSHIHARA, S ; OHTSU, M: Fabrication of a triple tapered probe for near-field optical spectroscopy in UV region based on selective etching of a multistep index fiber. In: *Optics Communications* Bd. 146 (1998), Nr. 1–6, S. 45–48

[NoHe06] NOVOTNY, LUKAS ; HECHT, BERT: *Principles of Nano-Optics* : Cambridge University Press, 2006 — ISBN 9781139452052

[Ohts04] OHTSU, MOTOICHI: *Progress in Nano-Electro Optics III: Industrial Applications and Dynamics of the Nano-Optical System* : Springer, 2004 — ISBN 9783540210504

[PSSJ99] PISKARSKAS, A. ; SMILGEVI?IUS, V. ; STABINIS, A. ; JARUTIS, V. ; PA?I?KEVI?IUS, V. ; WANG, S. ; TELLEFSEN, J. ; LAURELL, F.: Noncollinear second-harmonic generation in periodically poled KTiOPO4 excited by the Bessel beam. In: *Optics Letters* Bd. 24 (1999), Nr. 15, S. 1053–1055

[PuDa00] PUYGRANIER, B. A. F. ; DAWSON, P.: Chemical etching of optical fibre tips — experiment and model. In: *Ultramicroscopy* Bd. 85 (2000), Nr. 4, S. 235–248

[ShWi78] SHEPPARD, C. J R ; WILSON, T.: Gaussian-beam theory of lenses with annular aperture. In: *IEE Journal on Microwaves, Optics and Acoustics* Bd. 2 (1978), Nr. 4, S. 105–112

[SMOS96] SAIKI, T. ; MONONOBE, S. ; OHTSU, M. ; SAITO, N. ; KUSANO, J.: Tailoring a high-transmission fiber probe for photon scanning tunneling microscope. In: *Applied Physics Letters* Bd. 68 (1996), Nr. 19, S. 2612–2614

[TaYa00] TANAKA, TAKUO ; YAMAMOTO, SADAHIKO: Comparison of aberration between axicon and lens. In: *Optics Communications* Bd. 184 (2000), Nr. 1–4, S. 113–118

[TMCL09] TAN, K. M. ; MAZILU, M. ; CHOW, T. H. ; LEE, W. M. ; TAGUCHI, K. ; NG, B. K. ; SIBBETT, W. ; HERRINGTON, C. S. ; U. A.: In-fiber common-path optical coherence tomography using a conical-tip fiber. In: *Optics Express* Bd. 17 (2009), Nr. 4, S. 2375–2384

[Toma93] TOMANEK, P.: Fiber Tips for Reflection Scanning Near-Field Optical Microscopy. In: POHL, D. W. ; COURJON, D. (Hrsg.): *Near Field Optics, NATO ASI Series* : Springer Netherlands, 1993 — ISBN 978-94-010-4873-6, 978-94-011-1978-8, S. 295–302

[TTCG08] TSAMPOULA, X. ; TAGUCHI, K. ; CI?MÁR, T. ; GARCES-CHAVEZ, V. ; MA, N. ; MOHANTY, S. ; MOHANTY, K. ; GUNN-MOORE, F. ; U. A.: Fibre based cellular transfection. In: *Optics Express* Bd. 16 (2008), Nr. 21, S. 17007–17013

[Turn84] TURNER, DENNIS R.: Etch procedure for optical fibers.

[Vgar02] V GARCÉS-CHÁVEZ, D. MCGLOIN: Simultaneous micromanipulation in multiple planes using a self-reconstructing light beam. In: *Nature* Bd. 419 (2002), Nr. 6903, S. 145–7

[ViIn09] VISWANATHAN, NIRMAL K. ; INAVALLI, V. V. G.: Generation of optical vector beams using a two-mode fiber. In: *Optics Letters* Bd. 34 (2009), Nr. 8, S. 1189–1191

[WuHe93] WULLE, T. ; HERMINGHAUS, S.: Nonlinear Optics of Bessel Beams. In: *Physical Review Letters* Bd. 71 (1993), Nr. 1, S. 209–209

[YNHN06] YU, YOUNG-JUN ; NOH, HANEOL ; HONG, MUN-HEON ; NOH, HEUNG-RYOUL ; ARAKAWA, YASUHIKO ; JHE, WONHO: Focusing characteristics of optical fiber axicon microlens for near-field spectroscopy: Dependence of tip apex angle. In: *Optics Communications* Bd. 267 (2006), Nr. 1, S. 264–270

CHAPTER

6

Structured Light Beams Using Fiber Micro-axicon

Contents

6.1 Introduction

The output light beam from conventional sources such as lasers light, emitting diodes (LED) either have Gaussian or flat top intensity distribution in spatial dimension. Recent research developments in the area of complex intensity and polarization structured beams have shown that beams with unconventional intensity (dark hollow beams, optical cavities) and polarization structure (radial, azimuthal and hybrid etc.) are more efficient in many applications including in bio-physics[MiHa09], micro manipulation of particles and high-resolution microscopy etc. Though there are several methods available for the generation of such beams they all involve complex optical components and bulky systems. An optical fiber based technique for the generation of such complex light beams not only help in the miniaturization of the devices but can also extend the practical applications of such beams. The optical fiber based techniques can also provide high-throughput and energy efficient inexpensive devices.

This chapter deals with the use of various fiber micro-axicons fabricated via selective chemical etching method discussed in the previous chapter for the generation of intensity, phase and polarization structured beams. Dark hollow beams (DHB) and optical bottle beams are the most commonly used intensity modulated light beams. Chemically etched double concave micro axicon based techniques are developed for the generation of such beams. A convex micro-axicon in a tow-mode optical fiber is used for the generation of propagation-invariant vector beams.

6.2 Dark hollow beams from concave micro-axicon

Light beams with zero central intensity surrounded by one or more bright rings with cylindrical or conical intensity distribution are broadly classified as dark-hollow beams (DHBs)[YiGZ03]. Laguerre-Gaussian (LG) beam and higher order Bessel-Gaussian (BG) beams are some examples of DHB. Beams with specially engineered intensity and phase profiles are useful in various fields—for example, in optical trapping and manipulations, particularly in biophysical science for trapping living cells and organelles[GaSw98, MiHa09], and in atomic physics for manipulating neutral atoms[YZJW98, WaDL05]. Gaussian beams and flat top beams (FTB) are conventionally used for such applications but they are only capable of trapping particles with refractive index higher than that of the ambient

index. Whereas DHBs and optical vortex beams can overcome this and are capable of trapping objects with refractive index lower than the ambient also. In the case of atom cooling and guiding DHBs provides additional advantages like, atom confinement near the dark centre of the DHBs which suffer minimal light-shift effect of atomic levels, and also experience a low photon-scattering rate, and lower photon-assisted-collision rate, and no attractive potential from Van der Waals interaction of material walls[YZJW98, YiGZ03]. DHBs carrying lower-order optical vortices can propagate through atmospheric turbulence keeping their topological charge intact and thus find application in optical communication as information carrier[GbTy08]. Though there are several existing methods for generating DHBs such as refractive conical lens[ACPT03], holograms[Jarl98], diffractive optics[LDSL08], and specific waveguides[SNÖW10], optical fibers based methods would be interesting due its flexibility. DHBs generated using such fiber tips offer several advantages including the simplicity of fabrication, high coupling efficiency and with additional optical elements generation of special types of optical beams for imaging and communication applications are also possible.

The concave micro-axicons are fabricated in the optical fiber tip via selective chemical tube etching process which gives good quality tips suitable for generating DHBs. As mentioned in Chapter 5 the cone angle of the micro-axicon can be varied over a large range by changing the volume ratio of the constituent components of the etching solution(HF, NH_4F and DW) and any combination with HF/NH_4F volume ratio more that 1.7 would yield concave micro-axicons. The fibers are cleaved very close to the plastic jacket, fixed in Teflon fiber holders and dipped vertical in the etchant solution. The etchant solution is prepared in such a way that the core etch rate is more than that of cladding, resulting in negative cones in the fiber tips. Concave micro-axicons are fabricated in SMF630 and SMF28 optical fibers. For SMF630 fiber we used HF/Buffer (B) ratio of 6, 7, 8 and 9 and the etching was carried out for 10 minutes which was found to give good quality tips and DHBs. For SMF28 fiber we used HF/B ratios of 3.5, 4 and 4.25 and the etching was carried out for 15 minutes. After etching, the fibers are thoroughly rinsed in de-ionized water and then in NaOH solution repeatedly both to clean and to neutralize the HF acid from further reacting with silica fibers. The fiber tips are then imaged using a calibrated optical microscope (Olympus, Japan) fitted with CCD camera. Fig. 6.1 shows the microscope image of the concave micro-axicon fabricated in the optical fibers and the plot of the obtained cone angles as a function of HF/NH_4F ratio. Upon closer inspection it was also found

that the micro-axicons are double concave in nature where in the core and cladding cone angles are different.

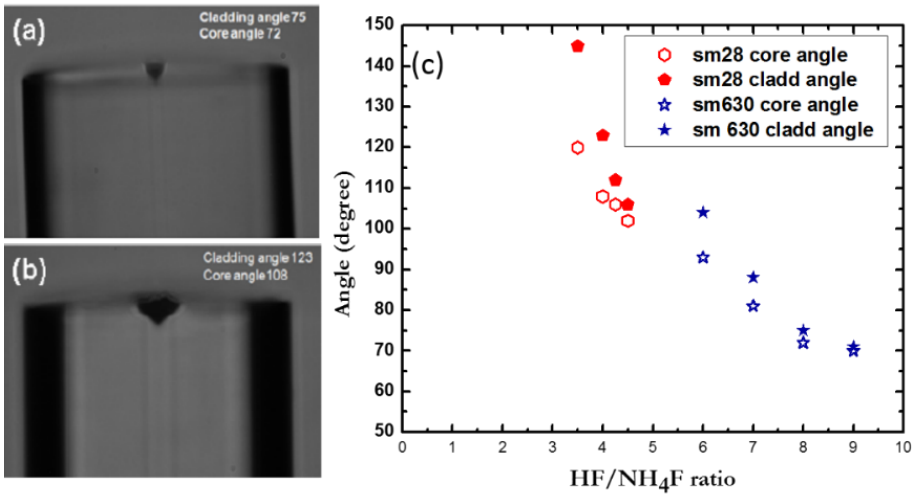

Fig. 6.1 Microscope images of concave micro-axicons fabricated in (a) SMF630 with HF/NH4F=8, (b) SMF28 with HF/NH4F=4 and (c) plot between cone angle and HF/NH4F ratio.

After imaging to measure the cone dimensions in the fiber, the output beam from different concave micro-axicons are characterized by launching light

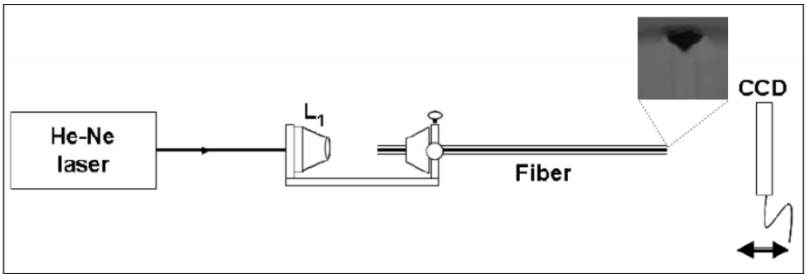

Fig. 6.2 Schematic of the experimental setup used for the generation and characterization of DHBs from concave micro-axicon

into these fiber. Fig. 6.2 shows a schematic of the experimental setup used for the characterization of the output beam from different micro-axicons. partially-polarized He-Ne laser beam (λ=632.8 nm) is coupled using a 20x, 0.40 NA microscope objective lens (L1) into the cleaved input end of the fiber without and with the device (concave micro-axicon) and the output beam is imaged using a CCD camera

mounted on a translation stage to enable measurement of the propagation characteristics of the output beam. The CCD is connected to a computer through IEEE 1394 card for data acquisition and analysis.

The DHBs are characterized by a set of parameters which describe the spatial properties of this class of beams[YiGZ03] defined as follows:

(i) *The dark spot size* (DSS) is defined as the full width at half maximum (FWHM) of the radial intensity distribution inside the ring of the DHB.

(ii) *The beam width* (W_{DHB}) is defined as the full width at $1/e^2$ of the maximum of the radial intensity distribution outside the core of the DHB.

(iii) *The beam radius* (r_0) is defined as the distance between the position of the maximum radial intensity and the centre of the light beam.

(iv) *The ring-beam width* (Wr) is defined as the fill width at $1/e^2$ of the maximum value of the radial intensity distribution, *ie* $W_r = W_{DHB} - 2r_0$

(v) *The width-radius ratio* (WRR) is defined as the ratio of the ring-beam width Wr to its beam radius r_0, *ie* $WRR = \frac{W_r}{r_0} = \frac{W_{DHB}}{r_0} - 2$

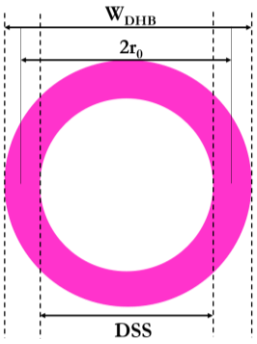

Fig. 6.3 Definition of DHB parameters

6.2.1 DHBs from SMF630 fiber micro-axicon

The He-Ne laser light is launched through the cleaved input end of the SMF630 fiber and the output beam from the device end is imaged using the CCD as shown in Fig. 6.2. Fig. 6.4 (a) and (b) respectively shows the output beam from

the cleaved SMF630 fiber and concave micro-axicon fabricated using an etchant solution of HF/NH4F=8 and Fig. 6.4 (c) shows the 3D intensity distribution in the

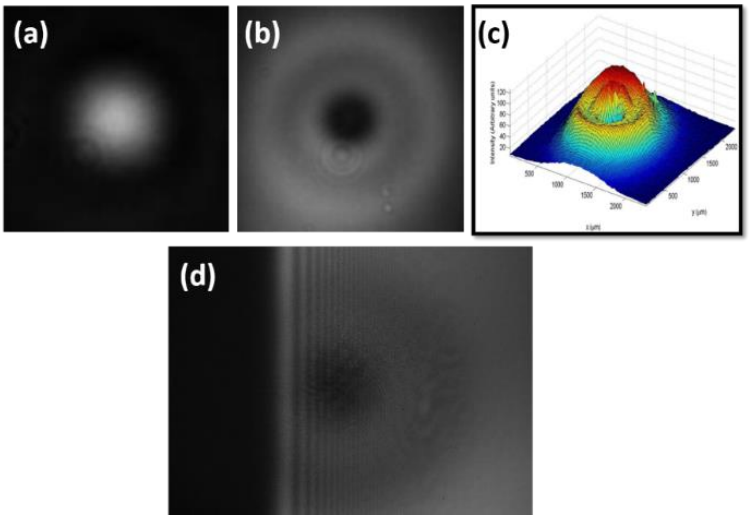

Fig. 6.4(a) Output beam from the cleaved SMF630 fiber, (b) DHB from the concave axicon chemically etched in SMF630 at z=0,(c) 3D intensity distribution in the cross section of the beam, (d) knife-edge diffraction pattern of the DHB.

beam cross section at z=0 (nearest to the micro-axicon). A knife edge diffraction of the DHB is done to verify the phase structure of the beam as shown in Fig. 6.4 (d) and it clearly shows that there is no phase difference between the rings since the diffraction fringes are all straight. The propagation characteristics of the DHB from the concave micro-axicon is measured by capturing the CCD images of the

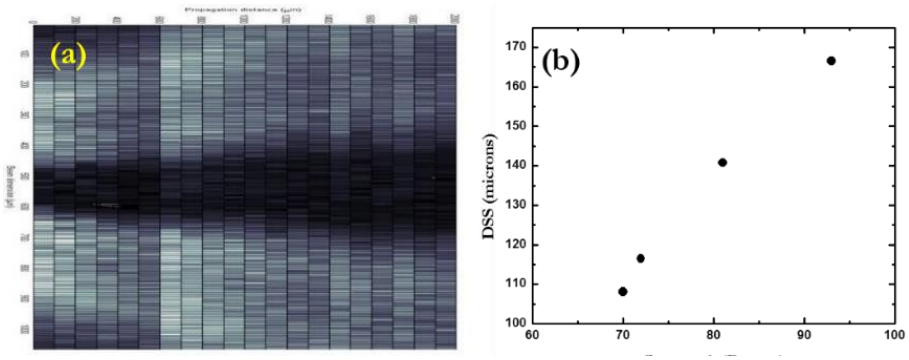

Fig. 6.5 (a) propagation of the DHB from the concave micro-axicon in SMF630 fiber, (b) plot between DSS and cone angle

beam at very close intervals and stitching the image using Matlab code. Fig. 6.5(a) shows the propagation of DHB from the SMF630 fiber. It is also interesting to note that the dark spot size (DSS) of the DHB generated form the concave micro-axicon depends on the cone angle (Fig. 6.5(b)). Thus the fiber micro-axicon based method for the generation of DHB gives an advantage to tune the DSS by varying the cone angle, which can be easily done by changing the volume ratio (HF/NH4F) of the etchant solution.

6.2.2 DHB from SMF28 fiber micro-axicon

The He-Ne laser light is launched in to the SMF28 fiber micro-axicon using the same experimental setup given in Fig. 6.2. Since the SMF28 fiber is multimode at 632.8 nm wavelength, the launching conditions are adjusted such that the output beam from the concave micro-axicon is a symmetric DHB. The propagation charecteristics of the DHB is measured by taking the CCD images of the beam at different distances from the micro-axicon tip (z=0) and processing the images using Matlab. Fig. 6.6 shows the output beam from a cleaved SMF28 fiber for on

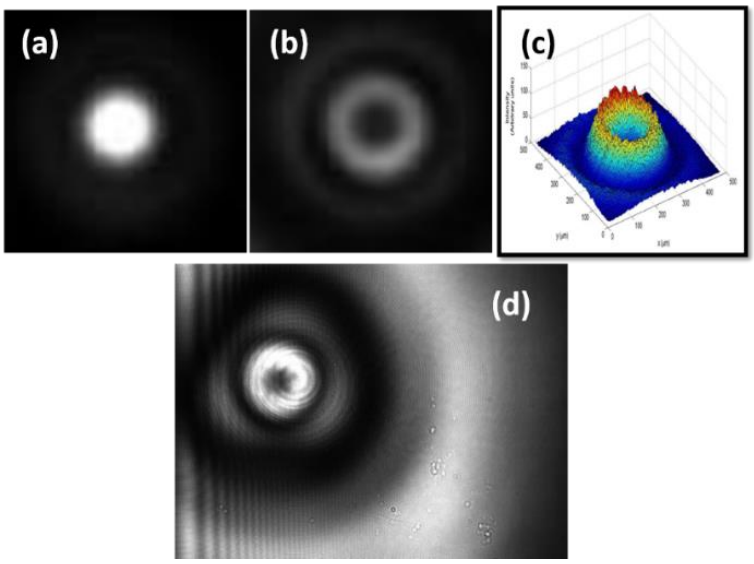

Fig. 6.6(a) Output beam from a cleaved SMF630 fiber, (b) DHB from the concave axicon in SM28 at z=0,(c) Intensity distribution in the cross section of the beam, (d) knife edge diffraction of the DHB

axis launch (a), the DHB produced by fabricating a concave micro-axicon in SMF28 fiber (b), the 3D intensity profile of the beam (c) and the knife-edge

diffraction pattern of the DHB (d). The knife-edge diffraction clearly shows that there is a π phase difference between the 2nd and 3rd rings a feature that will be made use of in generation of 3D bottle beams reported in the next section. Fig. 6.7 gives the propagation characteristics of the DHB(a) and the DHB parameters with propagation distance 'z'. The analysis of the parameters shows that they all diverge linearly with distance.

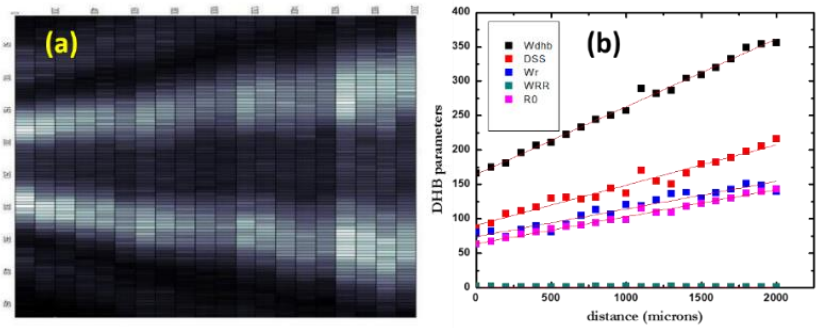

Fig. 6.7 (a) Propagation of the DHB from the micro-axicon, (b) plot of DHB parameters with distance of propagation, showing linear variation.

6.3 Tunable chain of optical bottle beams

Optical beams with zero on-axis intensity and surrounded in all three directions by regions of higher intensity are popularly known as optical bottle beams, a term proposed by Arlt and Padgett[ArPa00]. The interest towards these intensity structured beams are driven by applications such as dark optical traps for atoms[FKOD99], manipulation, guiding and binding of micro-particles and biological cells[ČRDA10], as erase beams for super-resolution fluorescence microscopy[WIOY03] etc. However, the generation of desired 3D light distribution is more difficult to achieve using simple diffractive and refractive optical elements as compared to that of the 2-D hollow laser beams[FKOD99]; [ČRDA10, YiGZ03] . As a result, a variety of methods using combinations of axicons and spherical lenses, diffractive optical elements or rapidly scanning laser beams are proposed and demonstrated for the generation of single laser beam based dark volume[ArPa00, BoDa06, WeSL05]; [ZeWu08, RySS09]. Recently one-dimensional traps with multiple longitudinal trap sites is gaining significant interest for optical binding, self-assembly and related studies[ČRDA10]. The non-diffracting and self-reconstructing properties of Bessel beams are used for the simultaneous micromanipulation in multiple planes along the axial

direction[GMMS02]. The generation of 3D light distribution with a dark core makes use of destructive interference in some region in space between two coherent light fields with different propagation characteristics. Outside this dark region the intensity will rise in all directions due to the different propagation constants, thus generating a well confined dark volume. This kind of chain of optical cavities along the longitudinal direction were proposed recently for trapping of multiple particles along the beam propagation and for controllable particle delivery[ACYZ06].

The multi-ring hollow Gaussian beam (HGB) with large difference in radial index k_r and small difference in the axial index k_z can be generated using a double-negative axicon chemically etched in the tip of a standard multimode optical fiber. If this HGB is focused by a high-numerical aperture (NA) lens it can result in a chain of 3-D optical bottle beams due to the axial interference of the Bessel beams generated by the focusing of individual rings in the multi-ring HGB. The requirement here is that the (NA) of the lens matches that of the diverging rings of the HGB. The radial and axial wave vectors of the two input HGB rings (k_{r1}, k_{r2}, k_{z1}, and k_{z2}) were first used to theoretically generate the output propagation-invariant beam and the chain of 3D bottle beams of different dimensions, which were found to agree well with experimental results. The advantage of this method of experimental generation of 3D bottle beams is that the 3D chain of optical bottles are formed in the propagation-invariant region of the Bessel beams thus have uniformity in cavity dimensions and intensity.

The Fig. 6.8 shows the experimental setup used for the generation of 3D optical bottle beams. Unpolarized light from a He-Ne (λ=632.8 nm) laser is launched into the multimode optical fiber (V =5.695) using a microscope objective lens L_1 (10x, NA=0.25). The output end of the fiber has the chemically etched double-negative axicon[PhVi10]. Details of the selective chemical etching process used to achieve the double-negative axicons in the fiber tip are discussed in Chapter 5. The etchant solution made of HF: NH_4F : DW in a volume ratio of X : 1 : X with X = 4 gives double-negative axicon of angles 96° and 110° respectively in the core and the cladding of the fiber due to the different etch rates. Optical microscope image of the etched fiber tip is shown in the inset (a) of Fig. 6.8 clearly shows the two cones of different angles in the core and the cladding of the fiber.

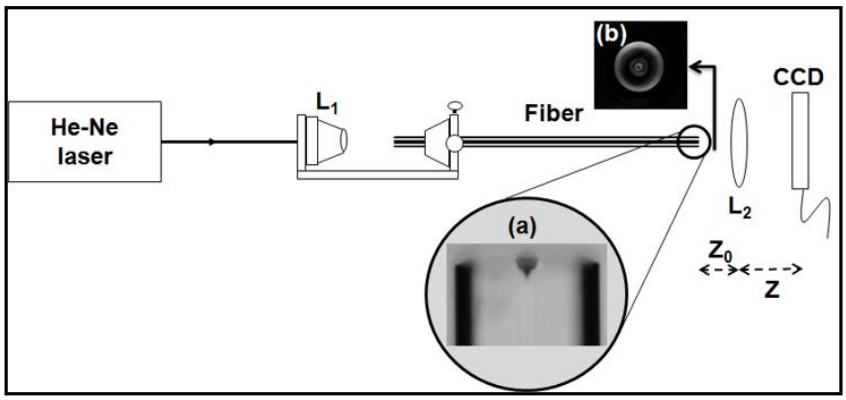

Fig. 6.8 Schematic of the experimental setup used to generate tunable 3D optical bottle beam. Inset: (a) microscope image of the chemically etched fiber tip showing double-negative axicon and (b) CCD image of the output beam from the fiber tip for a fixed input launch condition.

The output beam for a fixed input launch condition corresponds to the LP_{02} mode of the fiber with cleaved output end. The central bright spot of the LP_{02} mode splits into two rings upon passing through the double negative axicon with the third diffused ring appearing due to the large angle of the core-clad interface [inset (b) in Fig. 6.8]. The phase difference between the rings, measured using the knife-edge experiment reveals that there is no phase difference between the first two rings, as they are due to splitting of the central spot but there is a π phase difference with the third ring which confirms the modified LP_{02} mode assignment to the output pattern from the fiber[ViPJ10]. The free-space propagation characteristics of the three rings from the tip-modified optical fiber are first measured from Z = 0 to 4mm using a CCD camera mounted on a translation stage. The CCD camera is connected to the computer via IEEE-1394 card for data collection and analysis. From these measurements the diameter of the three rings at Z = 0 mm are calculated to be $r_1 = 78.84\mu m, r_2 = 146.062\mu m$ and $r_3 = 473.82\mu m$ and the corresponding divergence angles of the three rings are 4.18°, 10.51° and 17.23° respectively. The output microscope objective lens L_2 (20x, NA=0.40), mounted on a translation stage is moved to different fixed distances from the fiber tip (Z_0) to generate 3D bottle beams of different dimensions and periodicity. The characteristics of the focused beam along the propagation direction around the focal plane of the lens (ΔZ) are measured using the CCD camera mounted on the translation stage. By moving the lens L_2, mounted on a translation stage to different fixed distances (Z) from the fiber tip, the radius 'r' of the annular rings at the lens changes thereby changing the characteristics of the beam around the lens

focal plane[ZhWL08]. Under certain conditions this results in an intensity modulated 3D bottle beams with different dimension and periodicity formed along the entire length of the focal region of the beam.

Focusing a single annular ring beam using a lens with matching $\boldsymbol{k_r}$ and $\boldsymbol{k_z}$ values are known to generate non-diffracting Bessel beams[Chán99]. To understand the mechanism of the 3D cavity formation, two inner rings of the multi ring HGB are blocked using a mask and the focusing characteristics of the third ring was studied. For the lens L_2 positioned at a distance of Z_0 = 12 mm from the fiber tip, the third annular ring forms a propagation-invariant Bessel-Gauss beam with a central spot of width 23.5 μm and Z_{max} of 86mm. The radius of the third ring of 0.474 mm is used to calculate the $\boldsymbol{k_r}$ and Z_{max} values of the Bessel beam. The propagation of the Bessel beam is simulated using Equ. (6.1)

$$E(r,\emptyset,z) = \sqrt{2\pi k_r\,\omega_0}\,(Z/Z_{max})^{l+1/2} exp^{(-Z^2/Z_{max}^2)} exp^{\left[i\left(l\emptyset-\frac{l\pi}{2}-\pi/4\right)\right]} J_l(k_r r) \quad (6.1)$$

Fig.6.9 (b) shows the experimentally measured and simulated propagation of the Bessel beam generated by focusing only the third ring using L_2.

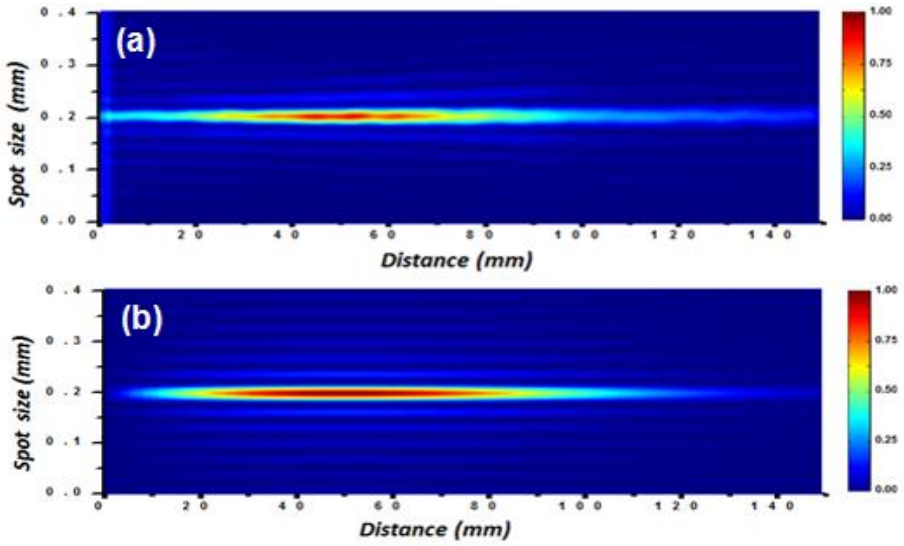

Fig. 6.9 (a) Free-space propagation of the experimentally generated non-diffracting Bessel beam formed by focusing the third annular ring using lens L2 kept at Z = 12mm. (b) Bessel beam propagation simulated using the input beam parameters in Equ. (6.1)

Next, by removing the masked glass plate all the three rings are included in the focusing and hence the generated Bessel beams were allowed to interfere along the propagation axis. For the fixed output lens position of Z_0 = 8.5 mm, the CCD camera is moved using a translation stage capturing images of the beam at an interval of 100μm. The interfering Bessel beams due to the three annular rings modulate the intensity profile along the propagation direction resulting in a 3D optical bottle beams along the entire range over which the Bessel-Gauss beam was formed with a single annular ring. The longitudinal period of this experimentally generated chain of 3D bottle beam is measured to be 6.18 mm. the superposition of two or more Bessel beams with different direction cosines creates periodic axial intensity distribution along the propagation axis. The spatially modulated Bessel beams generated due to two annular rings were simulated using Equ. (6.2) [ACYZ06]:

$$I(r,z) = a^2 J_0^2(k_{r1}) + b^2 J_0^2(k_{r2}) + 2abJ_0(k_{r1})J_0(k_{r2})cos[(k_{z1} - k_{z2})z + \varphi] \qquad (6.2)$$

The period of modulation of the bottle beam is calculated using the relation $\delta = 2\pi/(k_{z1} - k_{z2})$ to be 6.04 mm, which agrees well with the experimentally measured period of 6.18mm. Fig. 6.10 gives the generated optical bottle beams along with the corresponding theoretically simulated beam obtained by changing the output lens position. For the farthest distance of the lens L_2 from the fiber tip of Z = 14 mm, some part of the third ring is clipped by the fixed lens aperture (= 6 mm). In this case, the experimentally measured bottle beam period of 45 mm shown in Fig. 6.10 (e) deviates from the theoretically simulated period of 20.93 mm (Fig. 6.10 (f)) due to the effect of clipping of the third ring by the lens aperture and the related diffraction effects changing the beam propagation characteristics. The length and the diameter of the experimentally generated 3D bottle beam in this case increases to 10.75 mm and 211.5 μm respectively. Fig. 6.11 shows the peak intensity and the FWHM of the 3D chain of bottle beams corresponding to a L2 lens position Z=12 mm as a function of propagation distance The modulation period of the output beam intensity and its FWHM are determined from the $\boldsymbol{k_z}$ value of the rings forming the pattern. Clearly, the intensity of the beam is modulated with varying periodicity along the propagation direction[ChMH98]. The following table 1 gives the dimension and periodicity of the optical bottle beams generated by focusing multi ring HGB.

Table 6.1. Periodicity, length and diameter of the optical bottle regions generated by focusing multi ring HGB from double concave fiber micro-axicon

Position of lens L2 Z (mm)	Period (mm)		Length of dark region (mm)	Diameter of dark region (μm)
	Experimental	Theoretical		
8.5	6.18	6.03	1.1	37.6
12	13.7	13.08	5.5	61.7
14	45	20.93	10.75	211.5

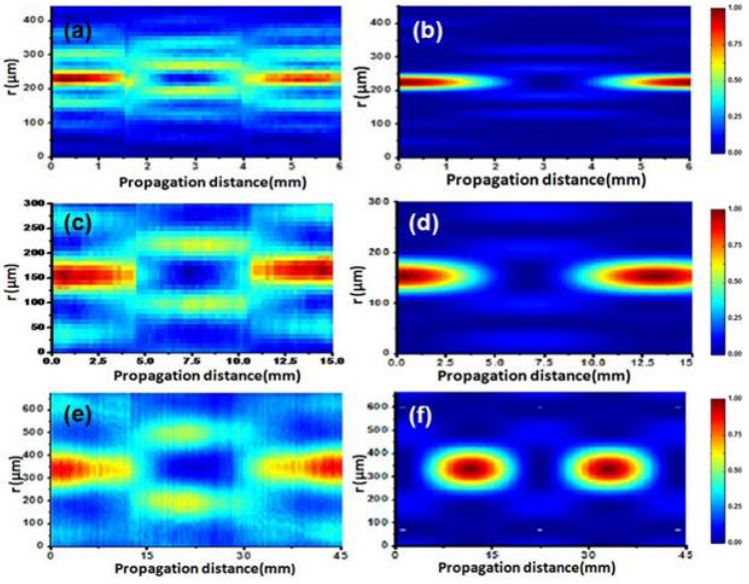

Fig. 6.10 3D optical bottle beams generated for different positions (z) of the L2 lens. (a), (c) and (e) are one period of the experimentally generated beams; (b), (d) and (f) are the corresponding simulation results; (a) & (b) z=8.5mm, (c) & (d) z=12mm and (e) & (f) z=14mm.

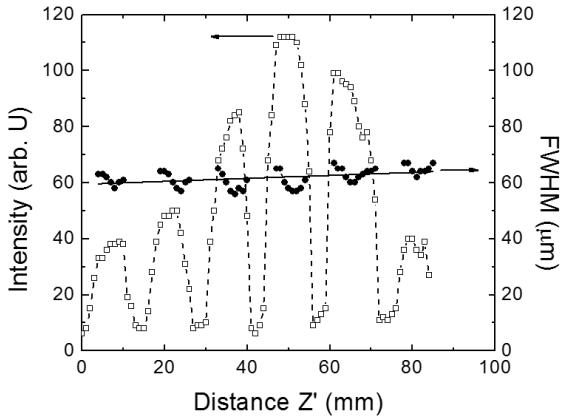

Fig. 6.11 Axial intensity and FWHM of chain of 3D bottle beam as a function of propagation distance (z´) for z= 12 mm.

6.4 Polarization structured propagation-invariant beams from convex micro-axicon

Propagation-invariant scalar fields have been studied extensively, both theoretically and experimentally since they were proposed by Durnin [DuME87]. Although there were considerable theoretical studies on propagation-invariant vector fields[Mish91]; [BoOl95] the experimental studies were limited due to the difficulty in generating these beams. Different experimental techniques were developed for the generation of propagation-invariant vector beams which include interferometric method[TiFK90], concentric-grating surface–emitting semiconductor diodes[EKWH92], and computer generated sub wavelength grating[NBKH04]. These propagation-invariant vector beams find application in super resolution microscopy[WRWJ06], laser focusing acceleration of electrons[RoKi90] and optical tweezers[RoJá08].

A Sagnac interferometer based method using a spiral phase plate and axicon is discussed in previous chapter (Chapter 2 Section 2.4) for the generation of propagation invariant vector beams (PIVB). The Sagnac interferometer with a combination of wave plates generates a vector beam and this beam is subsequently focused by an axicon to generate vector Bessel-Gauss beam. Recently it was shown that a two-mode optical fiber with proper launching conditions and input beam

polarization can produce vector beams[ViIn09]. So if one can combine these two, that is fabricate an axicon in the output end of the two-mode optical fiber, it can become a compact source of propagation invariant vector beam.

Towards developing a compact optical fiber based source for the generation of PIVBs a micro-axicon is fabricated directly in the tip of the two-mode optical fiber via selective chemical etching[Ohts04]. As discussed in the previous chapter for the tip fabrication the fiber is cleaved very closed to the plastic jacket and dipped normally in the etchant of constituting HF acid (50%), NH_4F (40%) and deionised water (DW). The etchant solution is prepared in the volume ratio 1:8:1 (HF: NH_4F: DW) and the fiber is kept dipped in the solution for 120 minutes at room temperature (T=25°C). The fiber is then taken out and cleaned for imaging using scanning electron microscope (SEM). The SEM image of the microaxicon is shown in Fig. 6.12 (inset). The apex angle of the micro axicon is measured to be 88°.

6.4.1 Spirally-polarized propagation invariant beam from fiber micro-axicon

Optical vector beams where in the state of polarization is varying in the transverse cross-section of the beam drove the attention of reseachers due to its applications. It has been shown that two-mode optical fiber excited with skew rays can be used aa a source of vector beams [ViIn09]. Thus by fabricating a micro axicon would give vector bessel beams. Schematic of the experimental setup used for the controlled generation of PIVBs from linearly polarized Gaussian beam using a two-mode optical fiber (TMF) with a micro-axicon at the tip is shown in Fig. 6.12. The Gaussian beam from a partially polarized, 5mW He-Ne laser light (λ=632.8nm) is first polarized using a Glan-Thompson polarizer P_1. The linearly polarized light then passes through a half-wave plate (HWP) mounted on a rotation stage to enable the adjustment of the plane of polarization of the input beam launched into the fiber. The beam is then focused using a 0.25NA 10X microscope objective lens (L_1) onto the cleaved end of the TMF which is positioned using a three-axis precision fiber launch stage. By adjusting the position of the focused input beam with respect to the fiber axis skew rays are launched into the fiber that selectively excites any of the guided vector modes or its combinations in the fiber. By changing the input beam polarization and the launch conditions LG_{01} beam output with different vector natures, from the TMF can be obtained[ViIn09]. This

vector beam focused by the micro-axicon fabricated at the output end of the optical fiber, leads to the formation of a combination of Bessel-Gauss beams (Chapter 2 Section 2.4). The output beam is then imaged using a CCD camera, connected through an IEEE 1394 card to a computer, fixed on a micro translation stage[PhVi11]. The output beam is then collimated using microscope objective lens (L_2) (40x, 0.65NA) for the polarization

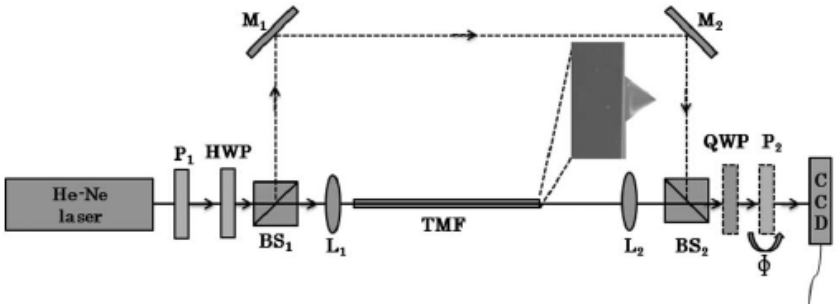

Fig. 6.12 Schematic of the experimental setup used for the generation of PIVB using fiber micro-axicon

characterization using imaging Stokes Polarimetry[Gold11] using a quarter-wave plate and a polarizer. A two-beam interferometer is constructed in parallel (dotted curve in Figure.6.12), to verify the presence of component vortices in the output beam. Fig. 6.13 shows the output beam with a intensity profile and theoretical fit according to the theoretical equations for the focusing of a spirally polarized beam by an axicon (Chapter 2 Section 2.4).

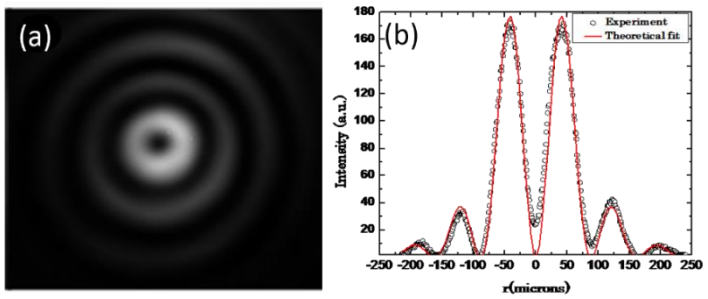

Fig. 6.13 (a) Output beam from fiber micro-axicon (b) intensity line profile and the theoretical fit along the horizontal direction.

The propagation characteristics of the output beam is measured by using the CCD and processing the images using Matlab. Fig. 6.14 shows the images of all the 100 measurements taken from very close to the micro-axicon(z= 0 μm) upto 1mm in steps of 10 μm. The propagation-invariant region of the spirally-polarized beam is measured to be ≈100 μm.

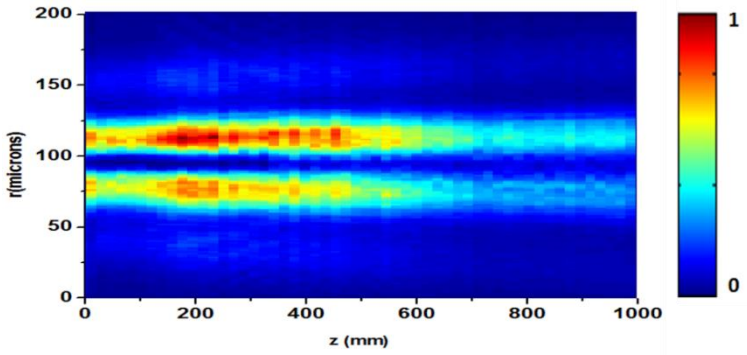

Fig. 6.14 Propagation characteristics of the spirally-polarized beam

The standard 2D Stokes parameter measurements were carried out on the higher-order Bessel beam output from the fiber micro-axicon to characterize the polarization charecteristics. From the Stokes parameter the polarization ellipse orientation and the ellipticity are calculated in the beam cross-section. The polarization ellipse plot of the centre ring of the beam is shown in Fig. 6.15. From the polarization ellipse map it is clear that the state of polarization at all points in the beam cross section is linear. Any spirally polarized beam can be considered as a linear combination of radial and azimuthal polarized vector beams[Gori01]. To get the exact nature of the spiral polarization we selected polarization ellipses with same 'b/a' (where 'a' and 'b' are semi-major and semi-minor axis of the polarization ellipse) ratio around the beam axis and plotted them in a polar plot shown in Fig. 6.15(c). The trajectory is fitted to a logarithmic spiral of the form $r = r_0 exp(\varphi/tan\gamma)$ with $r_0 = 26$ μm and $\gamma = 1.292\, rad$ (74°), indicating that the azimuthal contribution to the spirally-polarized beam is more than the radial part[Gori01].

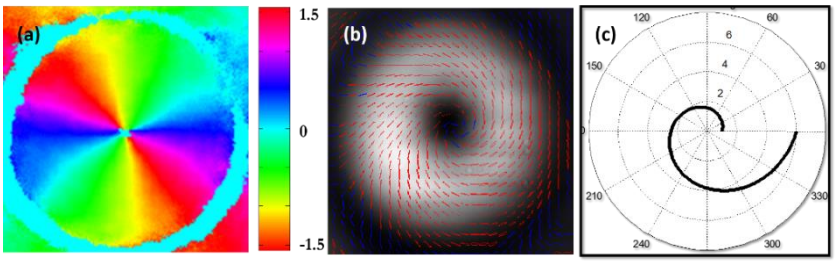

Fig. 6.15(a) Map of polarization ellipse major-axis orientation; (b) polarization ellipse plot on the beam cross-section; (c) logarithmic spiral fit for same 'b/a' values

Summary

Different types of double concave micro-axicons were fabricated in single-mode, few-mode and multi-mode optical fibers via selective chemical etching method. These micro-axicons were subsequently used for the generation of DHBs and the generated DHB, 3D chain of bottle and spirally-polarized Bessel-Gauss beam. The generated DHB parameters were found to depend on the cone angle of the micro-axicon. These HGBs upon high NA focusing gives tunable chain of optical bottle beams due to the axial interference of Bessel beams formed by individual rings. The period of the optical bottle was varied by changing the focusing lens position with respect to the fiber tip. By simply translating the focusing lens with respect to the fiber tip the size of the optical cavities have been varied from μm to mm. Convex micro-axicon fabricated in two mode optical fiber was used to generate spirally polarized propagation-invariant beams.

Reference

[ACPT03] DE ANGELIS, M. ; CACCIAPUOTI, L. ; PIERATTINI, G. ; TINO, G. M.: Axially symmetric hollow beams using refractive conical lenses. In: *Optics and Lasers in Engineering, Optics In Italy IV*. Bd. 39 (2003), Nr. 3, S. 283–291

[ACYZ06] AHLUWALIA, B. P. S. ; CHEONG, W. C. ; YUAN, X.-C. ; ZHANG, L.-S. ; TAO, S.-H. ; BU, J. ; WANG, H.: Design and fabrication of a double-axicon for generation of tailorable self-imaged three-dimensional intensity voids. In: *Optics Letters* Bd. 31 (2006), Nr. 7, S. 987–989

[ArPa00] ARLT, J. ; PADGETT, M. J.: Generation of a beam with a dark focus surrounded by regions of higher intensity: the optical bottle beam. In: *Optics Letters* Bd. 25 (2000), Nr. 4, S. 191–193

[BoDa06] BOKOR, NÁNDOR ; DAVIDSON, NIR: Generation of a hollow dark spherical spot by 4pi focusing of a radially polarized Laguerre-Gaussian beam. In: *Optics Letters* Bd. 31 (2006), Nr. 2, S. 149–151

[BoOl95] BOUCHAL, ZDENĚK ; OLIVÍK, MAREK: Non-diffractive Vector Bessel Beams. In: *Journal of Modern Optics* Bd. 42 (1995), Nr. 8, S. 1555–1566

[Cháv99] CHÁVEZ-CERDA, S.: A new approach to bessel beams. In: *Journal of Modern Optics* Bd. 46 (1999), Nr. 6, S. 923–930

[ChMH98] CHÁVEZ-CERDA, S. ; MENESES-NAVA, M. A. ; HICKMANN, J. MIGUEL: Interference of traveling nondiffracting beams. In: *Optics Letters* Bd. 23 (1998), Nr. 24, S. 1871–1873

[ČRDA10] ČIŽMÁR, T ; ROMERO, L C DÁVILA ; DHOLAKIA, K ; ANDREWS, D L: Multiple optical trapping and binding: new routes to self-assembly. In: *Journal of Physics B: Atomic, Molecular and Optical Physics* Bd. 43 (2010), Nr. 10, S. 102001

[DuME87] DURNIN, J. ; MICELI, J. J. ; EBERLY, J. H.: Diffraction-free beams. In: *Physical Review Letters* Bd. 58 (1987), Nr. 15, S. 1499–1501

[EKWH92] ERDOGAN, T. ; KING, O. ; WICKS, G. W. ; HALL, D. G. ; ANDERSON, ERIK H. ; ROOKS, M. J.: Circularly symmetric operation of a concentric-circle-grating, surface- emitting, AlGaAs/GaAs quantum-well semiconductor laser. In: *Applied Physics Letters* Bd. 60 (1992), Nr. 16, S. 1921–1923

[FKOD99] FRIEDMAN, NIR ; KHAYKOVICH, LEV ; OZERI, ROEE ; DAVIDSON, NIR: Single-Beam Dark Optical Traps for Cold Atoms. In: *Optics and Photonics News* Bd. 10 (1999), Nr. 12, S. 36–37

[GaSw98] GAHAGAN, K. T. ; SWARTZLANDER, G. A.: Trapping of low-index microparticles in an optical vortex. In: *Journal of the Optical Society of America B* Bd. 15 (1998), Nr. 2, S. 524–534

[GbTy08] GBUR, GREG ; TYSON, ROBERT K.: Vortex beam propagation through atmospheric turbulence and topological charge conservation. In: *Journal of the Optical Society of America A* Bd. 25 (2008), Nr. 1, S. 225–230

[GMMS02] GARCÉS-CHÁVEZ, V. ; MCGLOIN, D. ; MELVILLE, H. ; SIBBETT, W. ; DHOLAKIA, K.: Simultaneous micromanipulation in multiple planes

using a self-reconstructing light beam. In: *Nature* Bd. 419 (2002), Nr. 6903, S. 145–147

[Gold11] GOLDSTEIN, DENNIS H: *Polarized light*. Boca Raton, FL : CRC Press, 2011 — ISBN 9781439830406 1439830401

[Gori01] GORI, FRANCO: Polarization basis for vortex beams. In: *Journal of the Optical Society of America A* Bd. 18 (2001), Nr. 7, S. 1612–1617

[Jarl98] J. ARLT, K. DHOLAKIA: The production of multiringed Laguerre–Gaussian modes by computer-generated holograms. In: *Journal of Modern Optics* Bd. 45 (1998), S. 1231–1237

[LDSL08] LIU, ZHENGJUN ; DAI, JINGMIN ; SUN, XIAOGANG ; LIU, SHUTIAN: Generation of hollow Gaussian beam by phase-only filtering. In: *Optics express* Bd. 16 (2008), Nr. 24, S. 19926–19933. — PMID: 19030080

[MiHa09] MIYAZAKI, MASAYA ; HAYASAKI, YOSHIO: Motion control of low-index microspheres in liquid based on optical repulsive force of a focused beam array. In: *Optics Letters* Bd. 34 (2009), Nr. 6, S. 821–823

[Mish91] MISHRA, S. R.: A vector wave analysis of a Bessel beam. In: *Optics Communications* Bd. 85 (1991), Nr. 2–3, S. 159–161

[NBKH04] NIV, AVI ; BIENER, GABRIEL ; KLEINER, VLADIMIR ; HASMAN, EREZ: Propagation-invariant vectorial Bessel beams obtained by use of quantized Pancharatnam-Berry phase optical elements. In: *Optics Letters* Bd. 29 (2004), Nr. 3, S. 238–240

[Ohts04] OHTSU, MOTOICHI: *Progress in Nano-Electro Optics III: Industrial Applications and Dynamics of the Nano-Optical System* : Springer, 2004 — ISBN 9783540210504

[PhVi10] PHILIP, GEO M ; VISWANATHAN, NIRMAL K: Generation of tunable chain of three-dimensional optical bottle beams via focused multi-ring hollow Gaussian beam. In: *Journal of the Optical Society of America. A, Optics, image science, and vision* Bd. 27 (2010), Nr. 11, S. 2394–2401. — PMID: 21045904

[PhVi11] PHILIP, GEO M. ; VISWANATHAN, NIRMAL K.: Generation of spirally polarized propagation-invariant beam using fiber microaxicon. In: *Optics Letters* Bd. 36 (2011), Nr. 19, S. 3906–3908

[PuDa00] PUYGRANIER, B. A. F. ; DAWSON, P.: Chemical etching of optical fibre tips — experiment and model. In: *Ultramicroscopy* Bd. 85 (2000), Nr. 4, S. 235–248

[RoJá08] RODRÍGUEZ-LARA, B. M. ; JÁUREGUI, R.: Dynamical constants for electromagnetic fields with elliptic-cylindrical symmetry. In: *Physical Review A* Bd. 78 (2008), Nr. 3, S. 033813

[RoKi90] ROMEA, RICHARD D. ; KIMURA, WAYNE D.: Modeling of inverse Čerenkov laser acceleration with axicon laser-beam focusing. In: *Physical Review D* Bd. 42 (1990), Nr. 5, S. 1807–1818

[RySS09] RYZHEVICH, A. A. ; SOLONEVICH, S. V. ; SMIRNOV, A. G.: Method for creating hollow light beams with local intensity minima and possibilities for their application. In: *Journal of Applied Spectroscopy* Bd. 76 (2009), Nr. 4, S. 570–576

[SNÖW10] SCHWEIGER, GUSTAV ; NETT, RALF ; ÖZEL, BILAL ; WEIGEL, THOMAS: Generation of hollow beams by spiral rays in multimode light guides. In: *Optics Express* Bd. 18 (2010), Nr. 5, S. 4510–4517

[TiFK90] TIDWELL, STEVE C. ; FORD, DENNIS H. ; KIMURA, WAYNE D.: Generating radially polarized beams interferometrically. In: *Applied Optics* Bd. 29 (1990), Nr. 15, S. 2234–2239

[ViIn09] VISWANATHAN, NIRMAL K. ; INAVALLI, V. V. G.: Generation of optical vector beams using a two-mode fiber. In: *Optics Letters* Bd. 34 (2009), Nr. 8, S. 1189–1191

[ViPJ10] VISWANATHAN, NIRMAL K. ; PHILIP, GEO M. ; JAYASURYA, Y. V.: <title>Generic dark hollow beams using negative cones chemically etched in fiber In: GALVEZ, E. J. ; ANDREWS, D. L. ; GLÜCKSTAD, J. (Hrsg.): , 2010, S. 761307–761307–9

[WaDL05] WANG, ZHAOYING ; DONG, YIMING ; LIN, QIANG: Atomic trapping and guiding by quasi-dark hollow beams. In: *Journal of Optics A: Pure and Applied Optics* Bd. 7 (2005), Nr. 3, S. 147

[WeSL05] WEI, MING-DAR ; SHIAO, WEN-LONG ; LIN, YI-TSE: Adjustable generation of bottle and hollow beams using an axicon. In: *Optics Communications* Bd. 248 (2005), Nr. 1–3, S. 7–14

[WIOY03] WATANABE, TAKESHI ; IKETAKI, YOSHINORI ; OMATSU, TAKASHIGE ; YAMAMOTO, KIMIHISA ; SAKAI, MAKOTO ; FUJII, MASAAKI: Two-

point-separation in super-resolution fluorescence microscope based on up-conversion fluorescence depletion technique. In: *Optics Express* Bd. 11 (2003), Nr. 24, S. 3271–3276

[WRWJ06] WILLIG, KATRIN I. ; RIZZOLI, SILVIO O. ; WESTPHAL, VOLKER ; JAHN, REINHARD ; HELL, STEFAN W.: STED microscopy reveals that synaptotagmin remains clustered after synaptic vesicle exocytosis. In: *Nature* Bd. 440 (2006), Nr. 7086, S. 935–939

[YiGZ03] YIN, JIANPING ; GAO, WEIJIAN ; ZHU, YIFU: Chapter 3 Generation of dark hollow beams and their applications. In: E. WOLF, V. B., N. BOKOR, H. CAO, N. DAVIDSON, W. GAO, D. J. GAUTHIER, G. GBUR, I GLESK, P. R. PRUCNAL, B. C. WANG, L. XU, J. YIN AND Y. ZHU (Hrsg.): *Progress in Optics*. Bd. Volume 45 : Elsevier, 2003 — ISBN 0079-6638, S. 119–204

[YZJW98] YIN, JIANPING ; ZHU, YIFU ; JHE, WONHO ; WANG, ZUZHU: Atom guiding and cooling in a dark hollow laser beam. In: *Physical Review A* Bd. 58 (1998), Nr. 1, S. 509–513

[ZeWu08] ZENG, XIAHUI ; WU, FENGTIE: The analytical description and experiments of the optical bottle generated by an axicon and a lens. In: *Journal of Modern Optics* Bd. 55 (2008), Nr. 18, S. 3071–3081

[ZhWL08] ZHAO, CHENGLIANG ; WANG, LIGANG ; LU, XUANHUI: Focal shift of hollow Gaussian beams through a thin lens. In: *Optics & Laser Technology* Bd. 40 (2008), Nr. 1, S. 58–63

CHAPTER

7

Conclusion and Applications

Diffraction is an intricic property of the wave field affecting its charecteristics when the wave encounters an obstacle. In modern optics diffraction is treated as a natural property of any practicaly realizable beam with non-homogeneous transverse intensity distribution that leads to changes in both transverse and longitudinal amplitude, phase and polarization distribution of the beam field and is also responsible for the divergence in the free-space propagation of the light beam. The divergence of an optical beam was considered to be an unavoidable phenomenon in beam optics up to 1987, when Durnin showed physically possible solutions to Helmholtz wave equation which are independent of the propagation distance[DuME87] known as the Bessel beams. Though the Bessel beams were first generated experimentally by McLeod[Mcle54] sixty years ago, it became a more effective replacement to conventional beams only in the 90's. The far-field diffraction pattern of the field introduced by Durnin is delta-function rings rather than concentric intensity pattern around the optic axis. Hence the term *'propagation-invariant'* is more realistic and appropriate here than '*diffraction-free'* beams. In conventional propagation-invariant beams the state of polarization is same all over the cross-section of the beam and are also called scalar propagation-invariant beams. In the recent timed propagation invariant beams with spatially varying polarization in the cross-section als came up and are called vector propagation-invariant beams.

This thesis is focused on studies to highlight some of the salient experimental and theoretical aspects of propagation-invariant (PI) vector optical beams ranging from its generation methods (using bulk axicon and fiber micro-axicon) to studies on different manifestations of the fundamental aspects of the PI beams such as its self-reconstruction beyond obstruction, and the phase and polarization evolution in the vector regime and their characterization, all geared towards making use of the beam in emerging and future applications.

A theoretical formalism based on vector diffraction theory is developed for a complete understanding of axicon focusing of complex intensity, phase and polarization structured light beams. The theory developed also predicts the formation of optical needle beams (with spot size 0.43λ and propagation-invariant range 80λ) upon high-NA axicon focusing of vector-vortex beams. The beam dynamics and phase evolution with propagation is an important aspect to study especially in the case of propagation-invariant beams. This was carriedout using beams embedded with polarization singularities which clearly shows that the phase

of the beam remains invariant in the propagation-invariant region. As far as the self-reconstruction of the propagation-invariant beams are concerned our studies were focused on the polarization and phase reconstruction rather than the conventional amplitude reconstruction process. Using a polarization singular Bessel-Gauss beam wherein the amplitude, phase and polarization are mutually tied together we demonstrated the 3D self-reconstruction of the beam charecteristics. Miniaturization of the device is an important aspect in practical applications. In an effort towards designing a compact source for the generation of structured light beams, selective chemical etching method was carriedout for optical fibers with different core-cladding dopant and diameter ratios. The chemical process is calibrated to obtain optimum micro-axicon parameters for the generation of propagation-invariant vector beams are also discussed in the thesis. The fabricated micro-axicons in different types of optical fibers are used to generate intensity and polarization structured porpagation-invariant beams such as dark hollow beams, chain of optical bottle beams and spirally polarized beams.

Applications

The number of articles being published by Optical Society of America journals having the word 'Bessel' in their title has increased thirty times just in a span of ten years between 1990 to 2010 which shows the growing interest in this area among reasearchers[DLPF13]. Bessel beams that can self-reconstruct their initial beam profile even in the presence of phase perturbations are able to propagate deeper into inhomogeneous media. This ability has crucial advantages for light sheet-based microscopy in thick media, such as cell clusters, embryos, skin or brain tissue or plants, as well as scattering synthetic materials[FaRo12]. Conventional optical tweezer using Guassian beam can create only one trap location while the self-reconstruction and self-imaging properties of Bessel beams can create multiple longitudinal trap sites and allow simultaneos manipulation of particles and cells[GMMS02]. The ring structure of the Bessel beam also gives an additional advantage of trapping particles with different refractive index simultaneously. Higher-order Bessel beams carry a phase vortex at the centre and thus possess optical angular momentum(OAM) and this degree of freedom can be used to encode information in OAM basis. Higher-order Bessels beams also find applications in atom channeling and guiding. The concepts of vector beam with spatially varying polarization structure in the cross-section of the beam and propagation-invariance were connected to realize vector Bessel beams, first

introduced by Jordan and Hall [JoHa94] and Bouchal [BoOl95]. The vector beam have been reported to be efficient than the scalar beams especialy in microscpy, laser acceleration of particles and laser machining applications. The biological samples for example neurons cells, tissues etc.. are naturally birefringent and significantly modify the phase and polarization characteristics of the light beam incident on them. Together with the propagation invariance and the complete 3D self-healing property vector Bessel beams can considerably improve the existing bio-imaging techniques. In the case of optical trapping the trapping force experienced by the trapped particle not only on the intensity gradient but also on the polarization gradient. So propagation-invariant vector beams can be used for the trapping of cylindrically symmetric objects such as carbon nanotubes and metallic nano rodes.

References

[BoOl95] BOUCHAL, ZDENĚK ; OLIVÍK, MAREK: Non-diffractive Vector Bessel Beams. In: *Journal of Modern Optics* Bd. 42 (1995), Nr. 8, S. 1555–1566

[DLPF13] DUDLEY, ANGELA ; LAVERY, MARTIN ; PADGETT, MILES ; FORBES, ANDREW: Unraveling Bessel Beams. In: *Optics and Photonics News* Bd. 24 (2013), Nr. 6, S. 22–29. — 00005

[DuME87] DURNIN, J. ; MICELI, J. J. ; EBERLY, J. H.: Diffraction-free beams. In: *Physical Review Letters* Bd. 58 (1987), Nr. 15, S. 1499–1501. — 02042

[FaRo12] FAHRBACH, FLORIAN O. ; ROHRBACH, ALEXANDER: Propagation stability of self-reconstructing Bessel beams enables contrast-enhanced imaging in thick media. In: *Nature Communications* Bd. 3 (2012), S. 632. — 00046

[JoHa94] JORDAN, REBECCA H. ; HALL, DENNIS G.: Free-space azimuthal paraxial wave equation: the azimuthal Bessel?Gauss beam solution. In: *Optics Letters* Bd. 19 (1994), Nr. 7, S. 427–429

[Mcle54] MCLEOD, JOHN H.: The Axicon: A New Type of Optical Element. In: *Journal of the Optical Society of America* Bd. 44 (1954), Nr. 8, S. 592–592. — 00703

Appendix-I

AI.1 Stokes Parameters

For an electromagnetic wave propagating in 'z' direction with electric field oscillations in 'xy' plane and having a single frequency, the spectral density tensor or the coherence matrix is given by

$$\phi_{ij}(r,\omega) = \langle E_i^*(r,\omega)E_j(r,\omega)\rangle, i,j = x,y \qquad (AI.1)$$

Where the angle bracket denote statistical averaging and * stands for complex conjugate. The 2x2 coherence matrix is a non-negative definite and Hermitian matrix that entirely specifies the state of polarization (SOP) of the planar field. The 2D Stokes parameters *Sj* (j=0,1,2,3) are measurable quantities which comes as expansion coefficient of the 2D coherence matrix[SSKF02].

$$\phi_2 = \frac{1}{2}\sum_{j=0}^{3} S_j\sigma_j \qquad (AI.2)$$

where σs are Pauli matrices. Expanding (AI.2) by substituting the Pauli matrices, the coherence matrix are then becomes

$$\phi_2 = \begin{pmatrix} S_0 + S_1 & S_2 + iS_3 \\ S_2 - iS_3 & S_0 - S_1 \end{pmatrix} \qquad (AI.3)$$

$S_j = tr(\sigma_j\phi_2)$. So, each Stokes parameters can be expanded in terms of the electric field as:

$$\begin{aligned} S_0 &= \phi_{xx} + \phi_{yy} = E_xE_x^* + E_yE_y^* \\ S_1 &= \phi_{xx} - \phi_{yy} = E_xE_x^* - E_yE_y^* \\ S_2 &= \phi_{xy} + \phi_{yx} = E_xE_y^* + E_yE_x^* \\ S_3 &= i(\phi_{yx} - \phi_{xy}) = i(E_xE_y^* - E_yE_x^*) \end{aligned} \qquad (AI.4)$$

And the degree of polarization(DOP) in terms of the Stokes parameters is given by,

$$P_2 = \frac{[S_1^2 + S_2^2 + S_3^2]^{\frac{1}{2}}}{S_0} \qquad (AI.5)$$

When the field is fully polarized, the SOP can be represented as a point (S_1 ,S_2 ,S_3) on the Poincare sphere of radius S_0 (P_2=1). The equator of the sphere in the S_1S_2 plane corresponds to linearly polarized light, and the north and south poles to right-hand and left-hand circularly polarized light, respectively. Furthermore, all points in the Poincare sphere other than the equitorial line and both poles correspond to elliptic polarization with different eccentricity, orientation and handedness. So the Stokes parameters together with the polarization ellipse representation gives a complete description of the polarization of a plannar electromagnetic wave. Fig. AI.1 gives the polarization ellipse with relevent parameters.

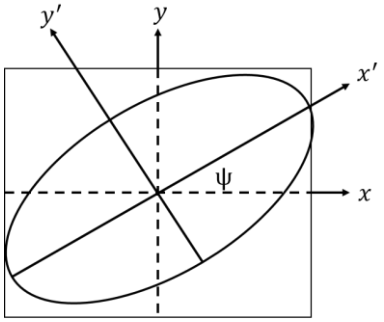

Fig. AI.1 Polarization ellipse

Consider a monochromatic plane wave at z=0 given by the following equations

$$E_x(t) = E_{0x}(t)\, cos[\omega t - \delta_x(t)] \qquad (AI.6)$$

$$E_y(t) = E_{0y}(t)\, cos\big[\omega t - \delta_y(t)\big] \qquad (AI.7)$$

where $E_{0x}(t)$ and $E_{0y}(t)$ are the instantaneous amplitudes, ω is the instantaneous angular frequency, and $\delta_x(t)$ and $\delta_y(t)$ are the instantaneous phase factors. After explicit removal of, ω the electric field can be written in the ellipse form given by the equation[Gold10]:

$$\frac{(E_x(t))^2}{(E_{0x})^2}+\frac{(E_y(t))^2}{(E_{0y})^2}-\frac{2E_x(t)E_y(t)}{E_{0x}(t)E_{0y}(t)}cos\delta=sin^2\delta \qquad (AI.8)$$

By substituting Equ.(AI.6) and (AI.7) in Equ. (AI.4) we get the Stokes parameters in terms of electric field as:

$$S_0=E_{0x}^2+E_{0y}^2$$

$$S_1=E_{0x}^2-E_{0y}^2 \qquad (AI.9)$$

$$S_2=2E_{0x}E_{0y}cos\delta$$

$$S_3=2E_{0x}E_{0y}sin\delta$$

The orientation of the major axis of the ellipse given by Equ.(AI.8) is given by[Gold10]

$$tan2\psi=\frac{2E_{0x}E_{0y}cos\delta}{E_{0x}^2-E_{0y}^2}=\frac{S_2}{S_1} \qquad (AI.10)$$

and the ellipticity of the polarization ellipse is given by

$$sin2\chi=\frac{2E_{0x}E_{0y}sin\delta}{E_{0x}^2+E_{0y}^2} \qquad (AI.11)$$

AI.2 Experimental measurement of Stokes parameters

We used the quarter-wave plate (QWP) retarder and linear polarizer(P) method to measure the Stokes parameter of the beam. The schematic of the experimental setup is shown in the Fig. AI.2.

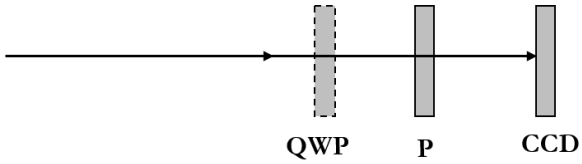

Fig. 2 Schematic of the setup used for the measurement of Stokes parameters

Six intensity images of the output beam are taken, first with the polarizer (P) orientations corresponding to 0° (I_0), 45° (I_{45}), 90° (I_{90}), and 135° (I_{135}), then a QWP is inserted before the polarizer and kept at 90° and keeping P2 at 45° (I_R) and 135° (I_L). And the Stokes parameters of the beam is calculated from the six intensity measurements using [Gold10]:

$$S_0 = I_0 + I_{90}$$
$$S_1 = I_0 - I_{90} \qquad (AI.12)$$
$$S_2 = I_{45} - I_{135}$$
$$S_3 = I_R - I_L$$

The polarization ellipse parameters calculated from the Stokes parameters are superposed on the beam and is used to study the change in their charecteristics under different experimental conditions as mentioned in the Chapters.

References

[Gold10] GOLDSTEIN, DENNIS H.: *Polarized Light, Third Edition*. 3 edition. Aufl. Boca Raton, FL : CRC Press, 2010. — 00000 — ISBN 9781439830406

[SSKF02] SETÄLÄ, T. ; SHEVCHENKO, A. ; KAIVOLA, M. ; FRIBERG, A. T.: Degree of polarization for optical near fields. In: *Physical Review E* Bd. 66 (2002), Nr. 1, S. 016615. — 00164

Appendix II

Polarization Singularities

In addition to the phase vortex or phase singularity paraxial optical fields also exhibit a variety of singular points which are classified into: *Vector* (V-point) singularities and *Elliptic* singularities[Freu02].

Vector singularities

This is a point in the beam field where the direction of the linearly polarized electric field vector is undefined as shown in Fig. AII.1. The V-singularity is charectarized by the Poincare–Hopf index η which descibe the orientation of the electric field vectors aroud the V-point.

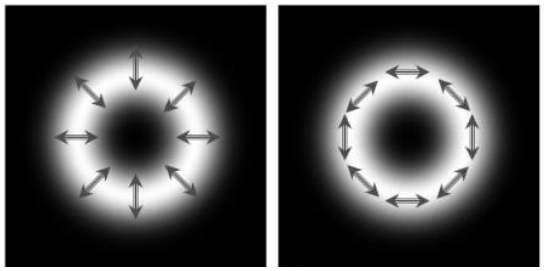

Fig. AII.1 Radial and azimuthal polarized beam showing V-singularities at the centre.

Elliptic point Singularities

In a sea of polarization ellipses prepared under certain some aspects of the polarization ellipse is undefined at certaing points in the beam field. There are two types of elliptic singularities: C-point and L-line.

C-point:

C-point is point where the orientation of the major axis of the polarization ellipse is undefined and is charecterized by C-point index I_C which defines the orientation of the polarization ellipses around the C-point. The C-point index I_C is defined as

$$I_C = \int_0^{2\pi} d\theta \qquad (AII.1)$$

where θ is the orientation angle of the major axis of the polarization ellipse. There are different morphological forms for C-point singularities. For example the C-point with index +1/2 is known as '*lemon*' and -1/2 is '*star*' and the linear combination of star and lemon is known as '*monstar*' [FODP08]. Fig. AII.1 shows the polarization ellipse structure of these C-point[I10] sructures.

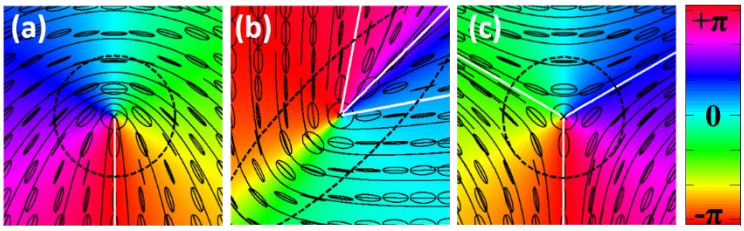

Fig. AII. 2 different morphological structures of the polarization singular pater of C-point index ± 1/2: (a) *lemon*, (b) *monster*, (c) *star* type polarization singular patterns

L-line:

L-lines is made by points od linear polarization where the handedness of the polarization ellipse is undefined (shown as dotted lines in Fig. AII.2) and happens where the intensity of the superposing beams are the same with the orientation depending on their phase differences

References

[FODP08] FLOSSMANN, FLORIAN ; O'HOLLERAN, KEVIN ; DENNIS, MARK R. ; PADGETT, MILES J.: Polarization Singularities in 2D and 3D Speckle Fields. In: *Physical Review Letters* Bd. 100 (2008), Nr. 20, S. 203902. — 00046

[Freu02] FREUND, ISAAC: Polarization singularity indices in Gaussian laser beams. In: *Optics Communications* Bd. 201 (2002), Nr. 4–6, S. 251–270. — 00068

[I10] I, FREUND: Multitwist optical Möbius strips. In: *Optics letters* Bd. 35 (2010), Nr. 2, S. 148–50. — 00007

List of Publications

Journal articles

- **Geo M. Philip** and Nirmal K. Viswanathan "Generation of tunable chain of three-dimensional optical bottle beams via focused multi-ring hollow Gaussian beam" **J. Opt. Soc. Am. A** 27, 2394-2401 (2010)
- N.K. Viswanathan, **G.M.Philip**, and Y.V.Jayasurya, "Generic dark hollow beams using negative cones chemically etched in the fiber tips," **Proc.SPIE** 7613, 761307-1(2010)
- **Geo M. Philip** and Nirmal K. Viswanathan, "Generation of spirally polarized propagation invariant beam using fiber microaxicon" **Opt. Lett** 36, 3906 (2011).
- **Geo M Philip**, Vijay Kumar, Giovanni Milione, and Nirmal K. Viswanathan "Manifestation of the Gouy phase in vector-vortex beams" **Opt. Lett** 37, 2667 (2012).
- Vijay Kumar, **Geo Philip** and N.K. Viswanathan, "Formation and morpholoical transformation of polarization singularities: Hunting the monstar," **J. Opt**.15, 044027 (2013)
- **Geo M. Philip** and Nirmal K. Viswanathan "Focusing of Optical Vector-vortex Beams" ***Physical Science International Journal*** 4(3), 434-446, 2014

Conference Papers

Oral Presentations:

- **Geo M. Philip** and Nirmal K. Viswanathan, "Fabrication of negative micro axicons in optical fiber via chemical etching," International Conference on Optics and Photonics, Chandigarh, India 2009.
- **Geo M. Philip** and Nirmal K. Viswanathan, "Sculpting Non-diffracting Beam from Gaussian beam using fiber axicon" International Conference on Contemporary Trends in Optics and Optoelectronics, XXXV OSI Symposium Trivandrum, India 2011.
- **Geo M. Philip** and Nirmal K. Viswanathan, " Gouy Effect in non-diffracting Beams" IONS India IIT Delhi.2011
- **Geo M. Philip** and Nirmal K.Viswanathan, "Long Range Longitudinally Polarised Optical Needle Beams", FIO 2013, Orlando, USA

Poster Presentations:

- **Geo M. Philip** and Nirmal K. Viswanathan, "Generation of higher-order Bessel like beams using a conical tip fiber," International Conference on Optics and Photonics, Chandigarh, India 2009.
- **Geo M. Philip** and Nirmal K. Viswanathan, "Polarization structuring of non-diffracting vortex beams" XXXVI OSI Symposium IIT Delhi India.2011
- **Geo M. Philip** and Nirmal K. Viswanathan, " Gouy Phase Measurement of non-diffracting Beams" Frontiers in Physics ,UOH.2011
- **Geo M. Philip** and Nirmal K Viswanathan, "Self-reconstructing singular beams" SPIE Photonics Europe 2014